

**CONFORMATIONAL CHANGES OF  
SINGLE DNA MOLECULES INDUCED  
BY H-NS AND HU PROTEINS IN A  
NANOSPACE**

**Durgarao Guttula**

{M.Sc., Banaras Hindu University, India.}

**A THESIS SUBMITTED FOR THE DEGREE OF  
DOCTOR OF PHILOSOPHY  
DEPARTMENT OF PHYSICS  
NATIONAL UNIVERSITY OF SINGAPORE**

**2014**

**CONFORMATIONAL CHANGES OF  
SINGLE DNA MOLECULES INDUCED  
BY H-NS AND HU PROTEINS IN A  
NANOSPACE**

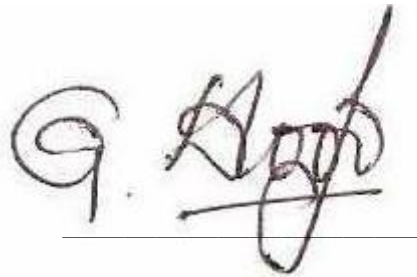
**Durgarao Guttula**

**NATIONAL UNIVERSITY OF  
SINGAPORE  
2014**

## DECLARATION

I hereby declare that this thesis is my original work and it has been written by me in its entirety. I have duly acknowledged all the sources of information which have been used in the thesis.

This thesis has also not been submitted for any degree in any university previously.

A handwritten signature in black ink, appearing to read 'G. Guttula', written over a horizontal line.

Durgarao.Guttula

17-January-2014

*I would like to dedicate this thesis to my loving parents,  
teachers and loved ones ...*

# Acknowledgements

*“ Sarve Jana Sukhino Bhavantu, Lokah Samastah Sukhino  
Bhavantu”*<sup>1</sup>

Firstly, I would like to express my great appreciation to my supervisor Associate Professor Johan R. C. van der Maarel, Department of Physics, National University of Singapore, for his patience, guidance, enthusiastic encouragement, and advice on this research work. His knowledge of polymer physics and insight into research trends has helped me to develop my professional skills and understanding. Moreover, the freedom in research that he allowed has greatly increased both my level of confidence in and enthusiasm for science. I have gained invaluable knowledge from him about how to do research and enjoy it.

Secondly, I would like to offer my special thanks to my co-supervisor Associate Professor Jeroen van Kan, Department of Physics, NUS, Singapore, for providing high-quality nanochannel stamps timely and inspiring me in nanotechnology. Special thanks to Dr P. P. Malar and Mr Liu Fan from Van Kan’s lab. Also, thanks to Mr Pei Ge Shao (may his soul rest in heaven), who guided me at the initial stage of Bio-Nano chip fabrication.

---

<sup>1</sup>Let all be happy. May the Lord bless the whole world with eternal peace and goodwill.

## Acknowledgements

---

I would like to thank Dr Ce Zhang for his technical knowledge of handling nanofluidic devices – my deepest gratitude to him. His knowledge of polymer behaviour in nanofluidic devices and creativity of manipulation of the microscope have guided me through the projects. I would also like to thank Associate Professor Yan Jie and his team, especially Mr Ci Ji of NUS, for helping me in protein purification and providing HU protein. Thanks to Professor Patrick S. Doyle and Dr Dai Liang (S.M.A.R.T/Massachusetts Institute of Technology) for contributing computer simulations, and Professor Arluison Veronique (CEA France) for providing other proteins.

My thanks are extended to Kai Jiang, Zongying Gong, Sarabjit Singh, Dr Siow Yee, Dr Binu Kundukad, and Dr Sreelatha (SMART/BioSyM), for their assistance in discussions and experiments, and for maintaining a good research environment. I would like to thank Mr Teo Hoon Hwee and Ms See Sin Yin for their technical support for Biophysics teaching lab instruments.

I also thank my friends in Singapore for making my life in NUS and Singapore “*happy and fun*”, especially Mr & Miss Dr Mallikarjunrao and Mr Anand Pratap Singh. Finally, this thesis would never have been possible without the love and support of Sailu (*bujji* ☺) who has become my life partner.

***“Hari om tatsat”***

# Summary

This thesis comprises two related projects. The effects of nucleoid-associated proteins H-NS and HU on the conformation of single DNA molecules in a nanospace were investigated with fluorescence microscopy. The nanospace was provided by nano channels of dimensions  $200 \times 300 \text{ nm}^2$  and  $150 \times 250 \text{ nm}^2$ . For H-NS project, temporal conformation changes were also investigated using cross channels of height 200 nm and widths of 250 and 150 nm.

In the first project, the effect of the bacterial heat-stable nucleoid structuring protein (H-NS) on the conformation of single DNA molecules confined in a nanochannel was investigated using fluorescence microscopy. With an increasing concentration of H-NS, the DNA molecules either elongate or contract. The conformational response is related to the filamentation of H-NS on DNA through oligomerisation and H-NS mediated bridging of distal DNA segments, and is controlled by the concentration and ionic composition of the buffer. Confinement in a nanochannel facilitates compaction of DNA into a condensed form for over-threshold concentrations of H-NS. Divalent ions such as magnesium facilitate but are not required for bridging or condensation. The time scale of the collapse of DNA after

exposure to H-NS was determined to be in the order of minutes, which is much shorter than the measured time required for filamentation of around 1 hr. The effect of H-NS is not only related to its binding properties, but also to the confinement, which is of paramount importance. The interplay between confinement, H-NS-mediated attraction, and filamentation controls the conformation and compaction of DNA.

In the second project, the effect of the heat-unstable nucleoid structuring protein (HU) on the conformation of single DNA molecules confined in a nanochannel was investigated using fluorescence microscopy. DNA molecules were pre-incubated with HU and confined inside an array of nanochannels with cross-sectional dimension of 200 by 300 nm. With an increasing concentration of HU, the pre-incubated DNA molecules contract in the longitudinal direction of the channel. This contraction is due to DNA bridge formation mediated by bound HU protein. For over-threshold concentrations HU, the DNA molecules condense into a compacted form. Divalent ions such as magnesium facilitate but are not required for condensation.

These findings might have implications in gene silencing and chromosome organisation, because the cross-sectional dimensions of the channels are comparable to those of the bacterial nucleoid.



# List of publications

1. Guttula, D., Zhang, C., Liu, F., Malar, P. P., Ng, S. Y., Dai, L., Doyle, P. S., van Kan, J. A., and van der Maarel, J. R. C. (2013). “*Effect of H-NS on the elongation and compaction of single DNA molecules in a nanospace*”. *Soft Matter* (2013), 9(40).
2. Zhang, C., Hernandez-Garcia, A., Jiang, K., Gong, Z., Guttula, D., Ng, S. Y., Malar, P. P., van Kan, J. A., Dai, L., Doyle, P. S., Vries, R. D., and van der Maarel, J. R. C. (2013). *Amplified stretch of bottlebrush-coated DNA in nanofluidic channels*. *Nucleic Acids Res.*, 41(20).
3. Zhang, C., Gong, Z., Guttula, D., Malar, P. P., van Kan, J. A., Doyle, P. S., and van der Maarel, J. R. C. (2012). *Nanofluidic compaction of DNA by like-charged protein*. *J. Phys. Chem. B*, 116(9).

# Contents

<b>Acknowledgements</b>	<b>iv</b>
<b>Summary</b>	<b>vi</b>
<b>List of publications</b>	<b>viii</b>
<b>Contents</b>	<b>ix</b>
<b>List of Figures</b>	<b>xiii</b>
<b>List of Tables</b>	<b>xv</b>
<b>Nomenclature</b>	<b>xviii</b>
<b>1 Introduction and Literature Review</b>	<b>1</b>
1.1 DNA organisation inside the cell . . . . .	2
1.1.1 Macromolecular crowding . . . . .	4
1.1.2 Negative supercoiling . . . . .	4
1.1.3 Nucleoid associated proteins . . . . .	5
1.1.3.1 H-NS . . . . .	6
1.1.3.2 HU . . . . .	10
1.1.3.3 Other nucleoid associated proteins . . . . .	12

1.2	DNA as a polymer . . . . .	16
1.2.1	Ideal chain . . . . .	16
1.2.2	Worm-like chain model . . . . .	19
1.2.3	Excluded volume interactions . . . . .	21
1.2.4	Physics of DNA in confinement . . . . .	23
1.2.4.1	De Gennes’s blob theory . . . . .	23
1.2.4.2	Odijk theory . . . . .	25
1.2.5	DNA in Nanochannel experiments . . . . .	28
1.3	Research Objectives . . . . .	33
1.4	Bibliography . . . . .	36
<b>2</b>	<b>Materials and methods</b>	<b>47</b>
2.1	T4-DNA . . . . .	47
2.1.1	YOYO-1 . . . . .	49
2.2	Fabrication of nanofluidic device . . . . .	50
2.2.1	Nanostructure fabrication by PBW . . . . .	50
2.2.2	Micro channel fabrication by UV-lithography . . . . .	52
2.3	PDMS . . . . .	54
2.3.1	Air plasma cleaning . . . . .	54
2.4	Fluorescence microscopy . . . . .	55
2.5	Data analysis . . . . .	57
2.5.1	Measurements of DNA length in nanochannels . . . . .	57
2.5.2	Measurement of DNA length in bulk phase . . . . .	59
2.6	Protein Purification . . . . .	60
2.6.1	Wt H-NS purification by ion exchange chromatography	62
2.6.1.1	First step – purification by Cellulose column	62
2.6.1.2	Second step – purification by Heparin column	64

2.6.2	His-tag H-NS purification . . . . .	66
2.6.3	Size Exclusion Chromatography (SEC) . . . . .	70
2.6.3.1	Calibrating the column . . . . .	71
2.6.3.2	Oligomerisation of H-NS . . . . .	73
2.6.4	Isolation and purification of HU . . . . .	74
2.7	Bibliography . . . . .	75

**3 Effect of H-NS on the elongation and compaction of single DNA molecules in a nanospace 77**

3.1	Introduction . . . . .	77
3.2	Materials and Methods . . . . .	81
3.2.1	Isolation and Purification of H-NS . . . . .	81
3.2.2	Sample preparation . . . . .	82
3.2.3	Fabrication of nanofluidic chips . . . . .	83
3.2.4	Single-channel array . . . . .	84
3.2.5	Cross-channel array . . . . .	85
3.2.6	Monte Carlo simulation . . . . .	86
3.3	Results . . . . .	87
3.3.1	Stretch of pre-incubated DNA . . . . .	87
3.3.2	Time-dependent conformational response . . . . .	91
3.3.3	Summary of observations . . . . .	96
3.4	Discussion . . . . .	97
3.4.1	Elongation by filamentation . . . . .	97
3.4.2	Contraction by bridging . . . . .	100
3.4.3	Condensation . . . . .	101
3.5	Conclusions . . . . .	105
3.6	Bibliography . . . . .	106

<b>4</b>	<b>Effect of HU protein on the conformation and compaction of single DNA molecules in a nanospace</b>	<b>110</b>
4.1	Introduction . . . . .	110
4.2	Materials and methods . . . . .	114
4.2.1	Isolation and purification of HU . . . . .	114
4.2.2	Sample preparation . . . . .	115
4.2.3	Fabrication of the Nanofluidic Chips . . . . .	115
4.2.4	Single-channel array . . . . .	116
4.3	Results and Discussion . . . . .	117
4.3.1	Compaction and Condensation of pre-incubated DNA	117
4.4	Conclusions . . . . .	121
4.5	Bibliography . . . . .	122
<b>5</b>	<b>Conclusions and future work</b>	<b>126</b>
5.1	Conclusions . . . . .	126
5.1.1	Overall conclusion . . . . .	128
5.2	Future work . . . . .	128
5.3	Bibliography . . . . .	132
<b>6</b>	<b>Over all references</b>	<b>133</b>
6.1	References . . . . .	133

# List of Figures

1.1	Conformational changes of DNA by different modes of nucleoid-associated proteins binding . . . . .	14
1.2	Schematic diagram of different confinement regimes . . . . .	27
2.1	Pulsed field gel electrophoresis of T4-DNA gel picture . . . . .	48
2.2	Nanostructure patterning in HSQ photoresist by Proton beam writing. . . . .	51
2.3	Super positioning of the SU8 microstructure on the HSQ nanostructure by UV lithography. . . . .	53
2.4	Intensity profile of a labelled DNA . . . . .	57
2.5	Fluorescence image of labelled T4-DNA in (A) bulk phase and (B) nanochannels. . . . .	58
2.6	Labelled T4-DNA in bulk phase and nanochannels. . . . .	59
2.7	Schematic drawing of separation principles in chromatography purification. . . . .	61
2.8	Protein purification by Cellulose column. . . . .	62
2.9	SDS-page picture of Cellulose column purification of H-NS. . . . .	63
2.10	Protein purification by Heparin column. . . . .	64
2.11	SDS-page picture of Heparin column purification of H-NS: . . . . .	65
2.12	Single step protein purification by His-trap column. . . . .	67
2.13	SDS-page picture of His-trap column purification of H-NS. . . . .	68

## List of Figures

---

2.14	SDS-page picture of His-tag digestion by TEV. . . . .	68
2.15	Circular dichroism spectrum . . . . .	69
2.16	Structure of the beads in the SEC media and elution process. . . . .	70
2.17	Calibration graph of SEC column with standards. . . . .	72
2.18	Size Exclusion Chromatography of H-NS. . . . .	73
3.1	Bright field optical image of the bonded cross-channel array device . . . . .	83
3.2	Montage of fluorescence images of T4-DNA in T-buffer with 3 mM NaCl and confined in $200 \times 300 \text{ nm}^2$ channels. . . . .	88
3.3	(A) Relative extension $R_{\parallel}/L$ of T4-DNA in T-buffer with 3 ( $\triangle$ ) or 30 ( $\nabla$ ) mM NaCl versus the concentration of H-NS. . . . .	89
3.4	Elongation of T4-DNA following a flush with a solution of $0.8 \mu\text{M}$ H-NS in T-buffer and 3 mM NaCl. . . . .	92
3.5	Condensation of T4-DNA following a flush with a solution of 1.0 ( $\triangle$ ), 1.2 ( $\circ$ ), and 1.6 ( $\nabla$ ) $\mu\text{M}$ H-NS. . . . .	93
3.6	Fluorescence intensity profile across the array of $200 \times 250 \text{ nm}^2$ channels imaged at the indicated. . . . .	94
3.7	Monte Carlo simulation results. . . . .	98
3.8	Relative persistence length $P/P_0$ of T4-DNA in T-buffer with 3 mM NaCl and confined in $150 \times 250$ ( $\blacktriangle$ ) . . . . .	99
4.1	Relative extension $R_{\parallel}/L$ of T4-DNA in T-buffer with 3 ( $\triangle$ ) or 30 ( $\nabla$ ) mM NaCl versus the concentration of HU . . . . .	118
4.2	(A) Montage of fluorescence images of T4-DNA in T-buffer with 3 mM NaCl and inside $200 \times 300 \text{ nm}^2$ channels. T-buffer is 8.1 mM TrisCl and 1.9 mM Tris, pH 7.5. . . . .	119

# List of Tables

1.1	Linear and volumetric compaction of DNA in different species.	3
2.1	Different types of liquid-chromatographic separation based on specific properties . . . . .	60
3.1	Relative decrease in extension $\Delta R_{\parallel}/L$ , decay rate $R$ , and lag-time $\tau_{lag}$ . . . . .	96



# Nomenclature

## Greek Symbols

$\lambda$	Deflection length of the polymer in Odijk theory, page 26
$\nu$	Flory exponent, page 21
$\sigma_k$	Kuhn renormalisation factor, page 18
$\theta$	Deflection angle of the polymer in Odijk theory, page 26
$\lambda - DNA$	Bacteria $\lambda$ -phage linear DNA, having 48,502 bp with 16.3 $\mu\text{m}$ length, page 48
$\lambda_{max}^{em}$	Wavelength at emission maxima, page 49
$\lambda_{max}^{ex}$	Wavelength at excitation maxima, page 49
$\sigma$	Superhelical density, page 5
$\sigma_C$	Constrain supercoiling, page 5
$\sigma_U$	Unconstrain supercoiling, page 5

## Superscripts

$h^2$	Mean square end to end distance, page 19
-------	--

## Subscripts

$F_{elas}$	Free energy of the coil from elasticity, page 18
$F_{rep}$	Free energy of the coil from repulsion, page 21

$k_B$	Boltzmann constant, page 18
$k_B T$	Thermal energy, page 18
$R_{\parallel}$	The extension of the chain along the channel direction, page 24
$R_g$	Radius of gyration, page 20
$w_{eff}$	Effective width of the polymer, page 24
$i$	$i^{th}$ segment of the polymer chain, page 16
$\theta_{ij}$	Angle between $i^{th}$ and $j^{th}$ position vectors along the contour, page 17
$L_k$	Linking number, page 5

### Symbols

$D$	Diameter of the confinement, page 23
$D_{av}$	Average diameter of the confinement with walls $D_1$ and $D_2$ , page 23
$g$	Number of links in the blob, page 23
$l_k$	Kuhn length factor, page 18
$L_p$	Persistence length, page 19
$N_k$	Kuhn segments factor, page 18
$L$	Contour length of the polymer, page 16
$l$	Segment length of the polymer, page 16
$N$	Number of segment in the polymer, page 16
$R$	Polymer size, page 16

### Acronyms

<i>E. coli</i>	<i>Escherichia coli</i> , page 3
AFM	Atomic Force Microscopy, page 13

## Nomenclature

---

DAPI	4',6-diamidino-2-phenylindole, page 49
DNA	Deoxy ribo Nucleic Acid, page 1
EtBr	Ethidium Bromide, page 49
FIS	Factor of Inversion Stimulation, page 6
H-NS	Histone like Nucleoid Structuring protein, page 6
<i>h</i>	Vector between first and last monomer of the polymer chain( <i>i.e.</i> end-to-end distance.), page 16
HU	Heat-Unstable nucleoid structuring protein, page 6
IEC	Ion Exchange Chromatography, page 61
IHF	Integration Host Factor, page 6
NAPs	Nucleoid Associated Proteins, page 3
PBW	Proton Beam Writing, page 52
RNA	Ribo Nucleic Acid, page 1
SEC	Size Exclusion Chromatography, page 61
SMC	Structure Maintenance of Chromosomes, page 3
T4-DNA	Bacteria T4-phage linear DNA, having ~169 kbp with 56 $\mu\text{m}$ length, page 48
UV	Ultra Violet light, page 52
YOYO-1	A fluorescent dye for DNA, page 49

# Chapter 1

## Introduction and Literature

### Review

Several decades of research has been done and still going on nucleic acids, because nucleic acids are the matter, on which life is built up. Nucleic acids store the genetic code (DNA) and translate genetic information into proteins and RNA etc.

Swiss scientist Johannes Friedrich Miescher first discovered DNA in 1869<sup>[1]</sup>. Six decades later, F. Griffith (1928) conducted the “*transforming principle*”<sup>[2]</sup> experiment on mice with virulent and non-virulent bacteria and hypothesised that the results could offer a clue to discovering genetic code. After 20 years, O. Avery et al. experimentally showed DNA to be the carrier of genetic information and confirmed the transforming principle<sup>[3]</sup>. In 1952, Alfred Hershey and Martha Chase confirmed that “*DNA*” itself is a *genetic* material. One year later, James D. Watson and Francis Crick resolved the spatial structure of DNA and proposed the *double-helix model*,

## 1.1. DNA organisation inside the cell

---

which won them the Nobel Prize. The double helix model is based on the basepair rules by Erwin Chargaff and X-ray diffraction results by Rosalind Franklin and Raymond Gosling<sup>[4]</sup>. This double-helix model itself not only complies with the known physical and chemical properties of DNA, but also explains how DNA fulfils biological functions such as replication, transcription, and translation<sup>[5]</sup>. The double-helix model was a turning point in the area of biology. Based on this model, major advancements have been made in the establishment of the foundation of modern molecular biology, leading to an upsurge in new experimental discoveries and techniques over the last half-century.

This chapter presents the study on bacterial chromosomal organisation and DNA conformational changes by nucleoid associated proteins. This is followed by the physics of DNA in non-confined (free space) and confined regimes, and some experimental studies reported on DNA conformation in nanochannels. The chapter concludes with the research object of this thesis. This introduction is helpful in understanding later chapters of this thesis.

## 1.1 DNA organisation inside the cell

The DNA in eukaryotes and prokaryotes is organised differently and establishes chromosome architecture at small and large scales. For example, 4.6 Mbp DNA with contour length 1.6 mm is present in 1  $\mu\text{m}$  diameter sized *Escherichia coli* (*E. coli*) of size 3-4  $\mu\text{m}$  (See table 1.1). The volumetric compaction is more than 350 times in *E. coli*. In other species such as

## 1.1. DNA organisation inside the cell

**Table. 1.1** Linear and volumetric compaction of DNA in different species.<sup>1</sup>

DNA	Sequence length bp	Physical length $\mu\text{m}$	Container diameter <sup>2</sup>	Linear reduction <sup>3</sup> $\mu\text{m}$	Volume of free DNA random coil $\mu\text{m}^3$	Container volume $\mu\text{m}^3$	Volume reduction <sup>4</sup>
<i>E. coli</i>	$4.6 \times 10^6$	$1.6 \times 10^3$	1.0	$1.6 \times 10^3$	$1.9 \times 10^2$	0.52	$3.7 \times 10^2$
Yeast	$2.8 \times 10^7$	$9.3 \times 10^3$	2.0	$4.7 \times 10^3$	$8.1 \times 10^3$	4.2	$1.9 \times 10^3$
Human	$6.0 \times 10^9$	$2.0 \times 10^6$	10.0	$2.0 \times 10^5$	$2.6 \times 10^7$	$5.2 \times 10^2$	$4.9 \times 10^4$

<sup>1</sup>This table is taken from Holmes (2000)<sup>[6]</sup>

<sup>2</sup>Nucleoid or nucleus

<sup>3</sup>Linear reduction = physical length/container diameter

<sup>4</sup>Volume reduction = volume of free DNA container volume

yeast and humans, the compaction is 2,000 and 50,000 fold respectively<sup>[6]</sup>.

In eukaryotes, DNA is confined in nucleus and compacted by histones. Histones organise DNA hierarchically into the higher-order structure called chromatin. *E. coli* does not have a nucleus; however, chromosomal DNA is compacted to a form called nucleoid. This compaction has no higher-order chromosomal organisation and represents a completely open structure. This compaction is caused by many factors: macro-molecular crowding, negative super coiling, segregation, compaction by nucleoid associated proteins (NAPs) and SMC complexes (structure maintenance of chromosomes) *etc.* DNA, as a macro object compacted inside a cell, performs enormous unique biological activities. The origin of prokaryotic chromosomal DNA compaction was poorly understood, and thus it is of scientific importance to discover its origin from both the biological and physical point of view. In the following sections, some of the effects of this compaction are described.

#### 1.1.1 Macromolecular crowding

Macromolecular crowding alters the properties of molecules (DNA) in a solution when high concentrations of macromolecules such as RNA and proteins are present<sup>[7]</sup>. For instance, the cytosol of *E. coli* contains about 300-400 mg/ml of macromolecules. Because of the hard sphere nature and excluded volume of the crowding agents, the effective available volume of DNA decreases as number of crowding molecules increases. This will cause an effective osmotic pressure imbalance that leads to attraction between the segments of the DNA. This force of attraction is also called depletion force. DNA is compacted due to depletion force, so the compaction by crowding is of entropic origin<sup>[8,9]</sup>. Electron microscopy and fluorescence studies of the nucleoid show that crowding plays a major role in compacting the genome, determining the distinct, well-defined structure of the nucleoid<sup>[10]</sup>. However, comparative studies on nucleoid, extracted from both wild type cells and mutants with deletions of NAPs show no apparent difference in the visual appearance of the nucleoids<sup>[11]</sup>. This study suggests that the contribution of crowding is considerably greater than the nucleoid-associated proteins (NAPs) to the large-scale structure and compaction<sup>[12]</sup>.

#### 1.1.2 Negative supercoiling

Chromosomal DNA in eukaryotes is in linear form and prokaryotic chromosomal DNA is in circular (or supercoiled) form, and multi-connected topology in cases of multiple chromosomes<sup>[13]</sup>. Conformational change from original relaxed DNA to supercoil form results in a reduced occupied volume. The volume is reduced due to the formation of super helical branches.

### 1.1.3. Nucleoid associated proteins

---

In DNA, the helix is repeated every 10.5 base pairs on average. DNA supercoiling is described by linking number  $Lk$ , and it is merely the number of crosses that a single strand makes across the other. A physical parameter *superhelical density*  $\sigma$ , describes the level of supercoiling. It is defined by the ratio of the linking number difference ( $Lk_0 - Lk$ ) of a supercoiled molecule to the linking number of a relaxed molecule under ideal conditions *i.e*  $\sigma = (Lk_0 - Lk)/Lk_0$ . In general it has the value of  $\sigma = -0.025$ , which means that the DNA is under-wound. Superhelical density ( $\sigma$ ) is the sum of constrained super coiling  $\sigma_C$  and unconstrained supercoiling  $\sigma_U$ . The action of NAPs and the counter activities of the DNA gyrase, introduce negative super coiling to DNA. For example, constrained supercoiling ( $\sigma_C$ ) increased by some NAPs are HU (30%), H-NS (3%) and FIS (15%) *in vivo*. Enzymes such as topo-isomerases (type-I and IV) remove supercoils<sup>[14]</sup>. Negative supercoiling is essential for folding, compaction, and untwisting. Untwisting is required for the initiation of transcription, replication, and recombination. Too much over-winding impedes transcription and replication<sup>[15]</sup>, and excessive under-winding is toxic and leads to poor chromosomal segregation<sup>[16]</sup>.

### 1.1.3 Nucleoid associated proteins

In eukaryotes, the organisation and control of genes is done by *histone* proteins, but in bacteria it is done by nucleoid-associated proteins (NAPs). These are the proteins that bind to DNA and alter its conformations. NAPs are not homologous with histones, but they functionally similar to them, so it is appropriate to call them “*histone-like*” proteins. There are many



NAPs, but the most important and abundant ones are HU, H-NS, IHF, and FIS. These proteins are present in the cells at concentrations up to or even exceeding  $10 \mu\text{M}^1$  depending on growth conditions<sup>[17,18]</sup>. In the exponential phase, the order of abundance is  $\text{FIS} > \text{HU} > \text{H-NS} > \text{IHF}$ , but it changes to  $\text{Dps}^2 > \text{IHF} > \text{HU} > \text{H-NS} > \text{FIS}$  in the stationary phase<sup>[19]</sup>. The stationary phase is more compacted than the exponential phase, which has a diffuse structure. The conformational effects of NAPs are discussed in detail in the following section.

#### 1.1.3.1 H-NS

H-NS was first identified as a thermostable protein acting on *in vitro* DNA transcription<sup>[20]</sup>, and has also been shown to stimulate DNA-directed RNA synthesis<sup>[21]</sup>. The name *histone like nucleoid structuring protein* or *heat-stable nucleoid structuring protein* (H-NS) was given during preliminary structural and functional studies of “*histone-like*” proteins. H1, B1<sup>[22]</sup>, *bglY*, H1a<sup>[23]</sup>, 16K, *osmZ*, *drdX*, *virR*, *cur*, and *pilG* all correspond to the gene *hns*. Any confusion regarding the name of this gene and its product was resolved in the early 90s, and *hns*/H-NS, with a few unfortunate exceptions, has been used almost exclusively since that time<sup>[24]</sup>. One of the similarities between H-NS and eukaryotic histones is the ability to compact and increase the thermal stability of the DNA. The difference is that HNS is not homologous to histone subunits and the manner it interacts with DNA.

---

<sup>1</sup>In this thesis most of the concentrations of the proteins are mention in nM or  $\mu\text{M}$  unit, because it is easy to compare with others literature work.

<sup>2</sup>stationary phase protein

H-NS is the most abundant protein present in cells (20,000 copies in the logarithmic phase, and 8,000 copies in the stationary phase). H-NS binds to DNA non-specifically; however, it shows higher binding affinity to intrinsic curve regions –that is, AT-rich regions<sup>[25,26]</sup>. The main function of H-NS is structuring DNA as well as the transcriptional regulator with predominant repressing functions<sup>[27,28,29]</sup>. This protein also influences cellular processes, such as adaptation to altered growth or stress conditions, regulation of bacterial virulence, DNA compaction, and silencing. Most interestingly, H-NS was also recently identified in the defence against foreign DNA<sup>[30,31]</sup>. In 1977, Varshavsky first described H-NS as a major component of the bacterial nucleoid<sup>[22]</sup>, a highly conserved structure and function in Gram-negative bacteria<sup>[32]</sup>. H-NS has a molecular weight of 15.6 kDa (137 amino acids). In wild-type cells, H-NS is found in three isoforms with different *pI* values. Experimentally, it was found that the predominant two forms have neutral *pI* at *pH* 7.5<sup>[23]</sup>, but the *pI* calculated from the amino-acid sequence is 5.1. H-NS is a global regulator of the bacterial cell, which together with other members of the NAPs contributes to the efficient adaptation of bacteria to different environmental conditions. Despite numerous investigations to understand the molecular mechanism of DNA binding and oligomerisation of H-NS, still little is known of the exact details of these interactions.

H-NS has two domains – N-terminal and C-terminal domains. The N-terminal causes dimerisation and the C-terminal causes DNA-binding. The complete crystal structure of H-NS is still unknown. However, 3D information has been derived from NMR data of the truncated N-terminal (1-64) and C-terminal (80-136) domains<sup>[33,34,35,36]</sup>. The independently folded

domains are connected by an unstructured flexible linker, which probably hinders the crystallisation of the native protein. It has been reported that the flexible linker may also participate in oligomerisation of H-NS. A truncated H-NS protein from *E. coli*, comprising only the first 46 N-terminal amino acid residues, has been described as the smallest H-NS derivative to dimerise, but incapable of forming higher oligomers<sup>[36]</sup>. Generally, mutations in the C-terminal domain can affect DNA binding, and mutations in the N-terminal domain affect the dimerisation (or oligomerisation) of H-NS. Since dimerisation (or oligomerisation) is an important prerequisite for DNA-binding, interpretations from binding studies with H-NS mutants are notoriously difficult.

H-NS acts as a global regulator, controlling the expression of more than 200 genes, most of which are related to environmental responses<sup>[37]</sup>. H-NS not only makes contact with itself, forming homo-dimers or higher oligomers, but is also known to undergo heteromeric contacts with a variety of other proteins. For example, the heterodimeric forms with StpA or other H-NS homologs, which share the dimerisation domain with H-NS<sup>[38]</sup>. Heteromeric contacts are also formed with more distantly related proteins, such as Hfq<sup>[39]</sup>, the phage T7 gene product 5.5<sup>[40]</sup>, FliG<sup>[41]</sup>, and Hha<sup>[42]</sup>. All such combinations of regulatory proteins may furnish the cell with a battery of regulatory tools, providing specificity and tuning mechanisms. This may be of special importance for adaptation reactions under rapidly changing environmental conditions, and is consistent with the involvement of H-NS in the modulation of bacterial gene expression in response to temperature and osmolarity<sup>[37,42,43]</sup>.

Two mechanisms are proposed for the H-NS inhibitory effect on gene expression by different groups. First, electron microscopy studies of DNA-HNS *in vitro* show that H-NS alters the DNA topology by coating along the DNA<sup>[44]</sup>, later confirmed by an elasticity measurement of the DNA-H-NS complex with magnetic tweezers by Amit et al. in 2003. It was shown that H-NS coats along the DNA and results in a large persistence length, and that the H-NS-DNA complex is sensitive to temperature and osmolarity<sup>[26,45]</sup>. This type of coating prevents the coated segment from being transcribed<sup>[46]</sup>. In the second mechanism, atomic force microscopy (AFM) studies by Dame et al. in 2000 discovered that H-NS bridges two distant segments of DNA<sup>[47,48]</sup>. Similar results have also been observed with microscopy studies by Woldringh et.al<sup>[49]</sup> and Spassky et al.<sup>[23]</sup>, Spurio et al.<sup>[50]</sup>, Stavans et al.<sup>[12]</sup>. This bridging traps the RNA polymerase and stops gene transcription<sup>[51]</sup>. Two hypotheses, that is, the formation of filaments and the formation of bridges are controversial. One stiffens DNA and the other compacts DNA. In 2005, Zhang et al. reported that bacteria such as *B. subtilis* does not have H-NS, but protein such as DnaB takes up this type of compaction by bridge distal segments on DNA<sup>[52]</sup>. From this study and the two hypotheses, it is clear that bridging needs coating. Finally, Liu et al.<sup>[53]</sup> in 2010 reported filamentation and bridging modes in a single experiment using magnetic tweezers. They concluded that these two modes are switchable by divalent cations such as magnesium and calcium.

### 1.1.3.2 HU

Histone-like protein from strain U93 is also known as *heat-unstable* nucleoid protein (*HU*). In *E. coli* HU is the most abundant protein. In the logarithmic phase there are 30,000 to 55,000 copies of HU and 15,000 in the stationary phase<sup>[54]</sup>. In the logarithmic phase there is one HU dimer per 190 bp of *E. coli* genome<sup>[55]</sup>. HU exists as a dimer with molecular weight  $\sim 18.5$  kDa with *pI* 9.5. In most bacteria, HU exists in homodimer form as  $HU_{\alpha\alpha}$  and  $HU_{\beta\beta}$ . In the enteric bacterium *E. coli* however, it exists as a heterodimer of  $HU_{\alpha}$  and  $HU_{\beta}$ , with each subunit being 9.5 kDa in size, encoded by the homologous *hupA* and *hupB* genes. All forms of HU have different binding properties<sup>[56,57,58]</sup>. HU exhibits sequence and structural homology with the IHF (integration host factor) protein. The HU subunits have 70% homology with each other and 30% homology with IHF. The first high-resolution structure derived from *B. stearothermophilus* depicts a dimeric molecule with two flexible basic arms, which fit into the minor groove of DNA<sup>[59]</sup>. HU binds sequence non-specifically to the DNA and induces bending<sup>[60]</sup>. The binding of HU to the minor groove of DNA causes two sharp kinks at a separation space of 9 bp by the insertion of prolines, which are located at the end of beta ribbons<sup>[61,61,62,63]</sup>. In the case of IHF, the intercalation of proline residues introduces and stabilises two kinks in the DNA. In recent binding studies, it was shown by FRET analysis that the interaction of HU with a 34 bp DNA fragment caused an almost 143° bending angle of the DNA<sup>[64]</sup>. This result is fully consistent with the resolved structure of co-crystals of *Anabaena*-HU and DNA. Beta ribbons reside on the minor groove of DNA, and beta ribbons of HU are very flex-

ible in solutions<sup>[65,66]</sup>. The bending of DNA by HU needs protein–protein interactions between the adjacent HU dimers<sup>[67,68]</sup>, but recent studies show that a single HU dimer is sufficient for bending<sup>[69]</sup>. HU is also able to form rigid nucleoprotein filaments at higher HU concentrations indicating the existence of two different HU-DNA nucleoprotein complexes; these filaments are arranged helically around the DNA<sup>[70,71]</sup>. HU plays an important architectural role in all kinds of DNA transactions, including replication<sup>[54]</sup>, transcription<sup>[72]</sup> regulation<sup>[73,74]</sup>, and reparation<sup>[75]</sup>. HU with other regulators often facilitates or even enables the formation of active DNA conformations through the formation of higher-ordered DNA-protein complexes. This type of complex structures often involves DNA loops— for example, in the case of gal-operon, HU binds within the inter operator region of the gal-operon, facilitating the interaction of two bound GalR dimers, which lead to a looped structure inadequate for transcription; these dimers are therefore called repressosome<sup>[76]</sup>. Another similar role for HU has also been described for the site-specific DNA inversion by the Hin recombinase. Here, the Hin dependent assembly of the invertasome is facilitated by HU, which enables the necessary DNA looping<sup>[77]</sup>.

The bending caused by a single HU at random positions would change the apparent flexibility. At a low HU concentration ( $\leq 50$  nM), the HU-DNA complex is more flexible (compacted by 50%) and at a relatively high HU concentration the HU-DNA complex is less flexible (leading to filamentation)<sup>[67,71]</sup>. Recent studies in 2010, with magnetic tweezers, reported that the bimodal binding (compaction and stiffening) behaviour is sensitive to the environmental salt conditions<sup>[78]</sup>. Bimodal was observed only for  $\leq 100$  mM, and compaction mode was observed for  $\geq 150$  mM of NaCl.

### 1.1.3.3. Other nucleoid associated proteins

---

In 2013, Kundukad et al. reported that the persistence and contour length of the HU-DNA complex depends on the incubation time<sup>[79]</sup>. The increase in bending flexibility and an increase in contour length was explained in terms of a decrease in the helical pitch of the duplex. Using single-molecule unzipping force analysis, Dame (2013) showed that individual bound HU proteins have no effect on the DNA helical stability, but HU protein bound to side-by-side within a filament increases DNA helical stability<sup>[80]</sup>.

### 1.1.3.3 Other nucleoid associated proteins

**IHF (*Integration Host Factor*)** has homology with HU. It is also one of the most abundant proteins, with  $\sim 6,000$  copies per cell in the logarithmic phase and 30,000 in the stationary phase (almost 5–6 times increment). IHF has a molecular weight of 22 kDa and exists as heterodimers with subunits having 30% homology. Unlike HU, IHF binds to the DNA sequence specifically, and DNA is wrapped around the protein body, indicating a bend of  $\geq 160^\circ$ <sup>[61,81]</sup>. This bending occurs at two large kinks by intercalation of hydrophobic proline residues on arms of  $\beta$  ribbons into the minor groove of DNA. IHF contacts the DNA exclusively via the phosphodiester backbone and the minor groove, and relies heavily on indirect readouts to recognise its binding sequence. One such readout involves a six-base pair tract, providing evidence for the importance of a narrow minor groove. The non-specific nature of IHF promotes the DNA compaction<sup>[82]</sup>. A hypothesis based on the increase of concentration of IHF in the stationary phase may help with introducing bends on DNA, which gives more compaction conformation; these compactions are stabilised by other NAPs such

### 1.1.3.3. Other nucleoid associated proteins

---

as Dps<sup>[19]</sup>.

**FIS** (*Factor of Inversion Stimulation*) also has a significant abundance in the logarithmic phase. The number of copies per cell in the logarithmic phase is  $\sim 3,30,000$  and in the stationary phase it is  $<100$ . FIS is a growth-phase-dependent expression. FIS binds to DNA both sequentially and non-sequentially. FIS has two intertwined  $\alpha$  helix subunits forming a helix-turn-helix (HTH) DNA motif that binds to the DNA's major groove. FIS bends the DNA, and the bending angle varies from  $50^\circ$  to  $100^\circ$  depending on the sequence of the binding site<sup>[83]</sup>. At high concentration, FIS binds non-sequentially to DNA<sup>[84]</sup>. In addition, FIS binds to DNA forming clusters and at crossovers and branched points. This type of binding suggests that FIS is important in organising branched plectonemic conformations in the nucleoid; this has been confirmed by AFM studies<sup>[84]</sup>.

Other NAPs such as Dps, Hfq, Lrp, CbpB and StpA all bind to DNA and change its conformation uniquely. Fig. 1.1 shows the different binding modes of NAPs to DNA and its corresponding AFM images. All these NAPs are important in bacterial chromatin compaction, dynamic modulation, and gene expression. NAPs not only affect the supercoiling of DNA, but also DNA transactions such as transcription and replication. Based on the expression levels in logarithmic and stationary phases, they act as environmental sensors. The structural changes of DNA by NAPs are bending, bridging, and wrapping<sup>[85,86]</sup>. All NAPs not only form homo/hetero complexes themselves, but also form complexes with other NAPs. An example is H-NS-StpA and HU-IHF. Some NAPs share the same binding sites of



### 1.1.3.3. Other nucleoid associated proteins

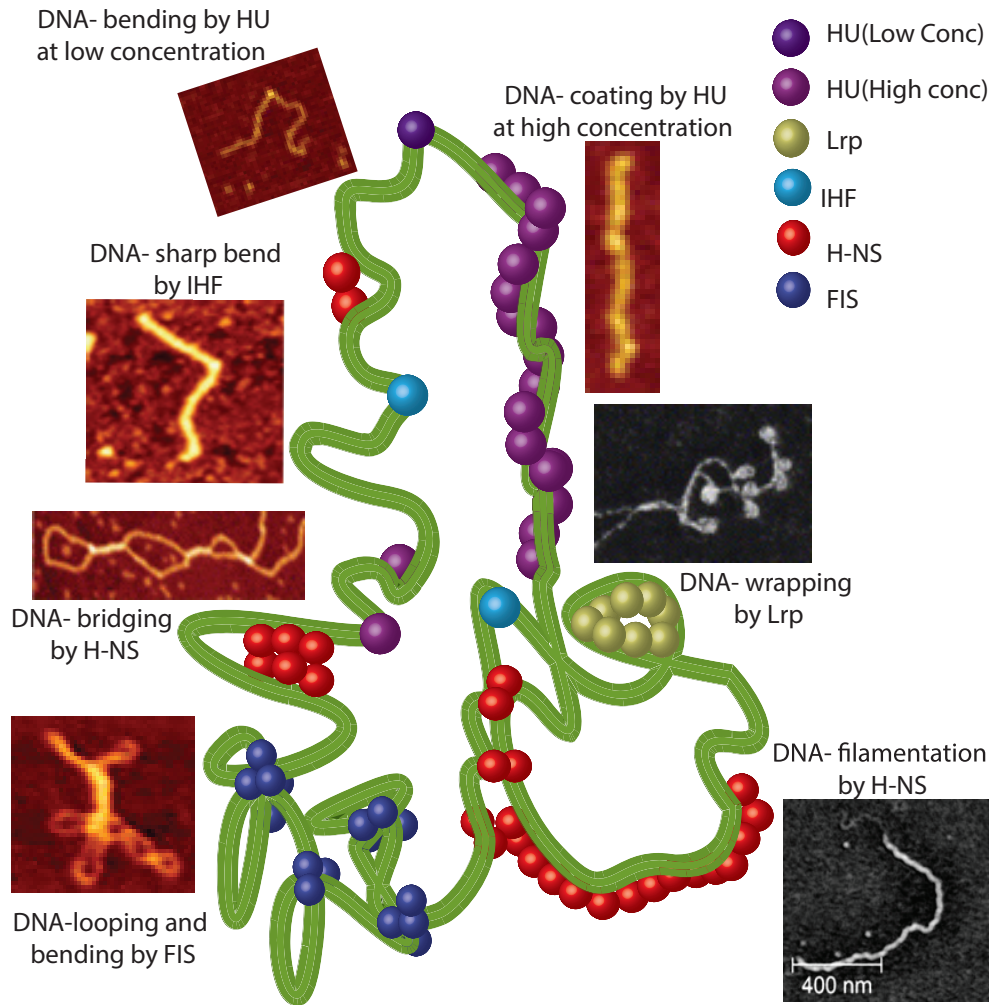


**Fig. 1.1** Conformational changes of DNA by different modes of nucleoid-associated proteins binding. For each DNA-NAP conformation, a schematic drawing and a corresponding AFM image is shown. Different effects of NAP binding on the target DNA are displayed: DNA-bending (at low [HU]), DNA-coating (at high [HU])<sup>[71]</sup>, DNA-wrapping (Lrp)<sup>[85]</sup>, DNA-filamentation (H-NS)<sup>[53]</sup>, plectonemic loop (FIS)<sup>[84]</sup>, DNA-bridging (H-NS)<sup>[47]</sup> and sharp DNA bends (IHF).<sup>[24]</sup> All cartoons are for illustrative purposes only. The exact mechanism of the NAPs binding to DNA and their interactions are completely unknown.

### **1.1.3.3. Other nucleoid associated proteins**

---

DNA, resulting in an antagonistic function, and also affecting the expression of other NAPs. All these effects together coordinate the regulation of a large number of different genes. The importance of NAPs as global regulators of the bacterial cell has become more and more evident.

In summary, NAPs play important roles in small-scale chromosome organisation, whereas in supercoiling, macromolecular crowding and segregation play important role in large-scale chromosome organisation.

## 1.2 DNA as a polymer

In the previous section, the organisation of genomic DNA in bacteria from a biological point of view was described. In this present section the physics of DNA as polymer is discussed. The basic definition of a polymer is the repeating of units (same or different, but all resembling units) to form a big molecule. The repeating unit is called a monomer. DNA is considered as a linear polymer chain with four bases as monomers. The four bases are Adenine (A), Cytosine (C), Guanine (G), and Thymine (T). The distance between the ends along the contour is called **contour length**  $L$ . This section briefly describes the three models of polymer in solutions. Each model predicts the relationship between equilibrium **polymer size** ( $R$ ) and contour length ( $L$ ) of the polymer.

### 1.2.1 Ideal chain

This is a simple model. In this model ( $N+1$ ) monomers with centre of mass position vectors  $\vec{R}_i$  are connected by a vector  $\vec{l}_i = \vec{R}_i - \vec{R}_{i-1}$ . Where  $|\vec{l}_i| = l$  is segmental length. The orientation of a specific segment is uncorrelated with that of the other segments. Furthermore, there are no interactions between segments, that are not directly linked with each other (no long-range excluded volume interactions). So the contour length  $L = N|\vec{l}_i|$ . Let  $\vec{h}$  be the vector between the first and last monomer (with index 0 and  $N$  respectively). The first moment of the end-to-end vector is (which gives the anisotropy of the molecule) zero, because there is no correlation between the bonds of the polymer. The second moment gives some indication of

### 1.2.1. Ideal chain

the average dimension of the polymer. The mean square end-to-end point distance is given as

$$\begin{aligned}
 \langle h^2 \rangle &= \langle \vec{h} \cdot \vec{h} \rangle = \left\langle \left( \sum_{j=1}^N \vec{l}_j \right) \cdot \left( \sum_{i=1}^N \vec{l}_i \right) \right\rangle = \sum_{i=1}^N \langle \vec{l}_i \cdot \vec{l}_i \rangle + 2 \sum_{i=1}^{N-1} \sum_{\substack{j=2 \\ i < j}}^N \langle \vec{l}_i \cdot \vec{l}_j \rangle \\
 &= Nl^2 + 2l^2 \sum_{i=1}^{N-1} \sum_{\substack{j=2 \\ i < j}}^N \langle \cos \theta_{ij} \rangle
 \end{aligned} \tag{1.1}$$

Where  $\theta_{ij}$  is the angle between  $i^{\text{th}}$  and  $j^{\text{th}}$  position vectors and the second term in Eq. (1.1) above is zero, because there is no correlation between the steps. So the mean square end-to-end distance and typical radius are given as

$$\langle h^2 \rangle = Nl^2 \tag{1.2}$$

$$R \simeq \langle h^2 \rangle^{1/2} \simeq N^{1/2}l = \sqrt{N}l \tag{1.3}$$

Note that the dependence on  $N$  (number of segments, and also related to molecular weight) and  $l$  (segment length) in Eq. (1.2) is the same as for a random walk with  $n$  steps having step size  $l$ . The second moment of the mass distribution, called the radius of gyration is given as

$$\langle R_g^2 \rangle = \frac{1}{N^2} \sum_{i=1}^{N-1} \sum_{\substack{j=2 \\ i < j}}^N \langle h_{ij}^2 \rangle = \frac{1}{6} Nl^2 \tag{1.4}$$

### 1.2.1. Ideal chain

If the orientation correlation between segments that are not too far separated from each other along the contour is considered, the chain is called a **Kuhn chain**. This model has two assumptions: (1) *the short range orientation correlations* between the segments separated by  $s$  were lost, that is  $\langle \cos \theta_{ij} \rangle = 0$  for  $j - i > s$ ; (2) *The chain is homogeneous and the end effects are neglected*. Under these two assumptions Eq. (1.1) becomes

$$\langle h^2 \rangle = Nl^2 + 2l^2 \sum_{j=2}^s \langle \cos \theta_{1j} \rangle \quad (1.5)$$

$$= Nl^2 \sigma_k \quad (1.6)$$

Where  $\sigma_k = 1 + 2 \sum_{j=2}^s \langle \cos \theta_{1j} \rangle$ , it is convenient to rescale the chain in terms of Kuhn segments  $N_k = N/\sigma_k$  and Kuhn length  $l_k = l\sigma_k$  such that the end-to-end distance can be written as  $\langle h^2 \rangle = Nl^2$  for any polymer. Note that the contour length of the polymer is constant  $L = Nl = N_k l_k$ , such that

$$\langle h^2 \rangle = Nl^2 = N_k l_k^2 \quad (1.7)$$

Thus, one can eliminate the short-range interaction by renormalising the Kuhn length. The entropy and free energy for the model (Ideal or Kuhn) are given by

$$S = S_0 - k_B \frac{3h^2}{2Nl^2} \quad (1.8)$$

$$F_{elas} = F_0 + k_B T \frac{3h^2}{2Nl^2} \quad (1.9)$$

## 1.2.2 Worm-like chain model

In ideal and Kuhn chain models there is no restriction on the orientations between the monomers, but in a real polymer chain the directions available for the contour are limited. Interaction between the monomers of the polymer leads to bending energy that makes some bending angles unfavourable or even impossible. Polymers such as DNA are modelled as thin, elastic filament obeying Hooke's elasticity law under small deformations. Such a model is called a **Kratky-Porod**, or **Persistence**, or **Worm-like chain** model. In this model, correlation between the tangent vectors, which are along the contour, decays exponentially because the polymer is randomly oriented.

$$\langle \cos \theta(s) \rangle = \exp\left(-\frac{|s|}{L_p}\right) \quad (1.10)$$

Where  $\theta$  is the angle between the tangent vectors separated at a distance  $s$  along the contour and  $L_p$  is the *persistence length*. The persistence length is the typical length scale over which the orientation correlation is lost – that is the distance along which contours change its direction. In continuous approximation, the end-to-end distance can be calculated as

$$\langle \vec{h} \rangle = \int_s^L l(\vec{s}) ds \quad (1.11)$$

### 1.2.2. Worm-like chain model

---

And the mean square end to end distance is given by

$$\langle h^2 \rangle = \int_S^L ds \int_0^L ds' \langle l(\vec{s}) \cdot l(\vec{s}') \rangle \quad (1.12)$$

$$= 2L_p^2 \left( \frac{L}{L_p} - 1 + \exp\left(-\frac{L}{L_p}\right) \right) \quad (1.13)$$

In two limiting cases  $L \ll L_p$  (rod) and  $L \gg L_p$  (coil), the Worm-like model gives

$$\begin{aligned} \langle h^2 \rangle &= L^2 & L \ll L_p \quad (\text{rod}) \\ \langle h^2 \rangle &= 2LL_p & L \gg L_p \quad (\text{coil}) \\ \langle R_g^2 \rangle &= \frac{1}{12}L^2 & L \ll L_p \quad (\text{rod}) \\ \langle R_g^2 \rangle &= \frac{1}{3}LL_p & L \gg L_p \quad (\text{coil}) \end{aligned} \quad (1.14)$$

Comparing the above equation with the Kuhn chain Eq. (1.2),  $\langle h^2 \rangle = LL_k$ , it follows  $l_k = 2L_p$  for coil type conformation. By definition, there is no orientation correlation between Kuhn segments, and thus the orientation correlation is lost over a distance of twice the persistence length.

Ideal, Kuhn and Worm-like chain models predict the size of the coil scales with the square root of the contour length (*i.e.*  $R = \sqrt{Ll}$  as in Eq. (1.3)). Orientation correlations have no effect at a large distance scale, but at a local distance scale results in an increase in step length and decrease in local flexibility of the chain. These models ignore the interaction between the segments, which are separated over large distances along the contour but close spatially due to the coiling of the chain.

### 1.2.3 Excluded volume interactions

Previous models consider the equilibrium conformations of the polymer that can pass through itself. Since the chain has a finite volume, no two monomers can occupy the same space. This will affect the characteristic size of the coil and is taken into account with excluded volume parameter  $\nu$  (Flory exponent); this effect is called the **excluded volume effect**. The coil swells if the interaction between monomers and solvent is favoured (called the positive excluded volume, and the solvent is “*good*”). When the interaction between monomers is favoured, then the coil shrinks (called the negative excluded volume, and the solvent is “*poor*”). In this discussion only good solvent is considered. The buffers used in our experiments are good solvents for DNA. The excluded volume effect was first discussed by Kuhn<sup>[87,88]</sup> and later developed by Flory<sup>[89,90]</sup>. Flory borrowed ideas from a model of non-ideal gases to describe the behaviour of a self-avoiding chain. If there are  $N$  particles in a coil of size  $R$ , then the concentration of the particle in the coil is  $c \sim N/R^3$ . The repulsive energy per volume is proportional to the density of the contact pairs. *i.e.*  $C^2$ . According to the equipartition theorem, each degree of freedom contributes  $1/2 k_B T$  to the free energy. The final free energy from repulsion is given by

$$F_{rep,coil}(R) \simeq k_B T \frac{BN^2}{R^3} \quad (1.15)$$

Where  $B$  is the excluded volume parameter and has a dimension of volume. As  $R$  is large, free energy decreases, and the chain swells. The swelling is counter balanced by the elastic force due to the restriction in



### 1.2.3. Excluded interactions

---

configurational degree of freedom of the monomer with increasing radius. The free energy from elasticity of the chain is given by Eq. 1.9. The equilibrium size of the chain can be derived from the minimisation of total free energy ( $F_{rep,coil} + F_{elast,coil}$ ) with respect to  $R$ . The Flory radius of the chain is given by

$$R_F \simeq (B/l^3)^{1/5} l N^{3/5} \quad (1.16)$$

By considering the excluded volume interaction, the above equation changes the scaling of the equilibrium size of the coil with molecular weight. In general, the characteristic size of a polymer chain scales with the number of links according to a power law

$$R_F \simeq l N^\nu \quad (1.17)$$

Where  $\nu$  is called the *Flory* scaling component. By self-avoiding random walk, the value of  $\nu$  is obtained as  $\sim 3/(d + 2)$ , where  $d \leq 4$  is dimensionality of the system. Calculations using the multi-body statistical method shows that the value of the Flory exponent for the dependence of radius on size ( $N$ ) is  $\nu = 0.589$ , which is, remarkably around  $3/5$ .

## 1.2.4 Physics of DNA in confinement

Previous section is about polymers in a solution (considered to be free space), and does not deal with the confinement. It is difficult to identify the random coil conformations experimentally. Because of thermal fluctuations, the coil quickly rearranges its conformations. To track the position of segments along the DNA contour there needs to be a one-to-one correspondence between space and position in the DNA sequence. For this correspondence to establish, the polymer must be confined in narrow channels with walls that impermeable to polymer. The following section, describes how polymer size is changed by the confinement width ( $D$ ). There are two major theories to describe the effect of confinement on the polymer. First, if the size of the confinement is larger than the persistence length ( $R_F \gg D \gg L_p$ ), the *de Gennes blob theory* will be considered. Second, if the confinement is less than the persistence length ( $D \ll L_p$ ), *Odijk's theory* will be considered.

### 1.2.4.1 De Gennes's blob theory

In this theory, a polymer chain is confined in a tube with diameter  $D$  ( $R_g \gg D \gg L_p$ ). The interaction between the monomers and walls of the confinement tube is ignored. Within the length scale on the order of the diameter of the tube  $D$ , the monomers are unaffected by the confinement, and they behave as if the tube does not exist. In the case of rectangular cross-section confinement by  $D_1$  and  $D_2$ , the channel diameter is replaced by  $D_{av} = \sqrt{D_1 D_2}$ . The domain  $D$ , commonly know as *blobs*, in which the chain is unperturbed and monomers feel no confinement. Let there be  $g$

#### 1.2.4. De Gennes's blob theory

---

links inside each blob ( $g < N$ ) of diameter  $D$ . The chain inside the blob has no confinement and follows the Flory theory (Eq. 1.17), which gives

$$D \simeq lg^\nu \tag{1.18}$$

The extension of the chain in the longitudinal direction ( $R_{parallel}$ ) induced by the confinement is given by

$$R_{parallel} = (N/g)D \simeq Nl(D/l)^{(\nu-1)/\nu} \tag{1.19}$$

As explained above in section 1.2.3 (Excluded volume interactions), the chain inside the blob is swollen and the Flory exponent  $\nu$  is  $3/5$ ; the longitudinal extension is given by

$$R_{parallel} \simeq \frac{L}{(D/l)^{2/3}}$$

or

$$R_{parallel} \simeq \frac{(w_{eff}L_p)^{1/3}}{D^{2/3}} \tag{1.20}$$

where  $w_{eff}$  is the effective width of the polymer, by considering the excluded volume effect and surrounding buffer effect. The longitudinal extension increases with the length of the polymer and decreases with the increase in diameter of the confinement as  $D^{-2/3}$ . The ionic strength of the surrounding buffer affects the effective width of the DNA and persistence length. The quantity  $(w_{eff}L_p)^{1/3}$  describes the effect of ionic strength on extension<sup>[91]</sup>. The polymer inside the confinement fluctuates because of

### 1.2.4. Odijk theory

---

thermal energy, and the mean squared average thermal fluctuation is described by the following equation; fluctuations are close to Gaussian<sup>[92]</sup>:

$$\langle \delta R_{parallel}^2 \rangle = (L_p W_{eff} D)^{1/3} L \quad (1.21)$$

The free energy of the polymer in this type of confinement is given by

$$F_{conf} \simeq kTN(L/D)^{5/3}; \quad D \gg L_p \quad (1.22)$$

De Gennes's blob theory describes only the statistics of the chain inside the confinement of  $D \gg L_p$ . The next section describes the polymer in a more confined region, in which the confined dimension is much smaller than the persistence length.

#### 1.2.4.2 Odijk theory

In smaller confinement  $D \ll L_p$ , the nature of confinement changes the conformation of the polymer compared with the de Gennes model, and thus a new theory is required. In this regime  $D \ll L_p$ , the excluded volume effects are negligible and the polymer (DNA) no longer forms coils in the confined region due to the fact that there is now much smaller space available. The polymer will undulate inside the channel and only bend when it bounces off the wall. It was first described in detail by *Odijk*<sup>[93]</sup>.

Following Odijk, a new length scale  $\lambda$  (deflection length) and  $\theta$  (deflection angle) appears to model the polymer dynamics as *aworm-like chain* in the confined ( $D \ll L_p$ ) regime. The deflection length and deflection angle are given by

$$\lambda = D^{2/3}L_P^{1/3} \tag{1.23}$$

$$\langle \theta^2 \rangle = 2\lambda/L_p \simeq (D/L)^2$$

The relative extension is  $R_{\parallel}/L \simeq (1 - (1/2)(D/L_p)^{2/3})$ . And the relative decrease in length with respect to the fully stretched configuration is  $\simeq (D/L_p)^{2/3}$ . With the increase in confinement diameter and decrease in persistence length, the polymer becomes more wrinkled inside the tube. The free energy (entropic origin) in the Odijk model is given as

$$F_{conf} \simeq LkT(D^2L_P)^{-1/3} \tag{1.24}$$

It results from fluctuations of the worm-like chain about the classical path induced by deflections from the wall.

Fig. 1.2 illustrates conformations of the chain in the de Gennes and Odijk regimes. The transition region between the two regimes is still unclear, and many researchers have attempted to bridge the gap. One way is to modify the de Gennes blob theory, in such a way that it extends to a more confined region. In this approach, the blob size is reduced, resulting in the volume interaction energy per blob becoming less than thermal energy ( $k_B T$ ), maintaining the same chain statistics within the blob<sup>[94]</sup>. The other approach is to modify the Odijk theory, in such a way that it extends to a less confined region. In this approach, the chain performs a one-dimensional walk through the formation of back-folded hairpin conformations<sup>[95]</sup>. This theory was found to have a huge discrepancy based on the simulation results of Wang et al. (2011). In 2012, Dai et al. reported

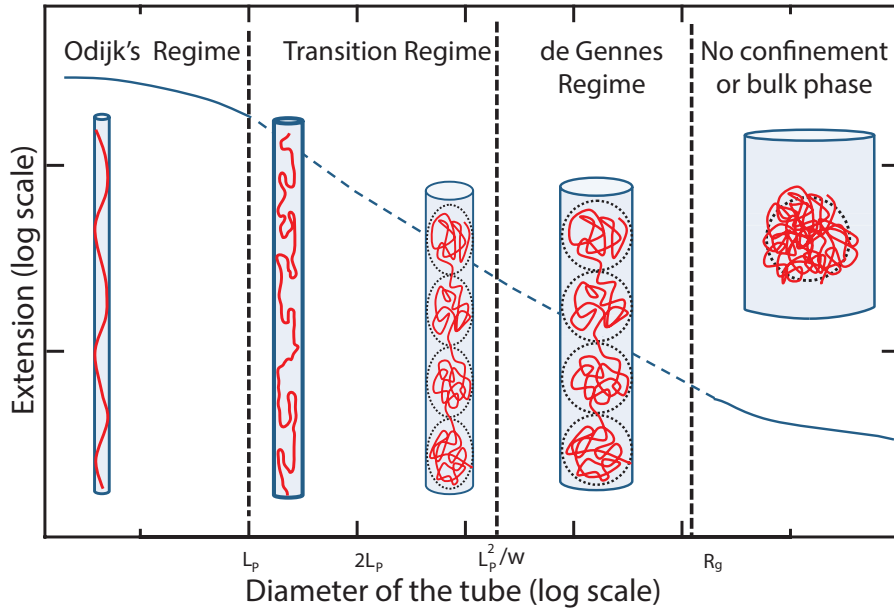


**Fig. 1.2** Schematic diagram of different confinement regimes. Relative extension curve as a function of channel diameter. Cartoons showing conformations in different regimes. Odijk regime  $D \ll L_p$  the polymer undulate inside the channel. In de Gennes regime ( $L_p \ll D \ll R_g$ ), the polymer exists as isometric blobs (shown as dashed circles) with diameter slightly less than the confinement diameter. The chain inside the blobs follows Flory excluded volume interactions and feels no confinement. In no confinement (bulk phase) regime the chain has Flory radius. The region in between Odijk and de Gennes is showed as transition regime. All cartoons are for illustrative purposes only.

a model for back-folding and looping of DNA confined inside a nanochannel. Back-folded hairpin conformations in the undulating Worm-like chain result in the formation of loops, which reduces the stretch of the molecule in the longitudinal direction of the channel. These predictions are in good agreement with the Monte Carlo simulations<sup>[96]</sup>.

### 1.2.5 DNA in Nanochannel experiments

In the early stage of DNA analysis, Gel electrophoresis was one of the techniques used to separate the DNA, because mobility of the DNA depends on the DNA size. Carlos Bustamante was the first person to use gels to image single extended DNA<sup>[97]</sup>. Later, Austin took up this idea and used nanofabrication of post-arrays to stimulate gel and elongate the DNA<sup>[98]</sup>. This elongation is greater than the DNA length of previous gel electrophoresis<sup>[99]</sup>. First a high-resolution image of extended DNA was reported by Bakajin et al. in a slit-like configuration<sup>[100]</sup>. In 2004 Guo et al. used nanofluidics via nano-imprinting techniques to extend the DNA<sup>[101]</sup>. The equilibrium extension of an individual DNA was observed to increase with decreasing channel size. However, no comparison was made between extension results and existing theories. In the same year, Tegenfeldt et al. systematically studied the extension of  $\lambda$ -DNA in 100 nm channels<sup>[92]</sup>. In this experiment, the extension of DNA scales linearly with the contour length and was well predicted by the de Gennes blob theory (Eq. 1.20).

Reisner et al. used nano channels ranging from 30 to 400 nm to extend the DNA ( $\lambda$ , and T2-DNA), and checked the validity of the theory. Interestingly, the crossover scale  $D_{critical}$  is roughly twice the persistence length that determines the degree of confinement at which bending rigidity becomes significant<sup>[102]</sup>. The DNA extension results were in good agreement with the prediction of the theory for  $D_{tube} \ll 2L_p$ . The extension for the widths greater than the crossover scale is consistent with a power law of the form  $D^{-0.85}$ . However, the value of the exponent is smaller than the predicted value by the theory (*i.e.*  $D^{-2/3}$ )<sup>[103]</sup>. The effect of ionic strength

## 1.2. DNA in Nanochannel experiments

---

on extension of DNA in confinement was reported by Reisner et al. in 2007<sup>[91]</sup>. The  $\lambda$ -DNA extension is measured in nanochannels having an average diameter of 50, 100, and 200 nm and ionic strength of TBE ranging from 4 to 300 mM. To explain the results, effective DNA width  $w_{eff}$  was introduced and  $(w_{eff}L_p)^{1/3}$  describes the effect of ionic strength on extension of DNA. The relative extension of the DNA as a function of ionic strength in larger channels is in good agreement with scaling theory prediction *i.e*  $R_{parallel} \simeq \frac{(W_{eff}L_p)^{1/3}}{D^{2/3}}$  (Eq. (1.20)). But the extension of DNA in narrow channels of width 50 nm ( $D \ll h, L_p$ ) was not in agreement with the theory prediction. A 50 nm channel is the threshold between the Odijk and de Gennes regimes, and the de Gennes scaling exceeds the measured extension values. Reisner and his colleagues also carried out in another study using the tapered nanochannels to probe the single DNA molecule, as well as the circular charomid DNA<sup>[104]</sup>. It was found that the extension of the circular charomid DNA scales was in accordance with the de Gennes exponent, but not the linear DNA. For the linear DNA, the exponent obtained was still similar to the work previously done<sup>[102]</sup>.

In 2008 Zhang et al. reported the effect of ionic strength on the persistence length. In their study, they used a PDMS-based biochip of depth 300 nm and width 150-300 nm and TBE ionic strength ranging from 0.3 to 35 mM. The equilibrium extension of DNA increases with decreasing ionic strength. The experimental results were interpreted by a modified version of the “blob theory” to account for the effects of the charge for a polymer in a good solvent, and also for finite chain segments within a blob. They concluded that the DNA extension with decreasing ionic strength is mainly caused by the increase of persistence ( $L_p$ ) as the excluded



## 1.2. DNA in Nanochannel experiments

---

volume effect is insignificant due to the relatively small number of statistical segments within each blob<sup>[105]</sup>.

Kim et al. observed that at very low ionic strengths, the DNA ( $\lambda$ -DNA usual length  $21.8\mu\text{m}$ ) extension is almost approaching its contour length ( $19.1\mu\text{m} \pm 1.1\mu\text{m}$ ), even though the DNA is confined in a wider nanochannel of dimension  $250\text{ nm} \times 400\text{ nm}$ . Besides this experiment, they also performed a Monte Carlo simulation using a “primitive DNA model” within a nanochannel. The simulation results were used to evaluate their experimental results as well as the Odijk theory. Overall, they demonstrated reasonable agreements among the experiment, computer simulation, and theory with some limitations<sup>[106]</sup>. Recently, using the same simulation model<sup>[107]</sup>, another analysis of theirs showed that formation of back-folding (hairpins) mostly occurs at both ends within the region of  $\sim 0.5\mu\text{m}$ , but a significant portion of the events still takes place in the middle region. They also claimed that they have observed the transition regime as classified by Wang et al.<sup>[94]</sup>

The effect of dextran nanoparticles on the conformation and compaction of single DNA molecules confined in a nanochannel was investigated with fluorescence microscopy by Zhang et al. in 2009. The DNA molecule elongates and eventually condenses into a compact form with increasing volume fraction of the crowding agent. The elongation is explained in terms of depletion of the DNA segments density nearer to channel walls. The compaction is explained in terms of nanochannels facilitating compaction with the crowding agent at low ionic strength. In 2012, the effects of the like-charge proteins such as bovine serum albumin and hemoglobin on the

## 1.2. DNA in Nanochannel experiments

---

conformation and compaction of single DNA molecules confined in rectangular nanochannels were investigated with fluorescence microscopy<sup>[108]</sup>. The sizes of the nanochannels ranged from 80 to 300 nm. In wider channels, with increasing protein concentration, the DNA molecules were compacted and eventually condensed into a compact form. In narrower channels ( $\sim 80$  nm), no condensation was observed. The threshold concentration for condensation depended on the channel's cross-sectional diameter as well as the ionic strength of the supporting medium. The critical values for full compaction were typically less than one-tenth of a millimolar. In the bulk phase and in the same environmental buffer conditions, no condensation was observed. Anisotropic nano-confinement hence facilitated compaction of DNA by negatively charged protein. They explained this behaviour in terms of enhanced depletion interaction between segments of the DNA molecule due to the orientation order imposed by the channel walls.

The extension of a confined DNA molecule results from a balance between entropy and excluded volume interactions within the DNA. The force from confinement is similar to other techniques like Optical and Magnetic tweezers for force-extension measurement of DNA for sub-100 pico-Newton force<sup>[104]</sup>. A systematic comparison of a polymer in confinement with applied force was done recently by Dai et al.<sup>[109]</sup>. Using Monte Carlo simulation, for a polymer in a good solvent, the effect of tensile force  $f$  on extension in the Pincus regime<sup>1</sup> was similar to the effect of cylindrical confinement in the de Gennes regime after mapping the characteristic length  $kT/f$  to the cylindrical diameter  $D$ . The extended de Gennes regime was

---

<sup>1</sup>In force extension measurements, the force applied to the end of the polymer introduces a characteristic length  $kT/f$  to describe the polymer conformations. Under tension, polymer can be considered as a string of tensile blobs in the Pincus regime.

## 1.2. DNA in Nanochannel experiments

---

analogous to the extended Pincus regime for a polymer under tension, but the scaling of the extension was different. In the extended Pincus regime the scaling followed  $L_{\parallel} = (k_B T/f)^{-1}$ , whereas the scaling in the extended de Gennes regime was  $R_{\parallel} = D^{-2/3}$ .

In conclusion, advancement in nanochannel technology provides a platform for physical and biological applications. From a physics point of view, it provides an experimental study of polymers in different confinements. From a biological point of view, it is capable of doing DNA sequencing, protein-DNA interaction studies *etc.*, similar to nanopore and tweezers experiments. Protein-DNA interaction studies are interesting because the nanoconfinement space is similar to the dimensions of the bacterial chromosomal nucleoid<sup>[110]</sup>.

## **1.3 Research Objectives**

The genome of *Escherichia Coli* bacteria has a  $4.6 \times 10^6$  Mbp with contour length of 1.6 mm, yet it is contained inside the nucleoid of about 1  $\mu\text{m}$  diameter. This linear compaction ( $\sim 1600$ ) and volumetric compaction ( $\sim 350$ ) has been attributed to many factors including supercoiling, nucleoid associated proteins (NAPs), and macromolecular crowding as described in introduction section. Despite being a topic of long standing interest, the exact mechanism is not clear. In particular, the interplay between the above mentioned compaction factors and confinement within a nanospace is not clear. The main aim of this thesis is to investigate the conformational response of DNA with nucleoid associated proteins H-NS and HU under various experimental conditions.

In particular, advances in nanofabrication have made it possible to fabricate quasi one-dimensional channel devices with cross-sectional diameters on the order of tens to hundreds of nanometers. These channels serve as a platform for studying single DNA molecules<sup>[111,112]</sup>. Furthermore, confinement in a nanospace results in significant modification of certain important biophysical phenomena, such as the knotting probability of circular DNA and the effect of macromolecular crowding<sup>[96,108,113,114]</sup>. In particular, it was shown that DNA can be compacted into a condensed form for over-threshold concentrations of dextran or like-charged proteins such as bovine serum albumin and hemoglobin. This thesis extends this idea to Protein–DNA interaction studies in nanospace, in particular nucleoid-associated proteins such as H-NS and HU.

Heat-stable nucleoid-structuring protein (H-NS, 15.6 kDa, *pI* 7.5) is

### 1.3. Research Objectives

---

implicated in transcriptional repression (gene silencing) as well as organisation of the bacterial genome<sup>[115]</sup>. H-NS binds and oligomerises along dsDNA to form a semi-rigid nucleoprotein filament, increases the thermal stability of the duplex, and inhibits transcription<sup>[26,45]</sup>. The histone-like function of H-NS in chromosome organisation is poorly understood. It has been proposed that the compaction into the nucleoid is related to, DNA supercoiling and osmotic stress through macromolecular crowding. Like-charge attraction between distal DNA segments by binding protein (bridging) is also thought to be important<sup>[49]</sup>. Indeed, it has been shown that H-NS reduces the physical extent of circular plasmids through side-by-side binding of opposing segments<sup>[47]</sup>. Divalent ions such as magnesium and calcium have been reported to play a pivotal role in the H-NS mediated bridging of DNA<sup>[53]</sup>. However, H-NS does not behave like a regular condensing multivalent cationic ligand, because it does not compact DNA into a structure with an ordered morphology (condensation) under physiological conditions<sup>[116]</sup>.

In *E. coli*, heat unstable nucleoid structuring protein (HU) is also most abundant protein<sup>[54,55]</sup>. HU exists as a dimer with a molecular weight of  $\sim 18$  kDa and an isoelectric point of  $pI$  9.5. The binding of HU on DNA is sequence unspecific, causes a kink in the duplex, and leads to underwinding of the helix by insertion of two proline residues separated by 9 bp along the contour<sup>[61,117]</sup>. Binding of HU on topologically constrained DNA affects supercoiling through modulation of the helical pitch. At high concentration, HU coats DNA and forms a rigid filament due to protein-protein interaction<sup>[118]</sup>.

The binding of HU on DNA affect the apparent flexibility of the duplex as inferred from the measurement of the persistence length. At low concentration of HU ( $\leq 50$  nM), the HU-DNA complex is more flexible compared to bare DNA because of HU induced bending at random positions along the contour. At high concentration of HU, a relatively stiff nucleo-protein filament is formed with about one HU dimer per every nine base pairs<sup>[67,71]</sup>. The variation in apparent persistence length also depends on the concentration of salt<sup>[78]</sup>. For a salt concentration exceeding 100 mM, the persistence length is rather insensitive to the binding of HU on DNA. The effect of HU on the persistence length, contour length, and supercoiling of DNA was previously observed to depend on the incubation time<sup>[79]</sup>. This time-dependence was rationalized in terms of the formation of a nucleo-protein filament followed by a structural rearrangement of the bound HU on DNA. The rearrangement results in a change in topology of closed circular DNA, an increase in bending flexibility, and an increase in contour length through a decrease in helical pitch of the duplex.

This thesis reports the effect of H-NS and HU in conjunction with confinement inside a nanochannel on the conformation and compaction of DNA. For this purpose, we have done two different, but related series of experiments. In the first series, we focus on equilibrium properties of DNA molecules that have been pre-incubated with protein (H-NS or HU). In the second series, the dynamic, conformational response of DNA molecules immediately following exposure to protein (H-NS) is investigated. Super-resolution fluorescence imaging of H-NS and HU in living *E. coli* cells has shown that it is clustered within the nucleoid with a diameter of a few hundred nanometers<sup>[110]</sup>. This diameter is comparable to the diameters of our

channel systems. Accordingly, we surmise that our results for nanochannel confined DNA have implications for gene silencing and chromosome organisation.

## 1.4 Bibliography

- [1] Dahm, R. (2008) Hum. Genet. **122**, 565–581. 1
- [2] Downie, A. (1972) J. Gen. Microbiol. **73**, 1–11. 1
- [3] Avery, O., MacLeod, C., & McCarty, M. (1944) J. Exp. Med. **79**, 137–158. 1
- [4] Watson, J. D. (2011) The double helix: A personal account of the discovery of the structure of DNA (Scribner). 2
- [5] Bates, A. D. & Maxwell, A. (2005) DNA topology (Oxford university press). 2
- [6] Holmes, V. F. & Cozzarelli, N. R. (2000) Proc. Natl. Acad. Sci. U.S.A. **97**, 1322–1324. 3
- [7] Ellis, R. J. (2001) Trends Biochem. Sci. **26**, 597–604. 4
- [8] Zimmerman, S. B. & Minton, A. P. (1993) Ann. Rev. Biophys. Biomol. Struct. **22**, 27–65. 4
- [9] Sear", R. (1998) Phys. Rev. E **58**, 724–728. 4
- [10] Robinow, C. & Kellenberger, E. (1994) Microbiol. Rev. **58**, 211. 4
- [11] Zimmerman, S. B. (2006) J. Struct. Biol. **153**, 160–175. 4

- [12] Stavans, J. & Oppenheim, A. (2006) Phys. Biol. **3**, R1. 4, 9
- [13] Egan, E., Fogel, M., & Waldor, M. (2005) Mol. MicroBiol. **56**, 1129–1138. 4
- [14] Wang, J. C. (1985) Annu. Rev. Biochem. **54**, 665–697. 5
- [15] Higgins, N. P. & Vologodskii, A. (2004) Topological behavior of plasmid DNA (Washington, DC: American Society for Microbiology Press). 5
- [16] Zechiedrich, E. L., Khodursky, A. B., & Cozzarelli, N. R. (1997) Gene. Dev **11**, 2580–2592. 5
- [17] Azam, T. A. & Ishihama, A. (1999) J. Biol. Chem. **274**, 33105–33113. 6
- [18] Ishihama, A. (2009) EcoSal–Escherichia coli and Salmonella: Cellular and Molecular Biology . 6
- [19] Kim, J., Yoshimura, S. H., Hizume, K., Ohniwa, R. L., Ishihama, A., & Takeyasu, K. (2004) Nucleic Acids Res. **32**, 1982–1992. 6, 13
- [20] Jacquet, M., Cukier-Kahn, R., Pla, J., & Gros, F. (1971) Biochem. Bioph. Res. Co. **45**, 1597–1607. 6
- [21] Cukier-Kahn, R., Jacquet, M., & Gros, F. (1972) Proc. Natl. Acad. Sci. U.S.A. **69**, 3643–3647. 6
- [22] Varshavsky, A., Nedospasov, S., Bakayev, V., Bakayeva, T., & Georgiev, G. (1977) Nucleic Acids Res. **4**, 2725–2746. 6, 7
- [23] Spassky, A., Rimsky, S., Garreau, H., & Buc, H. (1984) Nucleic Acids Res. **12**, 5321–5340. 6, 7, 9



- [24] Dame, R. R. T. & Dorman, C. J. (2010) Bacterial chromatin (Springer). 6, 14
- [25] Rimsky, S., Zuber, F., Buckle, M., & Buc, H. (2001) Mol. MicroBiol. **42**, 1311–1323. 7
- [26] Bouffartigues, E., Buckle, M., Badaut, C., Travers, A., & Rimsky, S. (2007) Nat. Struct. Mol. Biol. **14**, 441–448. 7, 9, 34
- [27] Schröder, O.oder, O. & Wagner, R. (2002) Biol. Chem. **383**, 945–960. 7
- [28] Rimsky, S. (2004) Curr. Opin. Microbiol. **7**, 109–114. 7
- [29] Fang, F. C. & Rimsky, S. (2008) Curr. Opin. Microbiol. **11**, 113–120. 7
- [30] Lucchini, S., Rowley, G., Goldberg, M. D., Hurd, D., Harrison, M., & Hinton, J. C. (2006) PLoS Pathog. **2**, e81. 7
- [31] Navarre, W. W., McClelland, M., Libby, S. J., & Fang, F. C. (2007) Gene. Dev. **21**, 1456–1471. 7
- [32] Bertin, P., Benhabiles, N., Krin, E., Laurent-Winter, C., Tendeng, C., Turlin, E., Thomas, A., Danchin, A., & Brasseur, R. (1999) Mol. MicroBiol. **31**, 319–329. 7
- [33] Shindo, H., Iwaki, T., Ieda, R., Kurumizaka, H., Ueguchi, C., Mizuno, T., Morikawa, S., Nakamura, H., & Kuboniwa, H. (1995) FEBS lett. **360**, 125–131. 7
- [34] Shindo, H., Ohnuki, A., Ginba, H., Katoh, E., Ueguchi, C., Mizuno, T., & Yamazaki, T. (1999) FEBS lett. **455**, 63–69. 7

- [35] Renzoni, D., Esposito, D., Pfuhl, M., Hinton, J. C., Higgins, C. F., Driscoll, P. C., & Ladbury, J. E. (2001) J. Mol. Biol. **306**, 1127–1137. 7
- [36] Bloch, V., Yang, Y., Margeat, E., Chavanieu, A., Augé, M. T., Robert, B., Arold, S., Rimsky, S., & Kochoyan, M. (2003) Nat. Struct. Mol. Biol. **10**, 212–218. 7, 8
- [37] Dorman, C. J. (2004) Nat. Rev. Micro. **2**, 391–400. 8
- [38] Williams, R. M., Rimsky, S., & Buc, H. (1996) J. Bacteriol. **178**, 4335–4343. 8
- [39] Kajitani, M. & Ishihama, A. (1991) Nucleic Acids Res. **19**, 1063–1066. 8
- [40] Liu, Q. & Richardson, C. C. (1993) Proc. Natl. Acad. Sci. U.S.A. **90**, 1761–1765. 8
- [41] Donato, G. M. & Kawula, T. H. (1998) J. Biol. Chem. **273**, 24030–24036. 8
- [42] Nieto, J., Madrid, C., Miquelay, E., Parra, J., Rodriguez, S., & Juarez, A. (2002) J. Bacteriol. **184**, 629–635. 8
- [43] Falconi, M., Colonna, B., Prosseda, G., Micheli, G., & Gualerzi, C. O. (1998) EMBO J. **17**, 7033–7043. 8
- [44] Tupper, A., Owen-Hughes, T., Ussery, D., Santos, D., Ferguson, D., Sidebotham, J., Hinton, J., & Higgins, C. (1994) EMBO J. **13**, 258–268. 9

- [45] Amit, R., Oppenheim, A., & Stavans, J. (2003) Biophys. J. **84**, 2467–2473. 9, 34
- [46] Caramel, A. & Schnetz, K. (1998) J. Mol. Biol. **284**, 875–883. 9
- [47] Dame, R., Wyman, C., & Goosen, N. (2000) Nucleic Acids Res. **28**, 3504–3510. 9, 14, 34
- [48] Dame, R. T., Noom, M. C., & Wuite, G. J. (2006) Nature **444**, 387–390. 9
- [49] Woldringh, C. & Nanninga, N. (2006) J. Struct. Biol. **156**, 273–283. 9, 34
- [50] Spurio, R., Dürrenberger, M., Falconi, M., La Teana, A., Pon, C. L., & Gualerzi, C. O. (1992) Mol. Gen. Genet. **231**, 201–211. 9
- [51] Dame, R. T., Wyman, C., Wurm, R., Wagner, R., & Goosen, N. (2002) J. Biol. Chem. **277**, 2146–2150. 9
- [52] Zhang, W., Carneiro, M. J., Turner, I. J., Allen, S., Roberts, C. J., & Soutanas, P. (2005) J. Mol. Biol. **351**, 66–75. 9
- [53] Liu, Y., Chen, H., Kenney, L., & Yan, J. (2010) Gene. Dev. **24**, 339–344. 9, 14, 34
- [54] Dixon, N. E. & Kornberg, A. (1984) Proc. Natl. Acad. Sci. U.S.A. **81**, 424–428. 10, 11, 34
- [55] Azam, T. A., Iwata, A., Nishimura, A., Ueda, S., & Ishihama, A. (1999) J. Bacteriol. **181**, 6361–6370. 10, 34
- [56] Claret, L. & Rouviere-Yaniv, J. (1997) J. Mol. Biol. **273**, 93–104. 10

- [57] Pinson, V., Takahashi, M., & Rouviere-Yaniv, J. (1999) J. Mol. Biol. **287**, 485–497. 10
- [58] Tanaka, H., Goshima, N., Kohno, K., Kano, Y., & Imamoto, F. (1993) J. Biochem **113**, 568–572. 10
- [59] White, S. W., Wilson, K. S., Appelt, K., & Tanaka, I. (1999) Acta Crystallographica Section D: Biological Crystallography **55**, 801–809. 10
- [60] Azam, T. A., Hiraga, S., & Ishihama, A. (2000) Genes. Cell. **5**, 613–626. 10
- [61] Swinger, K. K., Lemberg, K. M., Zhang, Y., & Rice, P. A. (2003) EMBO J. **22**, 3749–3760. 10, 12, 34
- [62] Rice, P. A. (1997) Curr. Opin. Struc. Biol. **7**, 86–93. 10
- [63] Bewley, C. A., Gronenborn, A. M., & Clore, G. M. (1998) Ann. Rev. Biophys. Biomol. Struct. **27**, 105–131. 10
- [64] Koh, J., Saecker, R. M., & Record Jr, M. T. (2008) J. Mol. Biol. **383**, 324–346. 10
- [65] Vis, H., Boelens, R., Mariani, M., Stroop, R., Vorgias, C. E., Wilson, K. S., & Kaptein, R. (1994) Biochemistry **33**, 14858–14870. 11
- [66] Vis, H., Mariani, M., Vorgias, C. E., Wilson, K. S., Kaptein, R., & Boelens, R. (1995) J. Mol. Biol. **254**, 692–703. 11
- [67] Tanaka, I., Appelt, K., Dijk, J., White, S. W., & Wilson, K. S. (1984) Nature **310**, 376–381. 11, 35

## Bibliography

---

- [68] Tanaka, H., Yasuzawa, K., Kohno, K., Goshima, N., Kano, Y., Saiki, T., & Imamoto, F. (1995) Mol. Gen. Genet. **249**, 570–570. 11
- [69] Goodman, S. D., Nicholson, S. C., & Nash, H. A. (1992) Proc. Natl. Acad. Sci. U.S.A. **89**, 11910–11914. 11
- [70] Dame, R. T. & Goosen, N. (2002) FEBS lett. **529**, 151–156. 11
- [71] van Noort, J., Verbrugge, S., Goosen, N., Dekker, C., & Dame, R. T. (2004) Proc. Natl. Acad. Sci. U.S.A. **101**, 6969–6974. 11, 14, 35
- [72] Balandina, A., Claret, L., Hengge-Aronis, R., & Rouviere-Yaniv, J. (2001) Mol. MicroBiol. **39**, 1069–1079. 11
- [73] Flashner, Y. & Gralla, J. D. (1988) Cell **54**, 713–721. 11
- [74] Lewis, D. E., Geanacopoulos, M., & Adhya, S. (1999) Mol. MicroBiol. **31**, 451–461. 11
- [75] Kamashev, D. & Rouviere-Yaniv, J. (2000) EMBO J. **19**, 6527–6535. 11
- [76] Semsey, S., Geanacopoulos, M., Lewis, D. E. A., & Adhya, S. (2002) EMBO J. **21**, 4349–4356. 11
- [77] Haykinson, M. J. & Johnson, R. (1993) EMBO J. **12**, 2503. 11
- [78] Xiao, B., Johnson, R. C., & Marko, J. F. (2010) Nucleic Acids Res. **38**, 6176–6185. 11, 35
- [79] Kundukad, B., Cong, P., van der Maarel, J. R. C., & Doyle, P. S. (2013) Nucleic Acids Res. **41**, 8280–8288. 12, 35

- [80] Dame, R. T., Hall, M. A., & Wang, M. D. (2013) ChemBioChem **14**, 1954–1957. 12
- [81] Rice, P. A., Yang, S.-w., Mizuuchi, K., & Nash, H. A. (1996) Cell **87**, 1295–1306. 12
- [82] Ali, B. J., Amit, R., Braslavsky, I., Oppenheim, A. B., Gileadi, O., & Stavans, J. (2001) Proc. Natl. Acad. Sci. U.S.A. **98**, 10658–10663. 12
- [83] Pan, C. Q., Finkel, S. E., Cramton, S. E., Feng, J.-A., Sigman, D. S., & Johnson, R. C. (1996) J. Mol. Biol. **264**, 675–695. 13
- [84] Schneider, R., Lurz, R., Lüder, G., Tolksdorf, C., Travers, A., & Muskhelishvili, G. (2001) Nucleic Acids Res. **29**, 5107–5114. 13, 14
- [85] Luijsterburg, M. S., Noom, M. C., Wuite, G. J., & Dame, R. T. (2006) J. Struct. Biol. **156**, 262–272. 13, 14
- [86] Luijsterburg, M. S., White, M. F., van Driel, R., & Dame, R. T. (2008) Crit. Rev. Biochem. Mol. Biol. **43**, 393–418. 13
- [87] Kuhn, W. (1934) Kolloid. Z. **68**, 2–15. 21
- [88] Kuhn, W. (1936) Kolloid. Z. **76**, 258–271. 21
- [89] Flory, P. J. (1949) J. Chem. Phys. **17**, 303. 21
- [90] Flory & J., P. (1953) Principles of polymer chemistry (Cornell University Press). 21
- [91] Reisner, W., Beech, J. P., Larsen, N. B., Flyvbjerg, H., Kristensen, A., & Tegenfeldt, J. O. (2007) Phys. Rev. Lett. **99**, 058302. 24, 29

- [92] Tegenfeldt, J., Prinz, C., Cao, H., Chou, S., Reisner, W., Riehn, R., Wang, Y., Cox, E., Sturm, J., Silberzan, P., & Austin, R. (2004) Proc. Natl. Acad. Sci. U.S.A. **101**, 10979–10983. 25, 28
- [93] Odijk, T. (1983) Macromolecules **16**, 1340–1344. 25
- [94] Wang, Y., Tree, D. R., & Dorfman, K. D. (2011) Macromolecules **44**, 6594–6604. 26, 30
- [95] Odijk, T. (2006) J. Chem. Phys. **125**, 204904. 26
- [96] Dai, L., Siow, Y. N., Doyle, P. S., & van der Maarel, J. R. C. (2012) ACS Macro Lett. **1**, 1046–1050. 27, 33
- [97] Bustamante, C. (1991) Annu. Rev. Biophys. Bio. **20**, 415–446. 28
- [98] Volkmuth, W. & Austin, R. (1992) Nature **358**, 600–602. 28
- [99] Volkmuth, W., Duke, T., Austin, R., & Cox, E. (1995) Proc. Natl. Acad. Sci. U.S.A. **92**, 6887–6891. 28
- [100] Bakajin, O. B., Duke, T. A. J., Chou, C. F., Chan, S. S., Austin, R. H., & Cox, E. C. (1998) Phys. Rev. Lett. **80**, 2737–2740. 28
- [101] Guo, L. J., Cheng, X., & Chou, C.-F. (2004) Nano Lett. **4**, 69–73. 28
- [102] Reisner, W., Morton, K. J., Riehn, R., Wang, Y. M., Yu, Z., Rosen, M., Sturm, J. C., Chou, S. Y., Frey, E., Austin, R. H., et al. (2005) Phys. Rev. Lett. **94**, 196101. 28, 29
- [103] De Gennes, P. G. (1979) Scaling concepts in polymer physics (Cornell university press). 28

- [104] Persson, F., Utko, P., Reisner, W., Larsen, N. B., & Kristensen, A. (2009) Nano Lett. **9**, 1382–1385. 29, 31
- [105] Zhang, C., Zhang, F., Van Kan, J. A., & van der Maarel, J. R. C. (2008) J. Chem. Phys. **128**. 30
- [106] Kim, Y., Kim, K. S., Kounovsky, K. L., Chang, R., Jung, G. Y., Jo, K., Schwartz, D. C., et al. (2011) Lab. Chip **11**, 1721–1729. 30
- [107] Chang, R. & Jo, K. (2012) J. Chem. Phys. **136**, 095101. 30
- [108] Zhang, C., Shao, P., van Kan, J. A., & van der Maarel, J. R. C. (2009) Proc. Natl. Acad. Sci. U.S.A. **106**, 16651–16656. 31, 33
- [109] Dai, L. & Doyle, P. S. (2013) Macromolecules **46**, 6336–6344. 31
- [110] Wang, W., Li, G.-W., Chen, C., Xie, X., & Zhuang, X. (2011) Science **333**, 1445–1449. 32, 35
- [111] Reisner, W., Pedersen, J., & Austin, R. (2012) Rep. Prog. Phys. **75**. 33
- [112] Levy, S. & Craighead, H. (2010) Chem. Soc. Rev. **39**, 1133–1152. 33
- [113] Jones, J. J., van der Maarel, J. R. C., & Doyle, P. S. (2011) Nano Lett. **11**, 5047–5053. 33
- [114] Zhang, C., Gong, Z., Guttula, D., Malar, P. P., van Kan, J. A., Doyle, P. S., & van der Maarel, J. R. C. (2012) J. Phys. Chem. B **116**, 3031–3036. 33
- [115] Browning, D., Grainger, D., & Busby, S. (2010) Curr. Opin. Microbiol. **13**, 773–780. 34



## Bibliography

---

- [116] Bloomfield, V. (1996) Curr. Opin. Struc. Biol. **6**, 334–341. 34
- [117] Swinger, K. K. & Rice, P. A. (2007) J. Mol. Biol. **365**, 1005–1016.  
34
- [118] Dame, R. T. (2005) Mol. MicroBiol. **56**, 858–870. 34

# Chapter 2

## Materials and methods

This chapter describes the materials and methods used in the experiments. The first section describes DNA labelling with YOYO-1, followed by biochip fabrication using a proton beam and UV lithography, followed by PDMS replication. The final section presents the data analysis

### 2.1 T4-DNA

T4-Phage DNA has provided countless research contributions to genetics and biochemistry. T4-bacteriophage is a bacteriophage that infects *E.coli*. Its complete genome sequence of  $\sim 169$  kbps ( $\sim 56 \mu\text{m}$ ) encodes about 300 gene products. T4-DNA is held in an icosahedral head, also known as a capsid of T4-phage. Single molecule studies generally use  $\lambda$  or T4-DNA. Dai et al. computer simulation suggests that  $\lambda$ -DNA is too short to enter the de Gennes regime and also to observe noticeable change in length. Even for the extended de Gennes regime, the corresponding range of channel size is

## 2.1. T4-DNA

rather small. It is possible to explore the extended de Gennes regime using T4-DNA in high-salt solution, and also possible to explore the de Gennes regime using T4-DNA in low-salt solution<sup>[1]</sup>. T4-DNA was purchased from Nippon Gene (Tokyo), and used without further purification. The integrity of T4-DNA was verified with pulsed gel electrophoresis (See Fig. 2.1). No detectable fragments of the order of several kbps were observed.

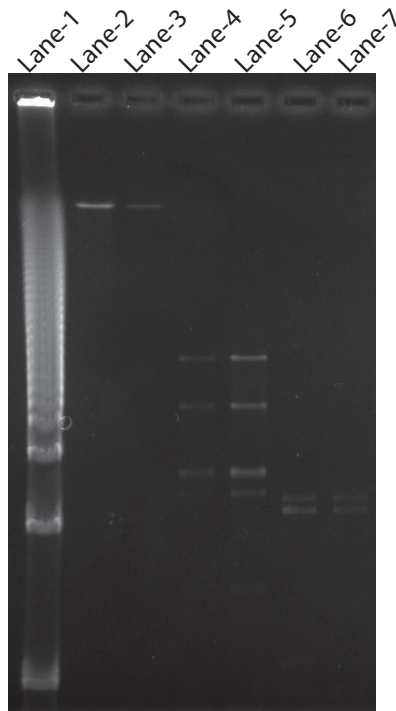


**Fig. 2.1** Pulsed field gel electrophoresis of T4-DNA gel picture. Lanes from left to right, 1. PFGE standard - 5 kb ladder, 2. T4 (0.01 g/l), 3. T4 (0.006 g/l)(1-year-old sample), 4. T4 digested by NruI (0.006 g/l), 5. T4 digested by NruI (0.01 g/l), 6. T4 digested by HindIII (0.01 g/l), 7. T4 digested by HindIII (0.006 g/l).

## 2.1.1 YOYO-1

DNA is not fluorescence itself, so it has to be labelled with fluorescent material. Some fluorescent dyes such as DAPI and Ethidium bromide (EtBr) have low quantum efficiency. Cyanine fluorochromes, such as **TOTO-1**<sup>1</sup> and **YOYO-1**<sup>2</sup>, are commonly used in fluorescence microscopy. These bis-intercalators exhibit high fluorescence enhancement ( $\sim 1000$  fold) upon binding to dsDNA, thus providing a high signal to noise ratio<sup>[2,3]</sup>. YOYO-1 was purchased from Invitrogen (Carlsbad, CA), and has excitation maxima ( $\lambda_{max}^{ex}$ ) at 491 nm and emission maxima ( $\lambda_{max}^{em}$ ) at 509 nm. YOYO-1 carries four positive charges<sup>[4]</sup>. As DNA carries a negative charge, the overall DNA-YOYO-1 charge is reduced and it depends on the amount of YOYO-1 added to the DNA. YOYO-1 alters the physical properties of the DNA, like contour length and helical pitch. The contour length of DNA is increased by 0.51 nm per YOYO-1 molecule and 36% increase in the fully saturated DNA<sup>[5,6,7]</sup>. The persistence length ( $l_p$ ) of DNA is constant and independent of the amount of concentration of YOYO-1<sup>[6,8]</sup>. All these effects were considered in the experiment. The intercalation ratio of 100 bp per one YOYO-1 molecule was used in the experiments. The length of T4-DNA increased by 0.85  $\mu\text{m}$  (i.e. from 56 to 56.9  $\mu\text{m}$ ). At such a low level of intercalation the distortion of the secondary structure of DNA is minimal.

<sup>1</sup>**TOTO-1**:(1,1'-(4,4,7,7-tetra methyl-4,7-diazaundecamethylene)-bis-4-[3-methyl-2,3-dihydro-(be-underlineoxazole-2-methyl-idenel]-quinoliniumolinium tetra-iodide)

<sup>2</sup>**YOYO-1**:(1-1'-(4,4,7,7-tetra methyl-4,7-diazaundecamethylene)-bis-4-[3-methyl-2,3-dihydro-(be-underlinethiazole-2-methyl-idenel]-quinoliniumolinium tetra-iodide)

## 2.2 Fabrication of nanofluidic device

A master stamp was produced in two steps. In the first step, nanochannels were produced using proton beam writing (PBW). In the second step, micro channels were produced by UV lithography, such that both nano and micro channels were connected. The fabrication of the stamp was carried out by Associate Professor Jeroen van Kan and his team (Piravi Malar. P, Liu. F) in the Centre for Ion Beam Applications (CIBA), Department of Physics, National University of Singapore, Singapore.

### 2.2.1 Nanostructure fabrication by PBW

Nanostructures were created using PBW with energies 500 keV to 2 MeV. The advantage of using a proton beam is that it penetrates deeply into the material with a minimal amount of surface disruption, and is less broadening than an electron beam<sup>[9]</sup>. The fabrication process is shown in Fig. 2.2. The process involves the following steps:

1. A 200-nm thick Cr and gold (Au) layer was pre-coated on the Si wafer. The metallic layer gives good adhesion of the resist to the wafer and easy removal for PDMS.
2. The required thickness (150-300nm) of a solution with hydrogen-silsesquioxane (HSQ) (Dow Corning Co), XR-1541 and FOX 12 in 4-methyl-2-pentanone was wet spun onto the Si/Cr-Au layer. The wafer was subsequently baked at 120°C in an oven for 2 h.

## 2.2. Nanostructure fabrication by PBW

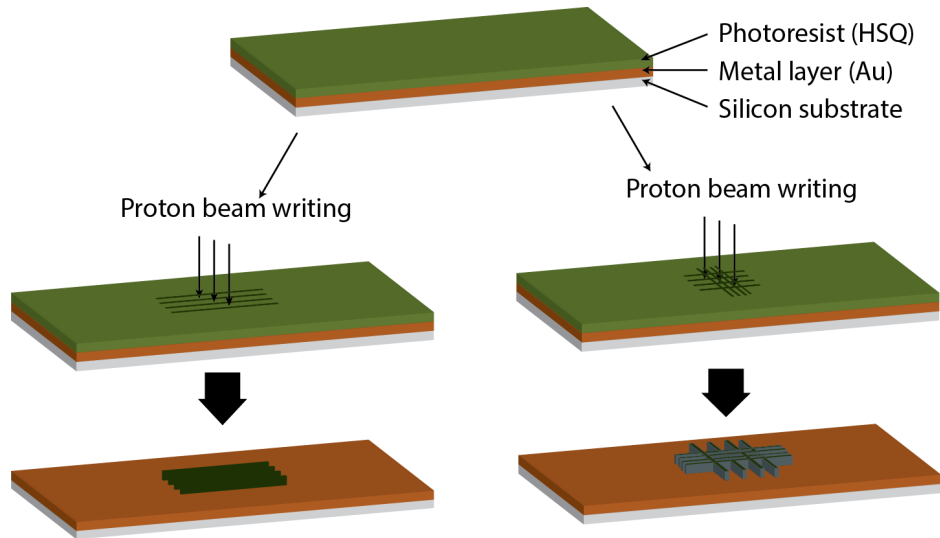


**Fig. 2.2** Nanostructure patterning in HSQ photoresist by Proton beam writing. Left side: regular channels; right side: cross channels. Top to bottom: A) Coating of Au and HSQ on substrate; B) Proton beam writing on HSQ; C) Positive structures after development.

3. The desired pattern on the HSQ layer was achieved by the PBW with the help of a scanning software. HSQ forms a cross-linked network by proton exposure; these structures are chemically strong.
4. Isopropanol-water (7:3) was used as a developer and developed in 10 min without agitation. The developer dissolves unexposed HSQ. After development, positive structures with widths of  $60$  to  $250 \pm 5$  nm were achieved.

In this way, nanochannels of heights 90, 150, 200 and 250 nm, and with widths 150, 200, 250, and 300 nm were obtained. The channel lengths were  $50 \mu\text{m}$ .

## 2.2.2 Micro channel fabrication by UV-lithography

1. The stamp with nanostructure prepared was heated to 200°C for 2 min. A 5  $\mu\text{m}$  SU-8 (Micro-Chem) layer was spin-coated on the preheated stamp at 2000 rpm for 30 s. The spin coated SU-8 was heated to 95°C for 2 min to evaporate the solvent.
2. The nanostructures on the substrate were aligned with the microstructure of the UV mask with the help of a mask aligner system. Due to low optical absorption of SU-8, the micro channels can be aligned to the underlying nanostructures. The substrate was exposed to UV light of wavelength 365 nm for 30 sec. The exposed substrate was post backed at 95°C for 2 min.
3. SU-8 developer (Micro Chem.) was used to develop the exposed SU-8 for 2 min. Finally, the substrate containing the nano and microstructures was backed to 150°C for 30 min to harden. The substrate was finally rinsed with IPA, followed by deionised water and a gentle stream of nitrogen gas. In this way, micro channels of dimensions  $5 \times 5 \mu\text{m}^2$  were obtained.

Using the combinations of PBW for nanostructures and UV lithography for microstructures, it is possible to produce a master stamp with positive structures of micro channels, which are superposed on underlying nanochannels.

### 2.2.2. Micro channel fabrication by UV-lithography

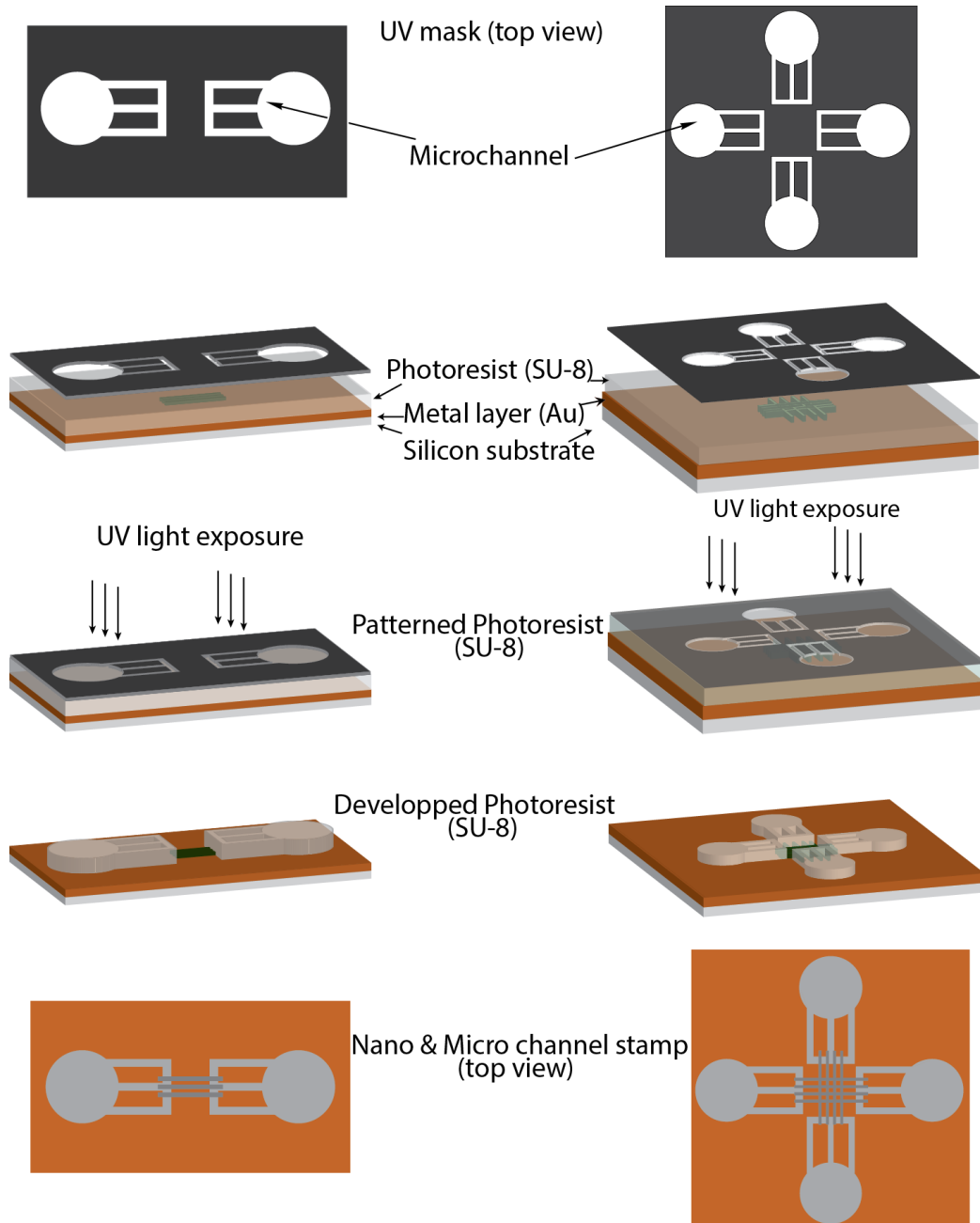


**Fig. 2.3** Super positioning of the SU8 microstructure on the HSQ nanostructure by UV lithography. Left side: regular channels; right side: cross channels.



## 2.3 PDMS

The advantage of PDMS is that it is biocompatible and more robust to replicate the master stamp. More than 100 replications can be done with one master stamp. The chemical formula of poly-di-methyl-siloxane (PDMS) is  $CH_3 - [Si(CH_3)_2O]_n Si - (CH_3)_3$ , where  $n$  is the number of repeating monomer  $[Si(CH_3)_2O]$ . The Sylgard<sup>TM</sup>184 (Dow Corning Corporation) kit contains a liquid silicon rubber base (vinyl-terminated PDMS) and a catalyst or curing agent (a mixture of a platinum complex and copolymers of methylhydrosiloxane). The curing agent was added to the base in a 1:10 weight ratio. Because the base is viscous it was thoroughly mixed. The mixture was degassed and poured onto the boat containing the master stamp, and degassed again to remove any air bubbles that were trapped in the nano/micro channels. The PDMS was then cured by placing it in an oven for 4 h at 65°C. The cured PDMS was carefully peeled off from the master stamp. The sources at the micro channel end were punched using a needle (Harris Uni-Core, Jed Pella Inc.)

### 2.3.1 Air plasma cleaning

The PDMS nanochannels prepared had three faces covered, the fourth face covered by a microscopic cover slip. The cured PDMS was naturally hydrophobic surface, so it was difficult for water based micro/nanofluidics. The pressure exerted on the channels was inversely proportional to the cross-sectional area of the channel. To make a good tight seal, and to enable fluid to flow in the channel, surface modification was needed. Atmospheric

## 2.4. Fluorescence microscopy

---

air plasma or argon plasma cleaning was the best methods to change the surface from hydrophobic to hydrophilic. Oxygen plasma changes the surface chemistry by converting the  $-O-Si(CH_3)_2-$  unit to silanol ( $-SiOH-$ ). This plasma cleaning also helps to remove surface contaminants and improves adhesion. The air plasma oxidised PDMS surface resists absorption of hydrophobic and negatively charged molecules. These hydrophobic surfaces are stable for few tens of hours in air/water. After a certain amount of time (aging) the hydrophobic property of the PDMS surface is recovered, irrespective of whether the medium is air, water, or a vacuum. The experiments were done below the aging time, so there is no hydrophobic effect on the results.

The PDMS chip was removed from the master stamp and cut to a little bit more than the actual chip dimensions. The PDMS chip and cover glass were placed in the cylindrical type glow discharge. Plasma energy of 10.5 W and a radio frequency of 40 kHz were applied for 30 s at air pressure of 0.3 torr. After air plasma cleaning, the PDMS stamp was immediately placed in contact with the cover slip for bonding. The bonding was further strengthened by post-backing the assembly on a hot plate at 95°C for 1 min.

## 2.4 Fluorescence microscopy

T4-DNA molecules having 165,600 base pairs (Nippon Gene) were suspended in the buffer of 10 mM Tris and 3 or 30 mM NaCl. For Protein-DNA experiments, a mixture of the Protein-DNA was prepared and incubated

## 2.4. Fluorescence microscopy

---

for more than 12 h. The DNA concentration was held constant at 0.003 g per L for all the nanochannel experiments. For visualisation of the DNA, the Protein-DNA complex mixture was fluorescently labelled with YOYO-1 and incubated overnight. The intercalation ratio was one YOYO-1 molecule per 100 base pairs. The Protein-DNA complex was loaded into the reservoirs of the micro channels, which flows through capillary action. The mixture was driven into nanochannels by application of an electric field, or sometimes by the application of minimal pressure of 0.7 kPa with the micro injector (Narishige, Tokyo). To apply the electric field, two platinum electrodes were immersed into the reservoirs of the two micro channels, and the electrodes were connected to a high-voltage power supply (Keithley 237 high voltage source measurement unit, Cleveland, Ohio), and voltage from 0.1 to 10 V was applied. Once the DNA molecules got into the channel, the electric field was switched off and the molecules were allowed to relax to their equilibrium state for at least 1 min. The fluorescently labelled DNA was visualised with the help of an inverted microscope (Nikon Eclipse Ti) equipped with a 200 W metal halide lamp, a filter set, and a 100X oil immersion objective. Videos were collected with a high gain EMCCD camera (iXon X3, Andhor) with 100 msec exposure and  $512 \times 512$  pixels.

## 2.5 Data analysis

The DNA lengths were measured with open source software ImageJ (<http://rsb.info.nih.gov/ij>) and Matlab. The size of the DNA along the long axis was obtained using the intensity profile of the DNA in ImageJ/ Matlab as shown in the Fig. 2.4 The DNA molecule average size was obtained by plotting a histogram of  $\sim 100$  molecules, and fitting the histogram with a Gaussian distribution.

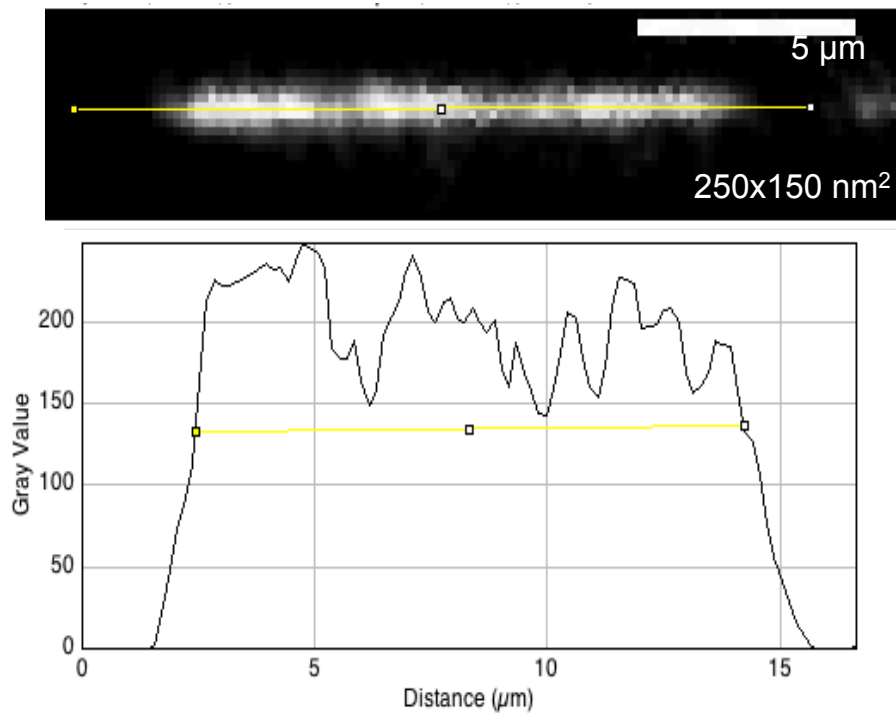


**Fig. 2.4**

Intensity profile of a labelled DNA and measurement of its length.

### 2.5.1 Measurements of DNA length in nanochannels

The DNA molecules in nanochannels are shown in Fig. 2.5(B). The figure shows a typical distribution of the measurements of more than 100

individual molecules. The distribution is approximately Gaussian. The fluctuation-induced distribution is close to Gaussian<sup>[10]</sup>. DNA fragments can easily be discerned, because their extensions fall below the values pertaining to the intact molecules. For the cut-off, the mean value minus 2 times the standard deviation was used. Resolution broadening can be neglected because the optical resolution is 1 order of magnitude smaller than the variance.

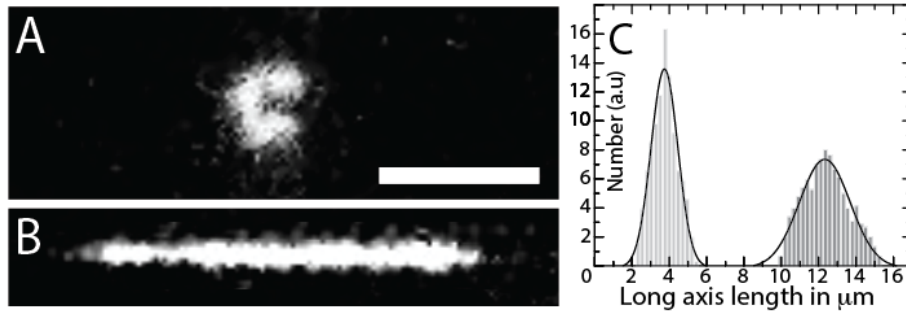


**Fig. 2.5** Fluorescence image of labelled T4-DNA in (A) bulk phase and (B) nanochannels. (C) Distribution in long axis extension of a population of more than 50 molecules in T-buffer with 3 mM NaCl inside the  $250 \times 140$  nm channels. 150 molecules in bulk phase with same buffer condition. A Gaussian fit gives  $R_{\parallel} = 12.3 \pm 1.5 \mu\text{m}$  and  $3.7 \pm 0.7 \mu\text{m}$  in nanochannels and bulk condition respectively. Scale bar is  $5 \mu\text{m}$ .

Fig. 2.5 shows the clear difference between the conformation of DNA in the bulk phase and nanochannels. In the bulk phase, the long axis length is about  $3.7 \mu\text{m}$ , and is extended to  $12 \mu\text{m}$  in the  $250 \text{ nm} \times 140 \text{ nm}$  channels. The conformational force extends the coil DNA along the channel direction.

### 2.5.2 Measurement of DNA length in bulk phase

The free space DNA molecules are shown in Fig. 2.5(A). The bulk phase experiments of the DNA-HNS complex for different HNS concentrations are shown in Fig. 2.6. Figure clearly shows that H-NS induces elongation and compaction, and not condensation, in the bulk phase. It may be observed that the DNA concentration is 100 times less than the nanochannel DNA concentration (0.003  $g/l$ ). However, DNA is condensed in the nanochannel (See chapter. 3).

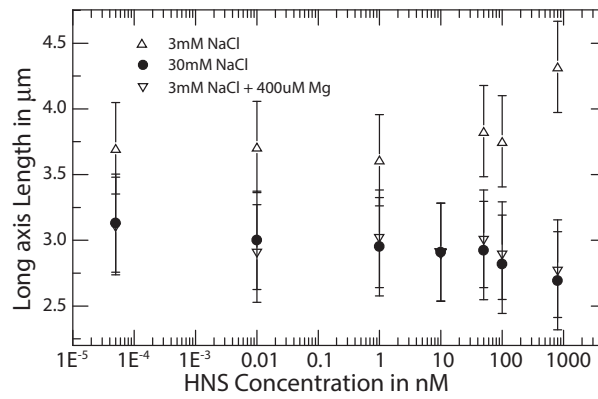


**Fig. 2.6** Labelled T4-DNA in bulk phase and nanochannels.

## 2.6 Protein Purification

Chromatography is a technique used to separate and/or analyze complex mixtures<sup>[11]</sup>. The technique has two phases –the stationary phase and the mobile phase. Based on geometry and nature of the phase, the chromatography can be classified into different types. The stationary phase chromatography (geometry based) can be further classified into *column chromatography* and *planar chromatography*. Similarly, the mobile phase chromatography (based on nature) has three different types of chromatographic techniques, namely *liquid-chromatography* (LC), *gas chromatography* (GC), and *supercritical-fluid-chromatography* (SFC). Using liquid chromatography, a lot of biomolecules such as DNA, proteins, peptides, and other charged molecules are purified. These molecules are purified/separated by using the differences in their specific properties. Today, many liquid chromatographic techniques are available; some of them are shown in the Table (2.1).

**Table. 2.1** Different types of liquid-chromatographic separation based on specific properties

Property	Technique
charge at certain pH	Ion exchange chromatography IEX
Size	size exclusion chromatography (SEC)
Hydrophobicity	Hydrophobic interaction chromatography(HIC) Reversed phase chromatography (RPC)
Biorecognition (ligand specificity)	Affinity chromatography (AC)
Isoelectric point	Chromatofocusing (CF)

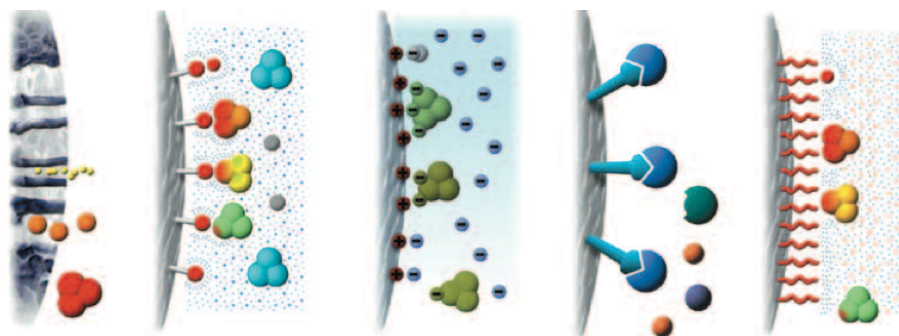


**Fig. 2.7** Schematic drawing of separation principles in chromatography purification. From left to right: GF, HIC, IEX, AC, and RPC. Figure adopted from GE Ion Exchange Chromatography & Chromatofocusing Principles and Methods. Figure was adapted from GE website

Ion Exchange Chromatography (IEX) uses the property of differences in net charge on the molecules to separate them. Many biomolecules have ionisable groups. Proteins are made up of amino acids containing weak acidic and basic groups, and their net charge depends on the pH, that is, *amphoteric* in nature. Proteins are built up by specific amino acid sequences, so each protein has its own net charge versus the *pH* relationship.

In IEX, the column was packed with ion exchange resin that could be a cationic or anionic exchanger. The anionic exchanger had positively charged groups and attracted negatively charged molecules, and the cationic exchanger attracted positively charged molecules. When samples were loaded to the column, molecules having opposite charges to the IEX resin bound to the resin; the greater the opposite charge, the stronger the bond. Proteins with the same charge as the IEX resin, and unbound molecules/proteins, were washed out by the buffer. Proteins were eluted by increasing ionic strength or changing the *pH* of the elution buffer (mobile phase). Proteins with a low net charge at a selected *pH* were eluted, followed by proteins having a higher net charge at that *pH*. The ionic strength



### 2.6.1. First step purification by Cellulose column

was increased in a gradient or stepwise fashion.

## 2.6.1 Wt H-NS purification by ion exchange chromatography

### 2.6.1.1 First step – purification by Cellulose column

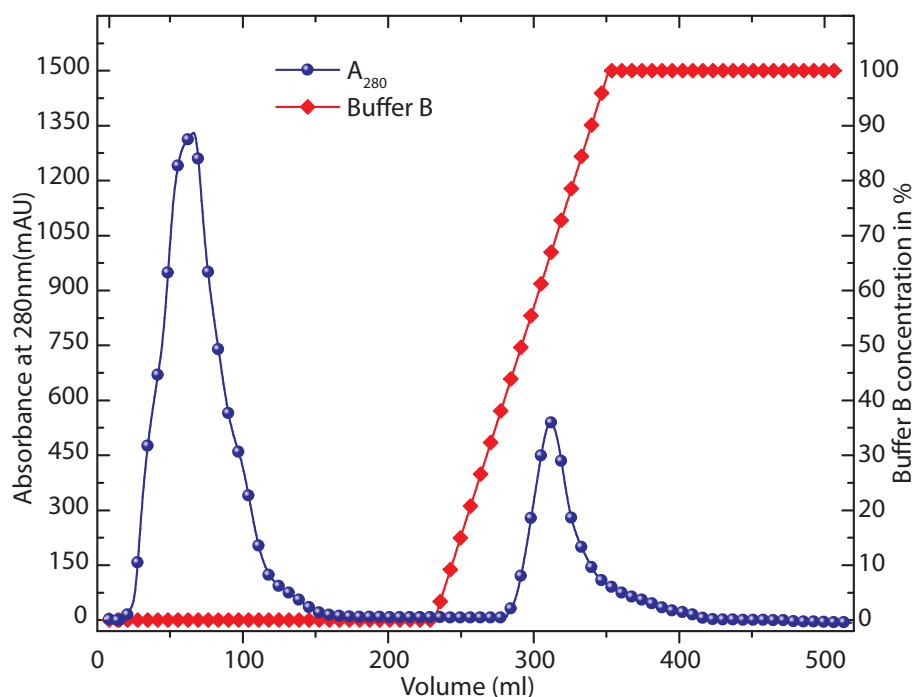


**Fig. 2.8** Protein purification by Cellulose column. Blue sphere represent arbitrary units of UV 280 readings and red diamonds represent the elution buffer concentration in percentage

H-NS purified by *K1746* bacteria transformed with pHOP-II<sup>[12]</sup> were grown on a Luria Broth (LB) plate with ampicillin (50 mg per L). A single colony was taken to grow a starter culture in a Luria Broth (LB) medium containing ampicillin at 310 K for 8 h ( $OD_{600} = 0.6$ ). The starter culture was then diluted 1,000 times into Luria Broth (LB) medium containing ampicillin and grown at 310 K for 2 h with vigorous shaking (280

### 2.6.1. First step purification by Cellulose column

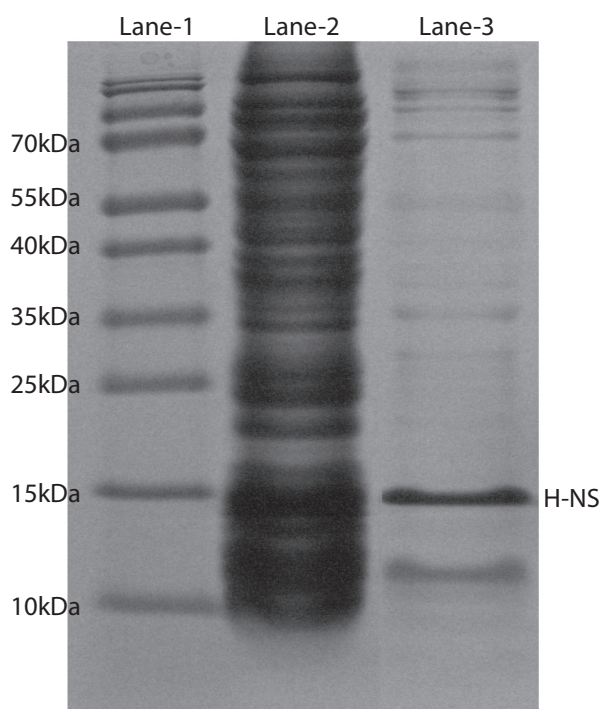


**Fig. 2.9** SDS-page picture of Cellulose column purification of H-NS. From left to right, lane-ladder; lane2-lysate; lane3-elute through cellulose column

rpm,  $OD_{600} = 0.6$ ). Protein expression was induced by the addition of isopropylthio- $\beta$ -galactoside (IPTG) to a final concentration of 1 mM. The bacterial cells were harvested by centrifugation at 6,000 g for 15 min at 277 K. The pellet was suspended in a buffer comprising 20 mM Tris-HCl, pH 7.2, 1 mM EDTA, 5 mM  $\beta$ -mercaptoethanol, 10% glycerol, 100 mg phenylmethylsulfonyl fluoride (PMSF) per L, 2 mM benzamidine, 100 mM  $NH_4Cl$ , and 1 mg Pefabloc SC per L. This was subsequently lysed with a sonicator (Sonic vibra) at 10,000 Joules, and followed by treatment with DNase-1 and RNase-A (Promega) on ice for 30 min. After centrifugation at 15,000 g for 2.5 h at 277 K, the supernatant was loaded onto a phosphocellulose (P11, Whatman) column (XK 50/30) equilibrated with 100 mM  $NH_4Cl$ , 1 mM EDTA, 10% glycerol and 20 mM Tris-HCl, pH 7.2 with an

### 2.6.1. Second step purification by Heparin column

AKTA explorer chromatography system (GE Life Sciences). The column was washed with the abovementioned 100 mM  $\text{NH}_4\text{Cl}$  buffer, and the protein was eluted with a gradient to 1 M  $\text{NH}_4\text{Cl}$ . The chromatogram showing the elution process is shown in Fig. 2.8. The elutes from the cellulose were checked with SDS-page gel. Fig. 2.9 Protein having a molecular weight of  $\simeq 15$  kDa was observed.

#### 2.6.1.2 Second step – purification by Heparin column

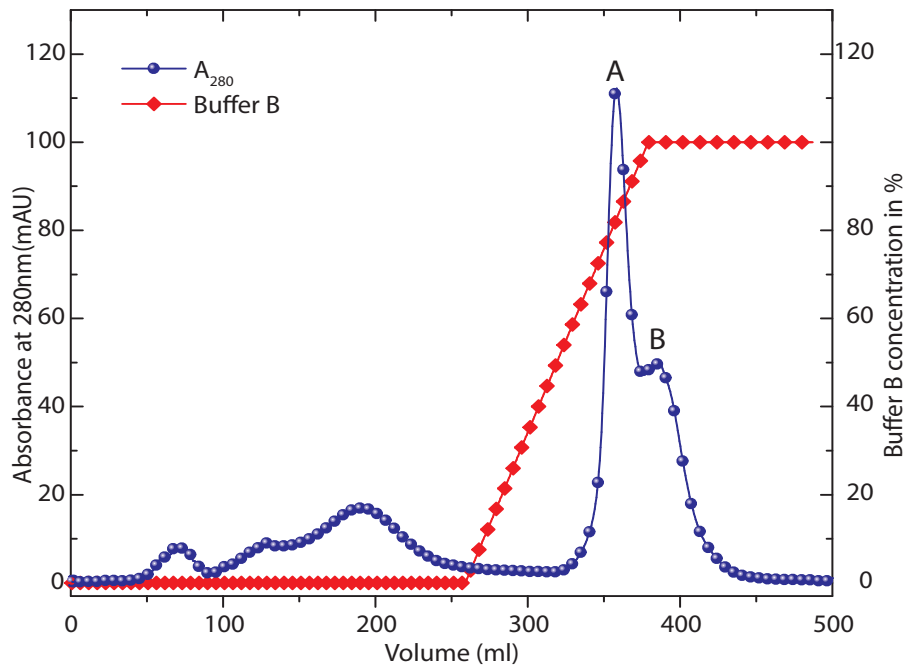


**Fig. 2.10** Protein purification by Heparin column. Blue sphere represent arbitrary units of UV 280 , and red diamonds represent the elution buffer concentration in percentage.

The results of purification from a cellulose column is usually not pure, so second step purification process was needed. The elute from the cellulose column was subsequently dialysed against 100 mM NaCl, 1 mM EDTA, 10% glycerol and 20 mM Tris-HCl,  $pH$  7.2. The dialysed sample was loaded

### 2.6.1. Second step purification by Heparin column

onto a heparin column equilibrated with the abovementioned 100 mM NaCl buffer followed by elution in a gradient to 1 M NaCl.

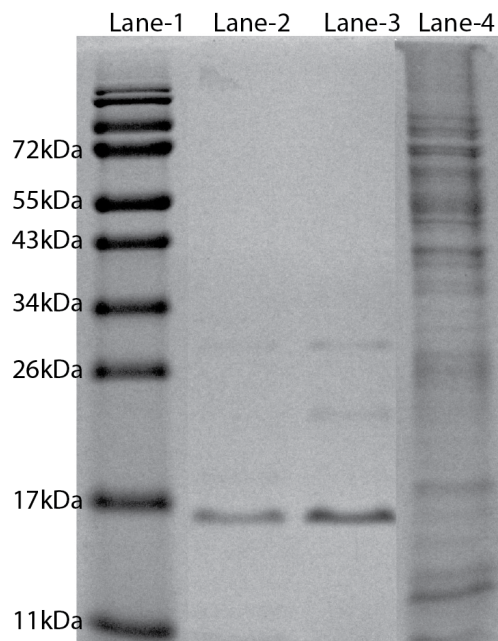


**Fig. 2.11** SDS-page picture of Heparin column purification of H-NS. From left to right: lane1-ladder; lane2, 3-elutes from heparin column at different times (peaks A and B in the Fig. 2.10); lane4-lysate.

The chromatogram showing the elution process is shown in Fig. 2.10. The purity of the H-NS was monitored by SDS-page gel to check the quality of the purification. From the picture of the gel (Fig. 2.11), it is clear that the H-NS was almost purified.

In Fig. 2.10 there are two peaks side by side, possibly due to two reasons — the column packing might not be good or the H-NS might exist in oligomers, which is clearly shown in the gel (Fig. 2.11) and further verified by size exclusion chromatography.

### 2.6.2 His-tag H-NS purification

This is a single-step purification process using a His-trap column. A BL21 (DE3) strain containing His-tag H-NS was grown in a Luria broth plate with 0.2% glucose with ampicillin (100  $\mu\text{g}$  per ml). A single colony was taken in a falcon tube containing a Luria Broth (LB) with glucose and ampicillin at 310 K for 8 h with shaking; the process stopped at  $\text{OD}_{600} = 0.7$ . The starter culture was then diluted 1,000 times into a Luria Broth medium containing 0.2% glucose and ampicillin (100  $\mu\text{g}$  per ml), and grown at 310 K for 2 h with vigorous shaking (280 rpm,  $\text{OD}_{600} = 0.7$ ). 1 ml from the culture was taken to check the expression. Protein expression was induced by the addition of isopropylthio- $\beta$ -galactoside (IPTG) to a final concentration of 500  $\mu\text{M}$ . Expression of the protein was checked by SDS-page gel; Fig. 2.13 shows that the protein was expressed well (lane 4, 3 before and after expression). The bacterial cells were harvested by centrifugation at 6,000 g for 15 min at 277 K. The pellet was suspended in a buffer, which is the same as described in the first section, including the 0.1 mM DTT that is then lysed with solicitor. The lysate after sonication was centrifuged at 25,000 g for 20 min at 277 K, and the supernatant was recovered. The supernatant was treated with RNase A with final concentration 10  $\mu\text{g}$  per ml and 100 U DNase per ml in room temperature with agitation for 1 h. RNase/DNase was deactivated by adding EDTA and again centrifuged for 15 min at 15,000 g at 277 K.

The supernatant was loaded onto a His-trap column (GE Life Sciences) with an AKTA explorer chromatography system (GE Life Sciences). The column was pre-equilibrated with an adsorption buffer (A1) containing 20

## 2.6.2. His-tag H-NS purification

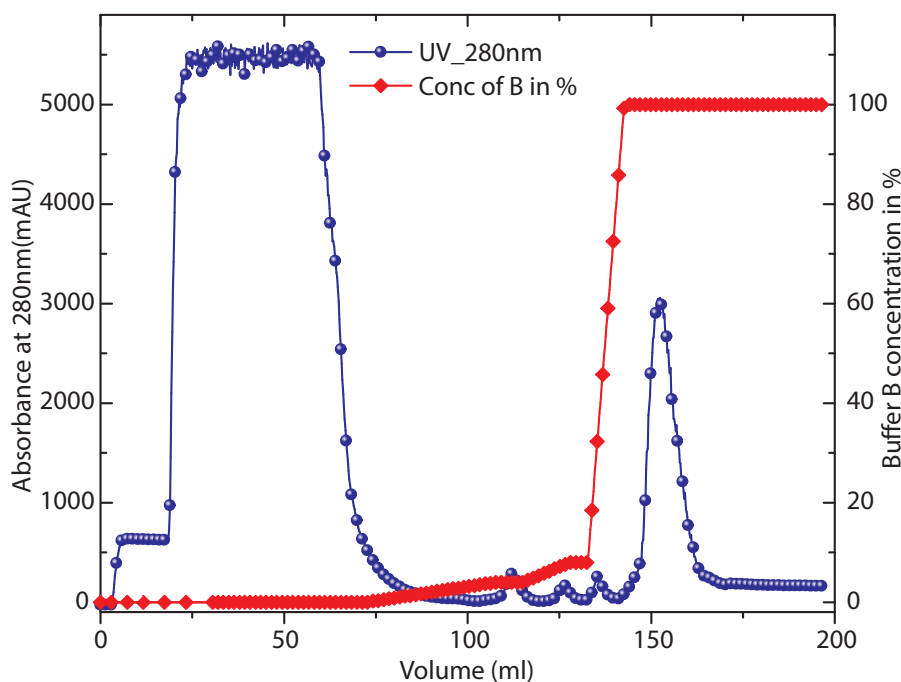


**Fig. 2.12** Single step protein purification by His-trap column. Blue sphere represent arbitrary units of UV 280 , and red diamonds represent the elution buffer concentration in percentage.

mM Tris-HCl, *pH* 8, 10% glycerol, 0.1% Triton and 0.5 M NaCl at 1 ml/min for 10 ml. The column was washed with a washing buffer (Tris-HCl, *pH* 8, 0.3 M NaCl), then followed by elution linearly with 4% elution buffer (20 mM Imidazole) which contained Tris-HCl, *pH* 8, 0.3 M NaCl and Imidazole 500 mM at 1 ml/min. After this, the percentage of Imidazole was increased to 8% linearly to make 40 mM Imidazole, which further washed out unbound protein. Finally the concentration of Imidazole was increased from 8% to 100% linearly at 0.25 ml/min. Fig. 2.12 shows the chromatogram for the His-trap column. The elutes were collected and checked for purity by SDS gel, which is shown in 2.13.

The His-tag was removed with cutting enzyme-TEV. Fig. 2.14 shows the progressive cutting action by TEV. Lanes from 3 to 7 are samples taken

## 2.6.2. His-tag H-NS purification

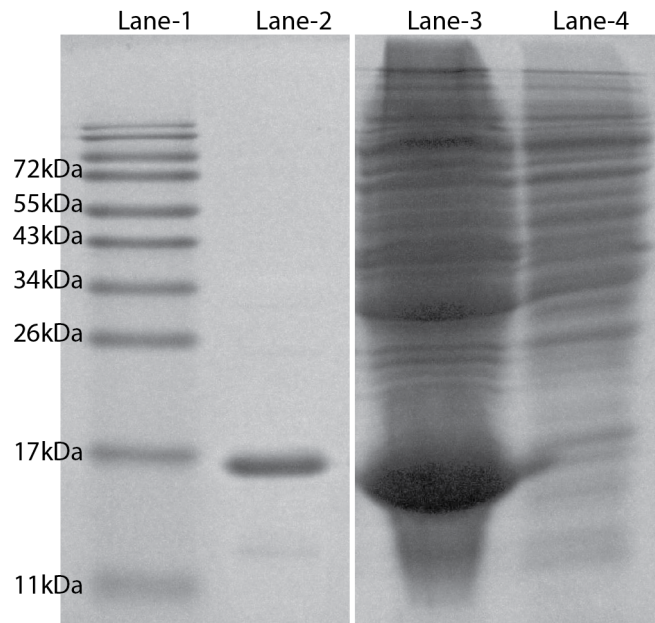


**Fig. 2.13** SDS-page picture of His-trap column purification of H-NS. From left to right: lane-ladder; lane2-elutes from his-trap column (purified H-NS); lane3- after induction by *IPTG*; lane4- before induction.

at 1, 2, 7, 12 h respectively. After overnight digestion all the His-tag were removed and quality of the protein was checked with gel.

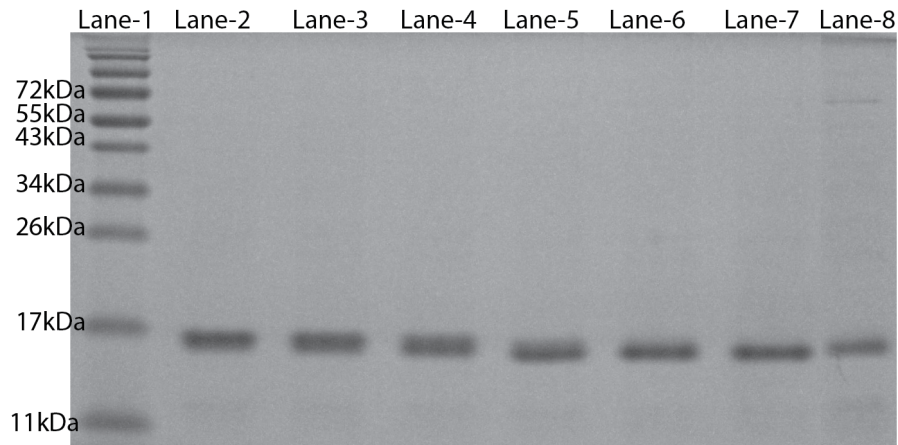


**Fig. 2.14** SDS-page picture of His-tag digestion by TEV. From left to right: lane1-ladder; lane2-elutes from His-trap column (purified H-NS with His-tag); lane3 to 7 are 1, 2, 7, 12 h, and overnight digestion; lane8-purified Wt-H-NS with two-step process.

## 2.6.2. His-tag H-NS purification

Experiments were done at 10mM Tris-HCl with 3 and 30mM NaCl. The stability (denaturing) of the protein need to check before the experiments. The circular dichroism technique was used to verify the protein stability at low ionic strength. Fig. 2.15 shows the stability at 3mM NaCl; the protein was denatured after adding  $H_2SO_4$ . It was clear that the protein at low salt concentration is still not denatured.

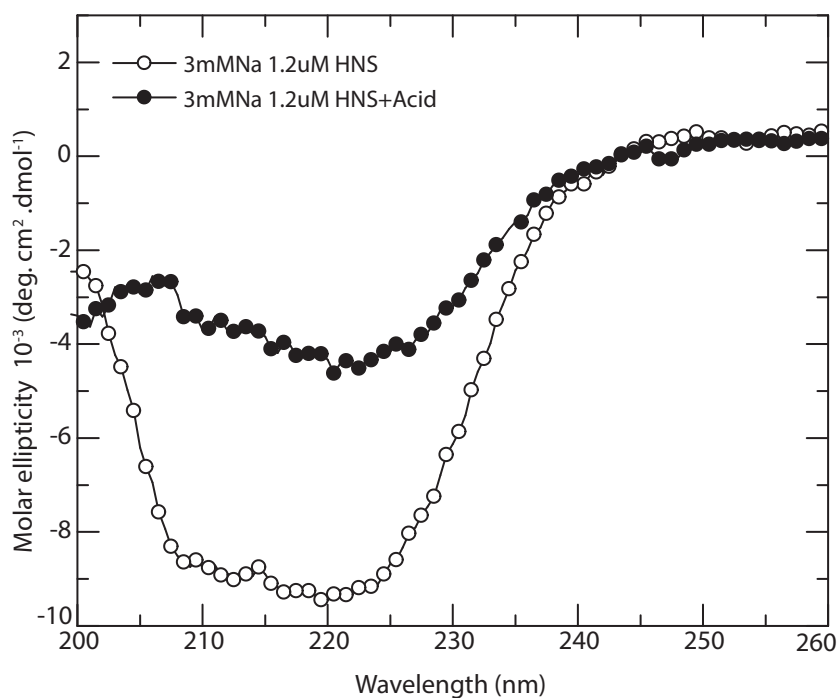


**Fig. 2.15** Circular dichroism spectrum of protein in 3mM NaCl before and after adding the acid. After adding acid protein becomes denatured. Open circles are protein in 10mM Tris-HCl and closed circles are after adding acid.



### 2.6.3 Size Exclusion Chromatography (SEC)

SEC, also called gel filtration (GF), was used for desalting the buffer<sup>[13]</sup>. In SEC, molecules are separated based on their size. The column is made up of sephadex, dextran, agarose, and polyacrylamide, or mixtures of these chemicals, like superdex (dextran + agarose). The medium consists of spherical particles with pores, and with physical and chemical inertness and stability. Fig. 2.16 shows the small particles go to pores of the stationary phase with a lag in motion; on the other hand, bigger particles are excluded from going into pores of the stationary phase and instead pass through the interstitial space of the stationary medium. The mid-range particle goes half way into the pores of the stationary phase. In this way, biggest molecules are first eluted, followed by the smaller particles. The elution of the sample is best characterised by a distribution coefficient  $K_d$

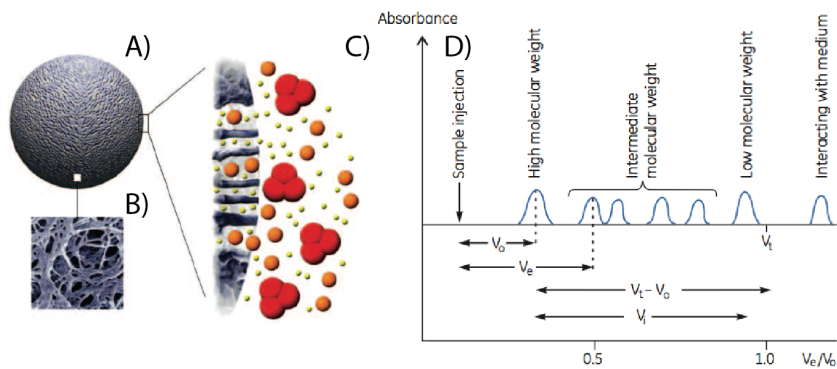


**Fig. 2.16** Structure of the beads in the SEC media and elution process. (A) Schematic picture of a bead. (B) electron microscopic enlargement of (A). (C) Schematic drawing of sample molecules diffusing into bead pores. Figure was adapted from GE website

### 2.6.3.1 Calibrating the column

If the molecule completely sieves from the column then  $K_d=0$ , and if the molecule goes in to pores of the stationary phase, lags, and comes last, then its  $K_d=1$ . For all intermediate molecules  $0 < K_d < 1$ . Let the volume of the mobile phase be  $V_0$ , *i.e.* the elution volume of the molecules, which are larger than the pore size of the gel. The volume of the stationary phase is  $V_s$  and the volume of the buffer inside the matrix is  $V_i$ , which is available to small molecules. It is clear that  $V_i$  is the elution volume of molecules that distribute freely between the mobile and stationary phases, minus the void volume.  $K_d$  represents the fraction of the stationary phase that is available for diffusion of a given molecular species:

$$K_d = \frac{V_e - V_0}{V_t - V_0 - V_{gelmatrix}} = \frac{V_e - V_0}{V_i} \quad (2.1)$$

In practice, the volume  $V_s$  or  $V_i$  stationary phase defined in the above equation is rather difficult to determine. It is much more convenient to substitute the term  $(V_t - V_0)$  for  $V_s$ , in which case  $k_{av}$  is defined as

$$K_{av} = \frac{V_e - V_0}{V_t - V_0} \quad (2.2)$$

For a given gel  $K_{av}/K_d$ , is a constant and is independent of the nature of the solute or its concentration.  $K_{av}$  is easily determined and, like  $K_d$ , defines solute behaviour independently of the bed dimensions and packing. Fig. 2.16(D) shows the different terms involved in the equations (2.1 and 2.2).  $K_{av}$  is related to the size of molecules as  $K_{av} = A \log M_r + B$ , where

### 2.6.3.1. Calibrating the column

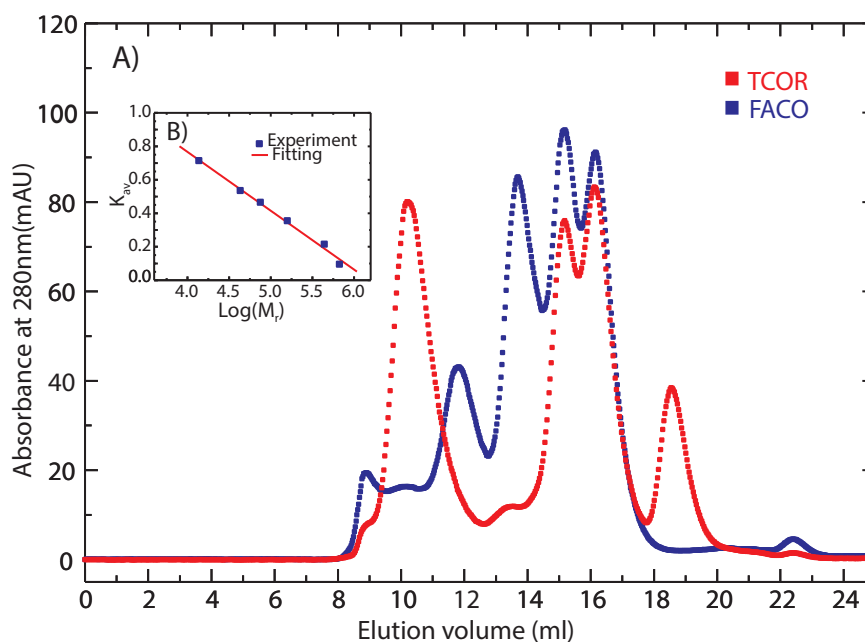


**Fig. 2.17** Calibration graph of SEC column with standards. The standards are T (Thyroglobulin  $M_r$  669 kDa), C (Conalbumin  $M_r$  75 kDa), O (Ovalbumin  $M_r$  43 kDa), R (Ribonuclease A  $M_r$  13.7 kDa) and F (Ferritin  $M_r$  440 kDa), A (Aldolase  $M_r$  158 kDa) and Blue dextran  $M_r$  2000. TCOR and FACO are in red and blue colour respectively. Insert shows calibration graph of  $K_{av}$  versus  $\text{Log}(M_r)$ .

A and B are constants and  $M_r$  is the molecular weight of the protein. Plot the  $K_{av}$  versus  $\log M_r$  using known molecular weight proteins, and one obtains the unknown protein molecular weight. Fig. 2.17 is a calibration graph with standards. Calibration was done with two standard samples with 500  $\mu\text{L}$  volume. The standards are T (Thyroglobulin  $M_r$  669 kDa), C (Conalbumin  $M_r$  75 kDa), O (Ovalbumin  $M_r$  43 kDa), R (Ribonuclease A  $M_r$  13.7 kDa) and F (Ferritin  $M_r$  440 kDa), A (Aldolase  $M_r$  158 kDa) and Blue dextran  $M_r$  2000. For best calibration, Conalbumin  $M_r$  75 kDa, Ovalbumin  $M_r$  43 kDa, and Blue dextran  $M_r$  2000 kDa are taken in both samples. Dextran has a very high molecular weight compared with all the components in the samples, so it was washed out as the first elute. This

### 2.6.3.2. Oligomerisation of H-NS

signal of the peak ensures that both samples are loaded at the same time, and it gives the value of  $V_0$  in Eq. 2.2. The calibration graph is plotted by using  $V_e$ ,  $V_0$  and  $V_t$  for  $K_{av}$  and  $\log(M_r)$ . An insert in Fig. 2.17 shows the final calibration graph for two standard samples. The values obtained from the graph are slope  $A = -0.35 \pm 0.01$  and intercept  $B = 2.17 \pm 0.08$ .

### 2.6.3.2 Oligomerisation of H-NS

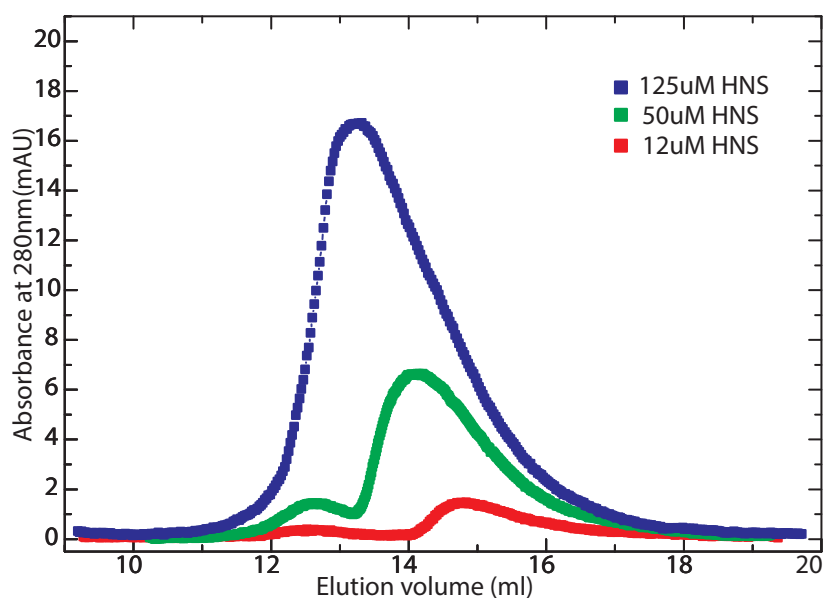


**Fig. 2.18** Size Exclusion Chromatography of H-NS. The concentrations are  $12 \mu\text{M}$  (red),  $50 \mu\text{M}$  (green),  $125 \mu\text{M}$  (blue).

The N-terminal of the H-NS is responsible for dimerisation or Oligomerisation. Falconi *et al.* found that in solution H-NS is in predominately dimeric form above concentrations of  $10 \mu\text{M}$ , and that at even higher concentrations a significant amount of H-NS can be found in trimers and tetramers<sup>[14]</sup>. Recent studies by Leonard also confirm this<sup>[15]</sup>. The Oligomerisation is needed for the filamentation process of the H-NS. Fig. 2.18 shows the size exclusion chromatography of the H-NS. H-NS has a molecular

#### 2.6.4. Isolation and purification of HU

---

weight 15.5 kDa, so its  $K_{av}$  is about 0.7. The molecular weights corresponding to 3 peaks are 84, 120, and 175 kDa for 12, 50, and 125  $\mu$ M H-NS, which directly shows the oligomer formation of H-NS. The graph is also skewed towards the less eluted volume side, that is higher molecular weight. This SEC experiment confirms the oligomer formation of the H-NS protein

#### 2.6.4 Isolation and purification of HU

Purification of HU was done in Associate Professor Yan Jie's lab, Department of Physics, NUS. DNA plasmid pET Duet-1, which was designed for coexpressing two genes  $HU\alpha$  and  $HU\beta$  ( $HU\alpha$  tagged with N terminal histag), was transformed into *Escherichia Coli BL21*. The cells were grown at 37°C in a Luria Broth medium containing ampicillin, and the overproduction of HU was induced by the addition of 4 mM IPTG at 20°C. The cells were lysed with a high pressure homogeniser. The lysate was cleared by centrifugation at 35,000 rpm for 30 min at 4°C. The lysate was then diluted with a buffer containing 250 mM NaCl, 10 mM Tris, and 10% glycerol and loaded into a His-trap HP column. The column was eluted with imidazole. The protein was further purified using a Superdex 75 gel filtration column and dispersed in a buffer comprising 500 mM KCl and 10 mM Tris. The concentration was determined by UV absorbance at 230 nm with  $A_{230} = 2.3$  per 1 g of HU per L<sup>[16]</sup>.

## 2.7 Bibliography

- [1] Dai, L. & Doyle, P. S. (2013) Macromolecules **46**, 6336–6344. 48
- [2] Rye, H. S., Yue, S., Wemmer, D. E., Quesada, M. A., Haugland, R. P., Mathies, R. A., & Glazer, A. N. (1992) Nucleic Acids Res. **20**, 2803–2812. 49
- [3] Glazer, A. N. & Rye, H. S. (1992) Nature **359**, 859–861. 49
- [4] Larsson, A., Carlsson, C., Jonsson, M., & Albinsson, B. (1994) J. Am. Chem. Soc. **116**, 8459–8465. 49
- [5] Bennink, M. L., Schärer, O. D., Kanaar, R., Sakata-Sogawa, K., Schins, J. M., Kanger, J. S., de Groot, B. G., & Greve, J. (1999) Cytometry **36**, 200–208. 49
- [6] Günther, K., Mertig, M., & Seidel, R. (2010) Nucleic Acids Res. **38**, 6526–6532. 49
- [7] Reuter, M. & Dryden, D. T. (2010) Biochem. Bioph. Res. Co. **403**, 225–229. 49
- [8] Zhang, C., Shao, P., van Kan, J. A., & van der Maarel, J. R. C. (2009) Proc. Natl. Acad. Sci. U.S.A. **106**, 16651–16656. 49
- [9] Watt, F., Breese, M. B., Bettiol, A. A., & van Kan, J. A. (2007) Mater. Today **10**, 20–29. 50
- [10] Tegenfeldt, J., Prinz, C., Cao, H., Chou, S., Reisner, W., Riehn, R., Wang, Y., Cox, E., Sturm, J., Silberzan, P., & Austin, R. (2004) Proc. Natl. Acad. Sci. U.S.A. **101**, 10979–10983. 58

## Bibliography

---

- [11] Wilson, K. M. & Walker, J. M. (2010) Principles and techniques of biochemistry and molecular biology (Cambridge University Press). 60
- [12] Tanaka, K., Yanada, H., Yoshida, T., & Mizuni, T. (1991) Agricultural and Biological Chemistry **55**, 3139–3141. 62
- [13] Porath, J. & Flodin, P. (1959) Nature **183**, 1657–1659. 70
- [14] Falconi, M., Colonna, B., Prosseda, G., Micheli, G., & Gualerzi, C. O. (1998) EMBO J. **17**, 7033–7043. 73
- [15] Leonard, P. G., Ono, S., Gor, J., Perkins, S. J., & Ladbury, J. E. (2009) Mol. MicroBiol. **73**, 165–179. 73
- [16] Krylov, A. S., Zasedateleva, O. A., Prokopenko, D. V., Rouviere-Yaniv, J., & Mirzabekov, A. D. (2001) Nucleic Acids Res. **29**, 2654–2660. 74

## Chapter 3

# Effect of H-NS on the elongation and compaction of single DNA molecules in a nanospace

### 3.1 Introduction

Heat-stable nucleoid-structuring protein (H-NS, 15.6 kDa, *pI* 7.5) is implicated in transcriptional repression (gene silencing) as well as organisation of the bacterial genome<sup>[1]</sup>. H-NS binds and oligomerises along dsDNA to form a semi-rigid nucleoprotein filament, increases the thermal stability of the duplex, and inhibits transcription<sup>[2,3]</sup>. The histone-like function of H-NS in chromosome organisation is poorly understood. It has been proposed that the compaction into the nucleoid is related to, among others, DNA super-



coiling and osmotic stress through macromolecular crowding. Like-charge attraction between distal DNA segments by binding protein (bridging) is also thought to be important<sup>[4]</sup>. Indeed, it has been shown that H-NS reduces the physical extent of circular plasmids through side-by-side binding of opposing segments<sup>[5]</sup>. Divalent ions such as magnesium and calcium have been reported to play a pivotal role in H-NS mediated bridging of DNA<sup>[6]</sup>. However, H-NS does not behave like a regular condensation agent, because, to the best of our knowledge, it has never been reported to compact DNA into a globular form (condensation) in physiological conditions<sup>[7]</sup>.

Advances in nanofabrication have made it possible to fabricate quasi one-dimensional channel devices with cross-sectional diameters on the order of tens to hundreds of nanometers. These channels serve as a platform for studying, single DNA molecules<sup>[8,9]</sup>. Furthermore, confinement in a nanospace results in significant modification of certain important biophysical phenomena, such as the knotting probability of circular DNA and the effect of macromolecular crowding<sup>[10,11,12,13]</sup>. In particular, it was shown that DNA can be compacted into a condensed form for over-threshold concentrations of dextran or like-charged proteins such as bovine serum albumin and hemoglobin. Here, we report the effect of H-NS in conjunction with confinement inside a nanochannel on the conformation and compaction of DNA. For this purpose, we have done two different, but related series of experiments. In the first series, we focus on equilibrium properties of DNA molecules that have been pre-incubated with H-NS. In the second series, the dynamic, conformational response of DNA molecules immediately following exposure to H-NS is investigated. Super-resolution fluorescence imaging of H-NS in living *Escherichia coli* cells has shown that it is clustered within

the nucleoid with a diameter of a few hundred nanometers<sup>[14]</sup>. This diameter is comparable to the diameters of our channel systems. Accordingly, we surmise that our results for nanochannel confined DNA have implications for gene silencing and chromosome organisation.

For the first type of experiments, T4-DNA (166 kbp) was incubated in buffers of various ionic composition and various concentrations of H-NS for at least 24 h. Some of the buffers also included divalent magnesium ions. The DNA molecules were stained with YOYO-1 with an intercalation ratio of 100 base-pairs per dye molecule. For such a low level of intercalation, the distortion of the secondary DNA structure is minimal. Furthermore, there is no appreciable effect on the bending rigidity, as inferred from previously reported measurements of the extension of DNA in nanochannels with different concentrations of dye<sup>[15]</sup>. The pre-incubated molecules were subsequently electrophoresed into a single array of long and rectangular nanochannels with average cross-sectional diameters of 200 or 250 nm. Our chips are made of polydimethylsiloxane (PDMS) casted on a high quality master stamp, obtained by proton beam writing and UV lithography<sup>[15,16,17]</sup>. The advantage of this technology is that about a hundred replicas can be made with a single stamp, so that a fresh chip can be used for every experiment. Once the pre-incubated molecules are equilibrated after switching off the electric field, their extensions along the direction of the channel (stretch) were measured with fluorescence microscopy. Depending on solution conditions, we observed an elongation or contraction of the stretch with respect to the protein-free state. Furthermore, as in the case macromolecular crowding, we observed a collapse to a condensed form for over-threshold concentrations of H-NS.

The second type of experiments was done with our recently developed cross-channel device<sup>[18]</sup>. As shown by its layout in Fig. 3.1, a centrally located grid of rectangular nanochannels is connected to two pairs of loading reservoirs with a set of microchannels. The grid features two arrays of parallel nanochannels in a perpendicular configuration. The average cross-sectional diameters of the channels pertaining to the respective arrays are 225 and 175 nm. DNA immersed in the relevant buffer, but without H-NS, was electrophoresed into the device through the array of wider channels in one direction. Once the molecules were equilibrated inside the channels after switching off the electric field, a buffered solution of H-NS was flushed through the intersecting array of channels in the other direction with a microinjector using a minimal pressure. During and after the flush, the conformational response of the DNA molecules was monitored with fluorescence microscopy. These experiments were done with a range of H-NS concentrations covering the critical concentration for condensation. Accordingly, the collapse to the condensed form following exposure to H-NS was observed in real time. Our observations will be analysed in terms of current knowledge of the binding properties of H-NS, in particular filamentation of H-NS on DNA and H-NS mediated like-charge attraction of distal DNA segments. However, it will be shown that, besides binding, confinement is of paramount importance in H-NS mediated control of the conformation and compaction of DNA.

## 3.2 Materials and Methods

### 3.2.1 Isolation and Purification of H-NS

K1746 bacteria transformed with pHOP-II were grown on a Luria Broth plate with ampicillin (50 mg per L). A single colony was taken to grow a starter culture in Luria Broth medium containing ampicillin at 310 K for 8 h ( $OD_{600} = 0.6$ ). The starter culture was then diluted 1,000 times into Luria Broth medium containing ampicillin and grown at 310 K for 2 h with vigorous shaking (280 rpm,  $OD_{600} = 0.6$ ). Protein expression is induced by addition of isopropylthio- $\beta$ -galactoside (IPTG) to a final concentration of 1 mM. The bacterial cells were harvested by centrifugation at 6,000 g for 15 min at 277 K. The pellet was suspended in a buffer comprising 20 mM Tris-HCl, pH 7.2, 1 mM EDTA, 5 mM  $\beta$ -mercaptoethanol, 10% glycerol, 100 mg phenylmethylsulfonyl fluoride (PMSF) per L, 2 mM benzamidine, 100 mM  $NH_4Cl$ , and 1 mg Pefabloc SC per L, subsequently lysed with a sonicator (Sonic vibra) at 10,000 Joules, and followed by treatment with DNase-1 and RNase-A (Promega) on ice for 30 min. After centrifugation at 15,000 g for 2.5 h at 277 K, the supernatant was loaded onto a phospho-cellulose (P11, Whatman) column (XK 50/30) equilibrated with 100 mM  $NH_4Cl$ , 1 mM EDTA, 10 % glycerol, 20 mM Tris-HCl, pH 7.2 with an AKTA explorer chromatography system (GE Life Sciences, columns and chromatography media were also purchased from GE). The column was washed with the above mentioned 100 mM  $NH_4Cl$  buffer and the protein was eluted with a gradient to 1 M  $NH_4Cl$ . The elute was subsequently dialyzed against 100 mM NaCl, 1 mM EDTA, 10 % glycerol, 20 mM Tris-HCl, pH 7.2. The

### 3.2.2. Sample preparation

---

dialyzed sample was loaded onto a heparin column equilibrated with the above mentioned 100 mM NaCl buffer followed by elution in a gradient to 1 M NaCl. At each step, the purity of H-NS was monitored by SDS-page gel chromatography. The secondary structure of H-NS in the prevalent buffers was confirmed with UV circular dichroism measurements.

### 3.2.2 Sample preparation

T4-DNA was purchased from Nippon Gene, Tokyo and used without further purification. The integrity of T4-DNA was verified with pulsed gel electrophoresis. No fragments of ones to tens of kbps were observed. YOYO-1 was purchased from Invitrogen, Carlsbad, CA. T4-DNA was stained with YOYO-1 with an intercalation ratio of 100 base-pairs per dye molecule. No anti-photo bleaching agent was used. Samples were prepared by dialyzing solutions of DNA against 10 mM Tris-HCl with the relevant concentration of NaCl and/or MgCl<sub>2</sub> in micro-dialyzers. Solutions of H-NS in the same buffer were also prepared. The Tris-HCl concentration is 10 mM Tris adjusted with HCl to pH 7.5, *i.e.* 8.1 mM TrisCl and 1.9 mM Tris). The ionic strength of the buffer was calculated with the Davies equation for estimating the activity coefficients of the ions and a dissociation constant  $pK = 8.08$  for Tris. For the measurement of the pre-equilibrated DNA molecules, solutions of H-NS and DNA were subsequently mixed and incubated for 24 h at 277 K. The final DNA concentration is 3 mg per L. Fluorescein 5-isothiocyanate (FITC) was purchased from Sigma-Aldrich. H-NS was labeled with FITC following standard protocol<sup>[19]</sup>. For the determination of the time required for the protein influx, a solution of 1  $\mu$ M of FITC labeled

H-NS in T-buffer was prepared.

### 3.2.3 Fabrication of nanofluidic chips

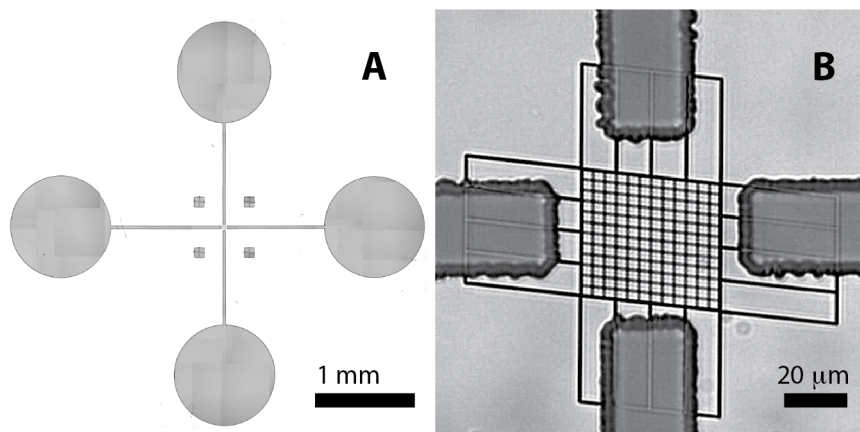


**Fig. 3.1** (A) Bright field optical image of the bonded cross-channel array device. The loading reservoirs are connected to the central grid of nanochannels by microchannels in SU-8 resin. (B) Optical image of the master stamp featuring the nanochannel grid with connecting microchannels. The channels have a uniform height of 200 nm and widths of 250 and 150 nm in the two perpendicular directions, respectively. The wider and narrower channels are laid on a rectangular grid and separated by 4 and 3.5  $\mu\text{m}$ , respectively<sup>[18]</sup>.

The nanofluidic devices were fabricated by replication in PDMS of patterned master stamps<sup>[15,17]</sup>. The nanochannels were made in HSQ resist (Dow Corning, Midland, MI) using a lithography process with proton beam writing<sup>[16]</sup>. Chips with two different channel layouts were made. For the measurement of the pre-incubated DNA molecules, a single array of nanochannels is connected to two punched loading reservoirs through a superposing set of microchannels made in SU-8 resin with UV lithography. For the investigation of the response to a change in solution conditions, a cross-channel device was made. In the latter device, there are two intersecting arrays of nanochannels connected to two pairs of loading

### 3.2.4. Single-channel array

---

reservoirs. The heights and widths of the positive channel structures on the stamps were measured with atomic force microscopy (Dimension 3000, Veeco, Woodbury, NY) and scanning electron microscopy, respectively. For the single-array device, two stamps were made featuring nanochannels of length  $60\ \mu\text{m}$  and rectangular cross-sections of  $150 \times 250$  and  $200 \times 300\ \text{nm}^2$ , respectively. The cross-sections pertaining to the two intersecting arrays of the cross-channel device are  $150 \times 200$  and  $200 \times 250\ \text{nm}^2$ . The connecting microchannels have a width and height of  $20$  and  $5\ \mu\text{m}$ , respectively. The stamp was coated with a  $5\ \text{nm}$  thick Teflon layer to guarantee a perfect release of the replicated PDMS chips<sup>[20]</sup>. The stamps were replicated in PDMS followed by curing with a curing agent (Sylgard, Dow Corning) at  $338\ \text{K}$  for  $24\ \text{h}$ . The PDMS replica was sealed with a glass coverslip, after both substrates were plasma oxidised (Harrick, Ossining, NY).

### 3.2.4 Single-channel array

The pre-incubated and stained DNA molecules dispersed in the relevant solution were loaded into one of the two reservoirs connected to the single array of nanochannels. The DNA molecules were subsequently driven into the channels by electrophoresis. For this purpose, two platinum electrodes were immersed in the reservoirs and connected to an electrophoresis power supply with a relatively low voltage in the range  $0.1\text{-}10\ \text{V}$  (Keithley, Cleveland, Ohio). Once the DNA molecules were localized inside the nanochannels, the electric field was switched off and the molecules were allowed to relax to their equilibrium state for at least  $60\ \text{s}$ . The stained DNA molecules were visualized with a Nikon Eclipse Ti inverted fluores-

### 3.2.5. Cross-channel array

---

cence microscope equipped with a 200 W metal halide lamp, a filter set, and a 100 $\times$  oil immersion objective. The exposure time was controlled by a UV light shutter. Images were collected with an electron multiplying charge coupled device (EMCCD) camera (Andor iXon X3) and the extension of the DNA molecules inside the channels was measured with IMAGEJ software (<http://rsb.info.nih.gov/ij/>). For the intensity threshold, we have used two times the signal to background noise ratio.

### 3.2.5 Cross-channel array

The protein-free, stained DNA molecules were loaded into the two reservoirs connected to the array of 200  $\times$  250 nm<sup>2</sup> nanochannels. To maintain the balance in pressure, T-buffer (without DNA) was loaded into the other two reservoirs connected to the perpendicular, intersecting array of 200 $\times$ 150 nm<sup>2</sup> channels. The DNA molecules were subsequently driven into the channels by electrophoresis and allowed to relax for at least 60 s as described above. At preset times, solutions of H-NS are flushed through the array of 200  $\times$  150 nm<sup>2</sup> channels into the 200  $\times$  250 nm<sup>2</sup> channels using a microinjector with a minimal injection pressure of 0.5 kPa (Narishige, Tokyo). During and following the flush with the solution of H-NS, the stained DNA molecules were visualized and their extensions were analyzed as described above.



### 3.2.6 Monte Carlo simulation

In the Monte Carlo protocol, the chain is modelled as a string of  $(N + 1)$  beads, which are connected by  $N$  inextensible bonds of length  $l_b$ <sup>[21,22]</sup>. Furthermore, the model consists of bond bending energy, hard-sphere repulsion between beads, and hard-wall repulsion between the beads and the wall. If the centre of a bead is beyond the channel wall, the potential becomes infinitely large and the configuration is rejected. The effective channel diameter is hence the real diameter minus the diameter of the bead. The diameter of the bead was set equal to the bond length  $l_b$ , which is equivalent to the chain width  $w$ . We have done two series of simulations. In the first series, the bending rigidity is set to reproduce a persistence length  $P = 50$  nm. The contour length of the chain with widths  $w = 5, 7.5,$  or  $10$  nm was fixed at  $L = 8 \mu\text{m}$ . The second series was done for a range in persistence length  $P = 50\text{-}160$  nm, but with a single width  $w = 10$  nm and contour length  $L = 16 \mu\text{m}$ . In each Monte Carlo cycle, we carried out one crankshaft and one reptation move. The simulation started from a random conformation and reached equilibrium after  $10^7$  cycles. In the production run, we generated  $10^{10}$  cycles and recorded the conformation every other  $10^5$  cycles. For each conformation, we calculated the extension as the maximum span of the molecule along the channel axis. Finally, the extension was averaged over the ensemble of  $10^5$  conformations. We have verified that effects of finite contour length on the relative stretch are unimportant for the relevant range of channel diameters.

---

## 3.3 Results

### 3.3.1 Stretch of pre-incubated DNA

In the first series of experiments, T4-DNA molecules were incubated with the relevant buffer for at least 24 h before they were brought into the channels of the single-array device. Montages of images of single DNA molecules confined in rectangular channels with a cross-section of  $200 \times 300 \text{ nm}^2$  are shown in Fig. 3.2. The images refer to well-equilibrated conformations. After the electric field has been switched off, the molecules relax to their equilibrium state within 60 s. We have verified that there is no further change in the extension of the molecules for more than 3 h. Furthermore, we observed no difference in extension between molecules inserted by electrophoresis or pressure. Video imaging was started 5-10 min after the molecules were brought into the channels and lasted for another 10 min. The equilibrated stretch in the longitudinal direction of the channel depends on the buffer conditions. In a buffer with a moderate ionic strength of around 11 mM (T-buffer with 3 mM NaCl, T-buffer is 8.1 mM TrisCl and 1.9 mM Tris,  $pH$  7.5), the DNA molecules elongate with increasing concentration of H-NS. In the case of a buffer with a higher ionic strength of about 38 mM, the molecules are contracted with respect to the protein-free situation. In the presence of sub-millimolar concentrations of magnesium ions, the H-NS induced contraction is minimal, if not negligible. For over-threshold concentrations of H-NS, condensation of the DNA molecules into a compact form is observed. Condensed DNA is visible as a bright fluorescence spot and can easily be discerned from the extended form. In channels

### 3.3.1. Stretch of pre-incubated DNA

with a smaller cross-section of  $150 \times 250 \text{ nm}^2$ , we observed the same qualitative behaviour. There are quantitative differences however in the values of the stretch and critical concentration of H-NS for condensation. Note that differences in width and brightness between molecules of similar extension are related to effects of photo-bleaching and have no physical meaning.

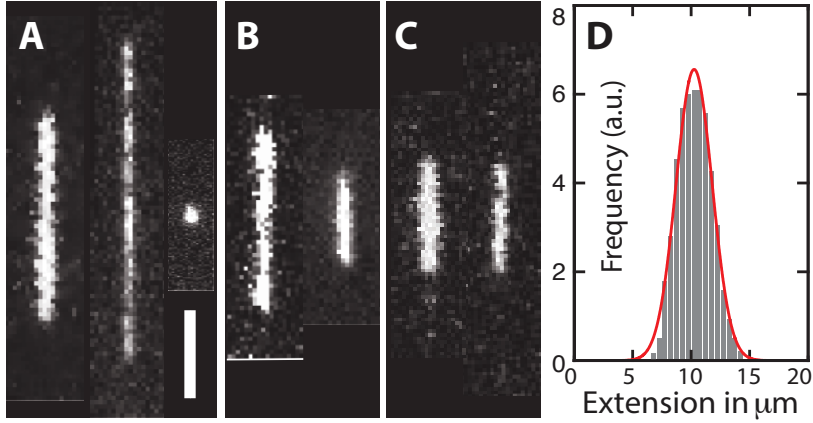


**Fig. 3.2** (A) Montage of fluorescence images of T4-DNA in T-buffer with 3 mM NaCl and confined in  $200 \times 300 \text{ nm}^2$  channels. T-buffer is 8.1 mM TrisCl and 1.9 mM Tris,  $pH$  7.5. The H-NS concentration is 0, 0.3, and  $0.6 \mu\text{M}$  from left to right. The scale bar denotes  $3 \mu\text{m}$ . (B) As in panel (A), but in T-buffer with 30 mM NaCl. The H-NS concentrations are 0 and  $0.3 \mu\text{M}$  from left to right. (C) As in panel (A), but in T-buffer with 3 mM NaCl and  $0.2 \text{ mM MgCl}_2$ . The H-NS concentrations are 0 and  $0.1 \mu\text{M}$  from left to right. (D) Distribution in extension of a population of 50 molecules in T-buffer with 3 mM NaCl and  $0.3 \mu\text{M}$  H-NS, inside  $200 \times 300 \text{ nm}^2$  channels, A Gaussian fit gives  $R_{||} = 10 \pm 2 \mu\text{m}$ .

We have measured the extension of the DNA molecules in channels with two different cross-sections:  $200 \times 300$  and  $150 \times 250 \text{ nm}^2$ . For each experimental condition, that is buffer composition, channel diameter, and H-NS concentration, we have used a fresh PDMS replica and measured around 50 molecules. The distribution in extension is close to Gaussian<sup>[23]</sup>. An example of such a distribution is also shown in Fig.3.2. Fragmented DNAs can easily be discerned, because their extensions clearly fall below

### 3.3.1. Stretch of pre-incubated DNA

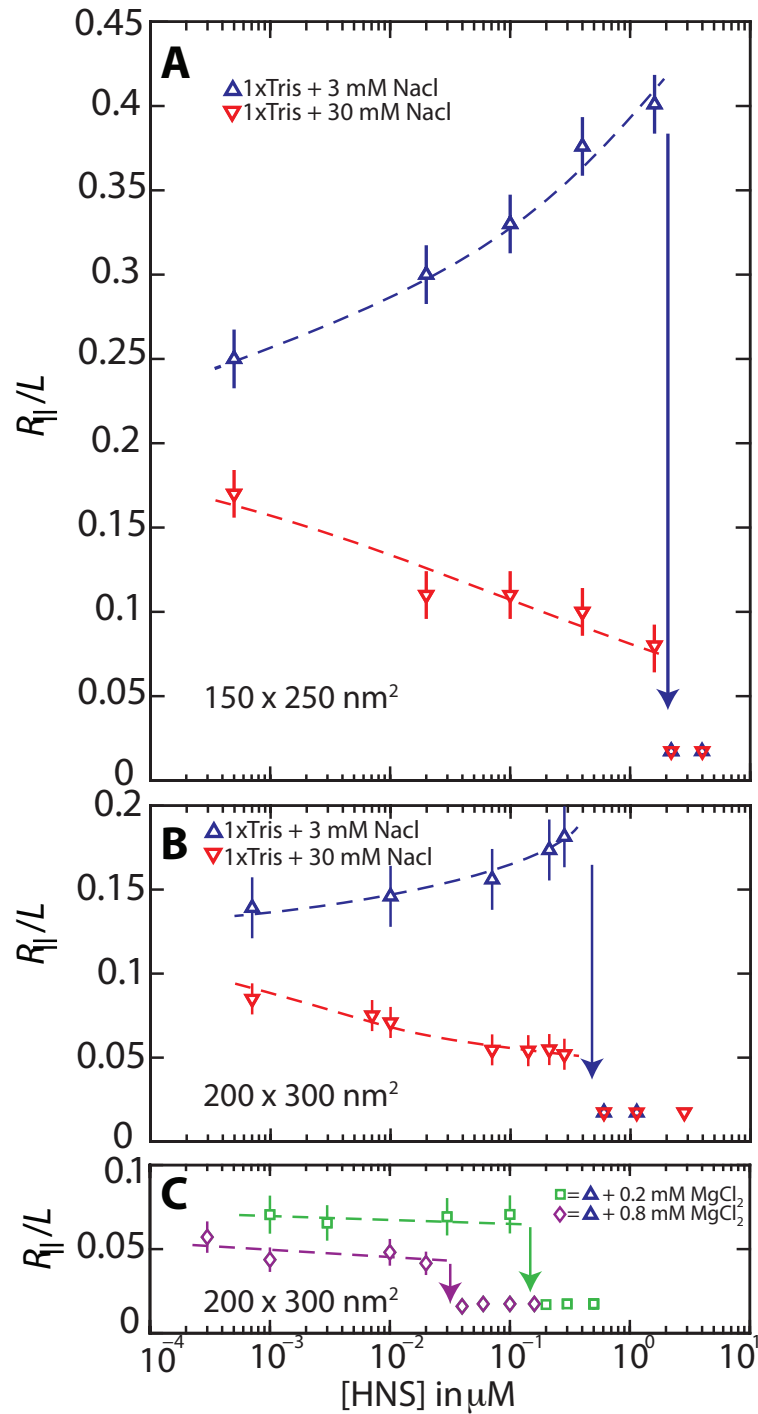


**Fig. 3.3** (A) Relative extension  $R_{||}/L$  of T4-DNA in T-buffer with 3 ( $\Delta$ ) or 30 ( $\nabla$ ) mM NaCl versus the concentration of H-NS. The molecules are confined in  $150 \times 250 \text{ nm}^2$  channels (B) As in panel (A), but in  $200 \times 300 \text{ nm}^2$  channels. (C) As in panel (A), but in T-buffer with 3 mM NaCl and 0.2 ( $\square$ ) or 0.8 ( $\diamond$ ) mM  $\text{MgCl}_2$ , inside  $200 \times 300 \text{ nm}^2$  channels. The dashed curves are drawn as an aid to the eye and the arrows denote the condensation thresholds.

### 3.3.1. Stretch of pre-incubated DNA

---

the values pertaining to the intact molecules. For the cut-off, we have used the mean value minus two times the standard deviation. Resolution broadening can be neglected, because the optical resolution is one order of magnitude smaller than the variance. The mean relative extension  $R_{\parallel}/L$ , that is the mean extension divided by the YOYO-1 corrected contour length of  $57 \mu\text{m}$ , is set out in Fig.3.3 as a function of the H-NS concentration. An enhanced stretch is observed if the molecules are bathed in a buffer of moderate ionic strength without divalent ions (T-buffer with 3 mM NaCl). In the case of a buffer of higher ionic strength (T-buffer with 30 mM NaCl), different behavior is observed. Now the molecules contract with increasing concentration of H-NS. The stretch is constant or slightly decreases with increasing H-NS concentration in the presence of 0.2-0.8 mM  $\text{MgCl}_2$ . Note that for sub-threshold concentrations of H-NS the relative extensions are in the range 0.05-0.4, which implies that the DNA molecules remain coiled. Furthermore, related to the stronger confinement, the stretch is more pronounced in the  $150 \times 250 \text{ nm}^2$  channel system.

For over-threshold concentrations of H-NS, the DNA molecules compact into a condensed form. This is facilitated by the confinement in the nanochannel, because we did not observe condensation in the feeding microchannels and/or the reservoirs of the chip. To the best of our knowledge, condensation of DNA by H-NS has not been reported before. In buffer composed of monovalent salts, the critical concentrations of H-NS for condensation are around 0.5 and  $2 \mu\text{M}$  H-NS for the  $200 \times 300$  and  $150 \times 250 \text{ nm}^2$  channel systems, respectively. The threshold shifts hence to a higher value with decreasing channel cross-sectional diameter. There is however no significant effect of the concentration of monovalent salts. On the other

### 3.3.2. Time-dependent conformational response

---

hand, the critical concentration for condensation are shifted downwards from, say, 0.05 to 0.03-0.1  $\mu\text{M}$  of H-NS in the presence of sub-millimolar concentrations of magnesium ions.

### 3.3.2 Time-dependent conformational response

The above described results refer to DNA molecules pre-incubated with H-NS for more than 24 h before they were brought into the nanochannels of the single-array device. In order to obtain more insight in the various mechanisms at hand, we have done a second series of experiments with the recently developed cross-channel device<sup>[18]</sup>. With the latter device, the conformational response of the DNA molecules to a change in environmental solution conditions can be investigated *in situ*. To avoid complications related to contraction prior to the collapse, we have used a buffer of moderate ionic strength and without divalent ions (T-buffer with 3 mM NaCl). In such a buffer, the pre-incubated DNA molecules are either elongated or condensed, depending on the concentration of H-NS. To cover the condensation phenomenon, we have done a series of experiments with a range of concentrations of H-NS through the threshold (0.8-1.6  $\mu\text{M}$ ).

Protein-free DNA molecules were electrophoresed into the array of wider  $200 \times 250 \text{ nm}^2$  channels of the cross-channel device. Filling the other two loading reservoirs with buffer minimized pressure gradients. Once the electric field is removed, the molecules equilibrate and remain stationary inside the array of wider nanochannels. The initial stretch is around 9  $\mu\text{m}$ . The H-NS containing buffer was loaded into the microinjector and subsequently flushed through the array of narrower  $150 \times 200 \text{ nm}^2$  channels

### 3.3.2. Time-dependent conformational response

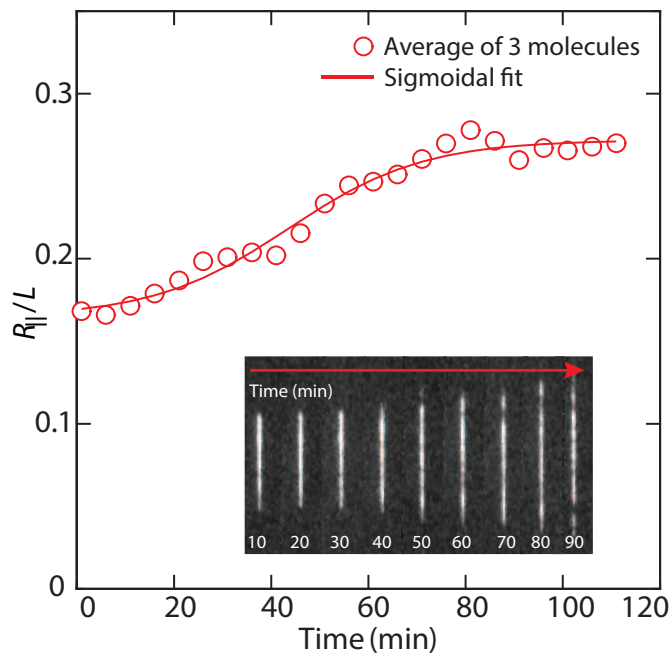


**Fig. 3.4** Elongation of T4-DNA following a flush with a solution of  $0.8 \mu\text{M}$  H-NS in T-buffer and  $3 \text{ mM}$  NaCl. The molecules are in  $200 \times 250 \text{ nm}^2$  channels and initially immersed in T-buffer with  $3 \text{ mM}$  NaCl. The red circles ( $\circ$ ) represents the average elongation of three different molecules. The solid curve ( $-$ ) represents a sigmoidal fit with a lag time of  $45 \text{ min}$ . The time-lapse series of fluorescence images (inset) illustrates the elongation following the flush. The start of the flush is at time zero. Notice the time scale of minutes.

into the wider channels with a pressure of about  $0.5 \text{ kPa}$ . Throughout the flush, the DNA molecules are imaged with fluorescence microscopy and were observed to remain inside the array of wider channels. The result pertaining to elongation with a flush of  $0.8 \mu\text{M}$  H-NS is shown in Fig. 3.4. Condensation following a flush with over-threshold concentrations of H-NS ( $1.0$ ,  $1.2$ , and  $1.6 \mu\text{M}$ ) is illustrated in Fig. 3.5. The threshold concentration for condensation inside the  $200 \times 250 \text{ nm}^2$  channels is  $0.9 \mu\text{M}$  H-NS. This value falls between the thresholds for pre-incubated DNA in slightly wider and narrower channels. We observed that the molecules remain mobile and that there is no H-NS-mediated sticking of DNA to the channel walls.

### 3.3.2. Time-dependent conformational response

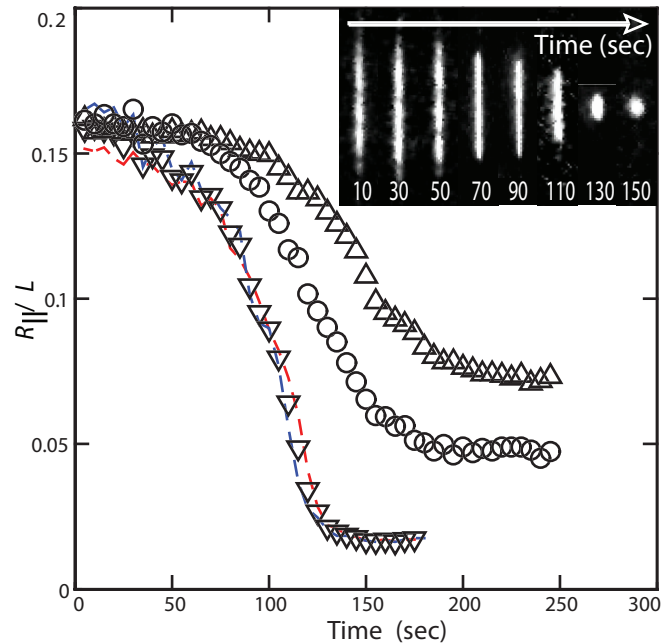


**Fig. 3.5** Condensation of T4-DNA following a flush with a solution of 1.0 ( $\Delta$ ), 1.2 ( $\circ$ ), and 1.6 ( $\nabla$ )  $\mu\text{M}$  H-NS in T-buffer with 3 mM NaCl. The molecules are in  $200 \times 250 \text{ nm}^2$  channels and initially immersed in T-buffer with 3 mM NaCl. The symbols represent averages pertaining to two different molecules for each buffer condition. Individual trajectories are denoted by the dashed curves (1.6  $\mu\text{M}$  H-NS only). The inset shows a time-lapse series of fluorescence images illustrating the compaction into the condensed form following a flush with 1.6  $\mu\text{M}$  H-NS. The start of the flush is at time zero. Notice the time scale of seconds.

In order to gauge the conformational response, it is necessary to determine the time required for the influx of protein. For this purpose, 1  $\mu\text{M}$  FITC-labelled H-NS was pipetted into one of the loading reservoirs connected to the array of narrow nanochannels. With fluorescence microscopy, it was monitored that the protein is transported through the microchannel and reaches the entrance of the nanochannels in about 30 s. Subsequently, the protein diffused through the narrow into the wide channels<sup>[18]</sup>. Fig 3.6 shows the time evolution of the integrated fluorescence intensity across the array of narrow channels. The buffer is progressively and uni-



### 3.3.2. Time-dependent conformational response

formly replaced within about 3 s from the moment H-NS enters the array of nanochannels. Eventually, the protein exits through the nanochannels into the microchannels connected to the other reservoirs. We have verified that, due to the continuous influx of H-NS, there is no appreciable drop in integrated fluorescence intensity and, hence, protein concentration for longer times. Furthermore, we did not observe adhesion of H-NS to the surface of PDMS.

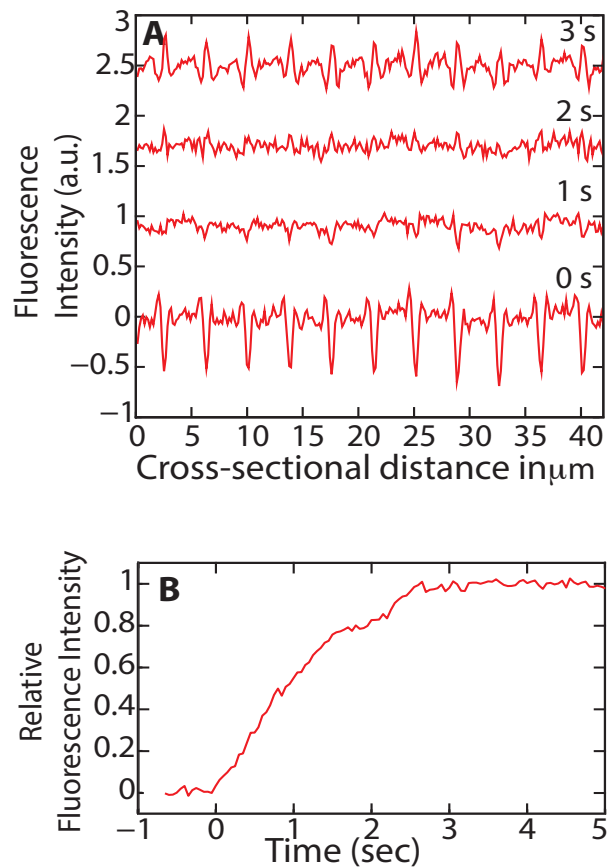


**Fig. 3.6** (A) Fluorescence intensity profile across the array of  $200 \times 250$  nm<sup>2</sup> channels imaged at the indicated times after injection of FITC-labeled H-NS through the intersecting array of  $150 \times 200$  nm<sup>2</sup> channels. The wider channels are separated by  $4 \mu\text{m}$ . (B) Integrated fluorescence intensity as a function of the elapsed time after injection. Time zero is defined as the time when the protein enters the channels and the fluorescence intensity starts to increase.

### 3.3.2. Time-dependent conformational response

---

As can be seen in the time-lapse series of fluorescence images and relative extensions in Fig. 3.4, for a sub-threshold concentration of H-NS the DNA molecules elongate in a sigmoidal fashion. We observed some variation in elongation pertaining to different molecules, but, overall, the rate and lag time are  $0.06 \pm 0.01 \text{ min}^{-1}$  and  $42 \pm 2 \text{ min}$ , respectively. The molecules reach the final stretch in around 90 min. These times are much longer than the time required for the influx of protein ( $<3 \text{ s}$ ). All molecules reach a final extension of around  $15 \mu\text{m}$ . With an extension prior to the flush of around  $9 \mu\text{m}$ , the stretch has increased by about 70%. The final extension falls between the extensions just prior to the collapse of pre-incubated DNA in slightly wider and narrower channels.

A time lapse series of fluorescence images captured after a flush with over-threshold concentrations of H-NS, as well as the corresponding relative extensions, are shown in Fig. 3.5. We have averaged the results obtained from two different DNA molecules for each buffer condition, because individual trajectories coincide within experimental error. The extensions decrease in a sigmoidal fashion and, eventually, level off at a level pertaining to the condensed form. The relative decrease in extension  $\Delta R_{\parallel}/L$ , decay rate  $R$ , and lag-time  $\tau_{lag}$  resulting from a fit of a sigmoid to the data are collected in Table. 3.1. With increasing concentration of H-NS, the rate and lag-time increases and decreases, respectively. Besides compaction time, the final extension of the condensed molecules inside the nanochannels depends on the concentration of H-NS. For 1.0, 1.2, and 1.6  $\mu\text{M}$  H-NS, the final extension is 4.0, 2.6, and 0.9  $\mu\text{m}$ , respectively. We have verified that there is no further decrease in extension for another 2 h.

### 3.3.3. Summary of observations

**Table. 3.1** Relative decrease in extension  $\Delta R_{\parallel}/L$ , decay rate  $R$ , and lag-time  $\tau_{lag}$  pertaining to condensation following exposure to an over-threshold concentration of H-NS

H-NS Conc.	$\Delta R_{\parallel}/L$	$R$ (s <sup>-1</sup> )	$\tau_{lag}$ (s)
1.0 $\mu\text{M}$	$0.087 \pm 0.002$	$0.048 \pm 0.002$	$144 \pm 2$
1.2 $\mu\text{M}$	$0.112 \pm 0.002$	$0.052 \pm 0.002$	$120 \pm 2$
1.6 $\mu\text{M}$	$0.141 \pm 0.004$	$0.069 \pm 0.004$	$100 \pm 2$

### 3.3.3 Summary of observations

For sub-threshold concentrations of H-NS, the molecules are either elongated or contracted with respect to the protein-free state. Elongation occurs in a monovalent buffer of moderate ionic strength. The final stretch is reached in about 90 min after exposure to H-NS. At higher ionic strength, the molecules contract. In the presence of sub-millimolar concentrations of magnesium ions, the H-NS induced contraction is minimal, if not negligible. DNA compacts into a condensed form for over-threshold concentrations of H-NS. The critical concentration depends on channel diameter (lower for wider channels), divalent salt (lower for sub-millimolar magnesium ions), but do not significantly depend on the concentration of monovalent salts. The time required for condensation after an exchange of buffer with H-NS is around a minute. Furthermore, the compaction time and the final extension of the condensates inside the channels depend on the concentration of H-NS, with shorter times and smaller extensions for higher concentrations of H-NS. We did not observe condensation of DNA with H-NS in the bulk phase and/or the microchannels of the chip in the prevalent solution conditions.

## 3.4 Discussion

### 3.4.1 Elongation by filamentation

H-NS is known to bind on DNA in a cooperative way and polymerizes along the contour to form a nucleoprotein filament<sup>[3]</sup>. The filamentation takes a few hours<sup>[6]</sup>. Furthermore, it has been shown that the persistence length  $P$  increases from the nominal value of 50 nm for bare DNA to around 140 nm in the presence of 4.0  $\mu\text{M}$  H-NS and 50 mM KCl<sup>[2]</sup>. With a DNA concentration of 3 mg per L, an H-NS concentration of 4.5  $\mu\text{M}$  corresponds with one H-NS dimer per base pair. Accordingly, with a range of four decades in H-NS dimer to base pair ratio, we cover the situation with sparsely bound H-NS on DNA for the lowest concentrations of H-NS to a fully coated nucleoprotein filament at H-NS concentrations exceeding, say, 1.0  $\mu\text{M}$ . The observed elongation in monovalent buffer of moderate ionic strength over a time span of 90 min is almost certainly due to filamentation with a concomitant increase in bending rigidity (stiffening). In order to verify this conjecture, we need to relate the stretch of the filament to its persistence length  $P$ . For this purpose, we have done Monte Carlo computer simulation of a wormlike chain confined in nanochannels of various cross-sectional diameter<sup>[21,22]</sup>.

For a self-avoiding, wormlike chain with persistence length  $P$  and width  $w$  in a wide channel with diameter  $D \gg P$ , Daoud and de Gennes' blob model predicts a scaling law  $R_{\parallel}/L \propto D^{-2/3} P^{1/3} w^{1/3}$ <sup>[24,25,26]</sup>. In particular, the scaling exponent for both  $P$  and  $w$  is predicted to be 1/3. The Monte Carlo simulation results for  $R_{\parallel}/L$  as a function of  $P$  for fixed  $w = 10$

### 3.4.1. Elongation by filamentation

nm as well as  $R_{\parallel}/L$  as a function of  $w$  for fixed  $P = 50$  nm are shown in Fig. 3.7. To a good approximation, the extension follows a power law in  $P$  and  $w$ , that is  $R_{\parallel}/L \propto P^{\alpha}w^{\beta}$ . The fitted values of the exponent  $\alpha$  depend on the value of the tube diameter  $D$ . Only for very wide channels with  $D = 400$  nm, the simulation result for  $\alpha$  approaches the prediction of blob theory. On the other hand, the simulation results for  $\beta$  are always close to the value given by the blob model, irrespective channel diameter.

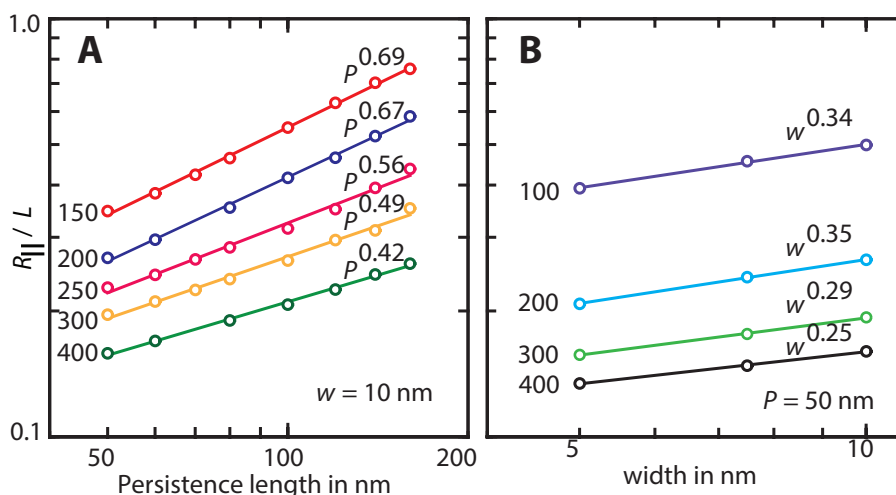


**Fig. 3.7** Monte Carlo simulation results. (A) Monte Carlo results of the relative extension  $R_{\parallel}/L$  versus persistence length  $P$  for a chain with cross-sectional diameter  $w = 10$  nm. (B) As in panel (A), but for the relative extension versus  $w$  for a chain with  $P = 50$  nm. The channel diameters and fitted scaling exponents are indicated.

The width of the filament is expected to be around 10 nm, as estimated from the diameter of the duplex (2 nm) and the diameter of H-NS (3.5 nm). In the absence of more detailed knowledge about the structure of the filament, we ignore a possible dependence of  $w$  on the concentration of H-NS. For the interpretation of the elongated stretch in terms of an increase in  $P$ , we accordingly use the Monte Carlo results obtained for  $w=10$  nm. The

### 3.4.1. Elongation by filamentation

scaling exponents  $\alpha = 0.56$  and  $0.67$  for the  $250$  and  $200$  nm, respectively. The increase in  $P$  with increasing H-NS concentration can then be obtained from  $P/P_0 = (R_{\parallel}/R_{\parallel}^0)^{1/\alpha}$ , with  $P_0$  and  $R_{\parallel}^0$  the persistence length and stretch for the protein-free state in otherwise the same conditions, respectively. The results are shown in Fig. 3.8. With increasing concentration of H-NS,  $P$  increases from the value pertaining to bare DNA ( $60$  nm in  $10$  mM salt<sup>[26,27]</sup>) to about  $130$  nm just prior to the collapse to the condensed form. This increase in  $P$  is in good agreement with the one reported in the literature obtained in  $50$  mM KCl<sup>[2]</sup>. Furthermore, the agreement of  $P$  obtained from channels of two different cross-sections confirms the scaling exponent  $\alpha$  and the cancellation of unknown, channel width dependent pre-factors in the relevant ratio of the extensions.

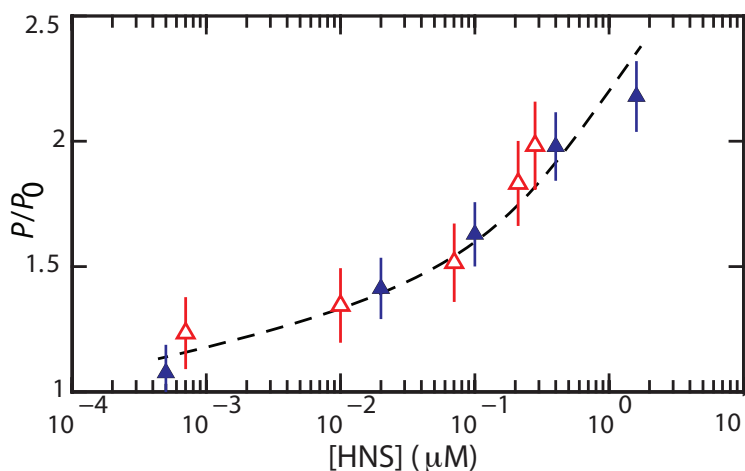


**Fig. 3.8** Relative persistence length  $P/P_0$  of T4–DNA in T-buffer with  $3$  mM NaCl and confined in  $150 \times 250$  ( $\blacktriangle$ ) and  $200 \times 300$  ( $\triangle$ ) nm<sup>2</sup> channels versus the concentration of H-NS. The dashed line is drawn as an aid to the eye.

Elongation of nano-confined DNA by crowding with dextran was reported before<sup>[11,12,13]</sup>. This effect was interpreted in terms of depletion of DNA segments and volume occupancy by neutral nanoparticles in the in-

### 3.4.2. Contraction by bridging

---

terfacial region next to the channel wall. Depletion can also play a role in the elongation of the nucleo-protein filament. However, such a role is minor at best, because the elongation of DNA induced by H-NS is more pronounced despite the fact that the concentrations of H-NS are an order of magnitude lower than those of dextran. Furthermore, unlike the situation for dextran, the molecules contract in a buffer of higher ionic strength.

### 3.4.2 Contraction by bridging

Another aspect is the disappearance of the elongation in the presence of sub-millimolar concentrations of magnesium ions and the contraction in a monovalent buffer of higher ionic strength. An increase in ionic strength reduces the binding efficiency of H-NS<sup>[28,29]</sup>. However, in the present range of salt concentrations (below 50 mM) the concomitant effect on the bending rigidity of the filament is moderate<sup>[2]</sup>. Furthermore, an explanation of a *contraction* with respect to the protein-free state in terms of a decrease in bending rigidity requires a value of  $P$  less than the one pertaining to bare DNA. Although this can be envisaged by, for instance, sharp bends or kinks in the duplex, a more plausible explanation is H-NS mediated side-by-side binding of distal segments of the DNA molecule (bridging). In atomic force microscopy and single-molecule manipulation studies, bridging was observed to be induced by divalent ions such as magnesium and calcium<sup>[5,6]</sup>. Here, we show that for DNA in a nanochannel the switch is merely controlled by screened electrostatics through a variation in the concentration of monovalent salt. The enhanced sensitivity of the conformation of the filament to the concentration and ionic composition of the

supporting medium is plausibly related to confinement induced segment orientation order (see below).

Nanochannel confined DNA was previously observed to contract in the presence of bovine serum albumin or hemoglobin irrespective of the ionic strength<sup>[13]</sup>. The latter contraction was explained by depletion of like-charged protein in the interior of the DNA coil and the concomitant osmotic pressure gradient. Since H-NS is net electroneutral at pH 7.5<sup>[30]</sup>, such a mechanism does not explain the switch from elongation to contraction with a change in the ionic composition and/or concentration of the buffer.

### 3.4.3 Condensation

A unique feature of the nanoconfinement is the compaction of DNA into a condensed form for over-threshold concentrations of H-NS. Condensation of DNA in a nanochannel by crowding with dextran as well as like-charged proteins has been reported before<sup>[11,13]</sup>. A fundamental difference is the critical concentration of the crowder or like-charged protein in the range of tens to hundreds of micromolars. In the case of H-NS in monovalent buffer, the critical concentration is at least one order of magnitude less and around one micromolar. This concentration corresponds to a fully coated nucleoprotein filament. The threshold concentration for the filament (pre-incubated DNA) is however about the same as the one observed for bare DNA following exposure to H-NS. Furthermore, the time scale of filamentation (hours) is much longer than the one for condensation (minutes). Accordingly, condensation is not related to filamentation *per se*, but to H-NS mediated attraction of like-charged, distal DNA segments.



Such a notion is also supported by the order of magnitude downward shift in threshold concentration in the presence of magnesium ions, which are known to promote the formation of H-NS bridges<sup>[5,6]</sup>. In this respect, H-NS acts as a multivalent condensing ligand such as polyamines, despite its net neutral charge. Indeed, the threshold concentration and final extension of the condensates for H-NS are similar to those obtained for protamine in the same cross-channel device<sup>[18]</sup>. Protamine induced condensation occurs however markedly faster on a time scale of a few seconds. Another important difference is that H-NS only facilitates condensation once the molecule is confined in a nanospace, whereas protamine also condenses DNA in the bulk phase<sup>[31]</sup>.

An effective attractive interaction by bridging ligands requires the juxtaposition of two almost parallel DNA segments<sup>[32]</sup>. Once the segments are skewed, the contact area is reduced and the attraction disappears. A plausible mechanism for the nanochannel-facilitated condensation is the increase in contact pairs of (almost) parallel-aligned and juxtaposed segments due to orientation order imposed by the channel walls. The critical concentration for condensation hence depends on two factors: the orientation order and probability of a contact. With decreasing channel diameter, the orientation order increases. Concurrently, the contact probability decreases, because the correlation length of the volume interaction is on the order of the channel diameter. In the blob model, the contact probability is proportional to the number of segments per blob, that is  $\propto D^{5/3}$  with diameter  $D$ <sup>[24]</sup>. The increase in critical concentration with decreasing channel diameter can hence be explained by a decrease in contact probability despite the increase in orientation order.

The decrease in extension and eventual condensation following exposure to over-threshold concentrations of H-NS is sigmoidal Fig.3.5. In a coarse grained simulation model, it was seen that DNA compaction is controlled by competing factors<sup>[33]</sup>. These factors include several binding modes of H-NS to DNA and confinement to a planar interface. In particular, it was observed that additional bridges are preferentially formed at sites close to a first bridge, provided that other H-NS dimers are available. The first bridge accordingly act as a seed to propagate compaction. Such a mechanism in which a dimer D is converted into a bridge B can be represented by an auto-catalysed reaction



with  $k^+$  and  $k^-$  being the rate constants for bridge formation and destruction, respectively. The concentration of dimers  $c_D$  can be considered constant due to the continuous influx of protein. A sigmoidal increase in concentration of bridges is obtained from integration of the logistic rate equation,

$$c_B(t) = \frac{K_{c_D}}{1 + \exp(-k^+ c_D t)(K_{c_D}/c_B^\circ - 1)} \quad (3.2)$$

with seed concentration  $c_B^\circ$  at  $t = 0$  and equilibrium constant  $K = k^+/k^-$ . One may assume that the decrease in extension of the DNA molecule inside the nanochannel is proportional to the density of bridges. The decay rate  $R = k_{c_D}^+$  and maximal decrease in extension  $\Delta R_{\parallel} \propto K_{c_D}$  should then be proportional to the concentration of protein. As shown by the relevant entries in Table. 3.1, this proportionality is indeed observed within experi-

### 3.4.3. Condensation

---

mental error. Once the rates are divided by the concentrations of H-NS, we obtain a rate constant of bridge formation  $k^+ = (4.5 \pm 0.3) \times 10^4 s^{-1} M^{-1}$ . To the best of our knowledge, this quantity has not been reported before. We did not observe a systematic H-NS concentration dependence in the fitted values of the shift factor  $K_{c_D}/c_B^\circ = 800 \pm 200$ , so that the lag-time is approximately inversely proportional to the decay rate. Overall, the sigmoidal decrease in extension, time required for condensation (rate and lag-time), and final extension of the condensate agree with compaction driven by like-charge attraction of distal DNA segments and mediated by bridging H-NS.

Condensed DNA has usually an ordered morphology, in which the segments are arranged in a hexagonal fashion<sup>[7,34]</sup>. The structural arrangement of compacted molecules inside nanofluidic channels is probably also hexagonal. This could, however, not be confirmed, because of difficulties associated with molecular imaging of enclosed molecules.

## 3.5 Conclusions

Overall, our observations on nanochannel-confined DNA agree with the two main features of H-NS, that is filamentation of H-NS on DNA and H-NS mediated bridging of distal DNA segments. Filamentation with a concomitant increase in bending rigidity occurs over a time span of about an hour, as determined from the elongation of DNA along the direction of the channel in a buffer of moderate ionic strength. Elongation is suppressed and the DNA molecule may even contract once bridging comes into play. For DNA in a nanospace, bridging is not only induced by divalent ions such as magnesium, but also by screened electrostatics through the concentration of monovalent salts. Another unique feature of nano-confinement, in conjunction with H-NS mediated bridging, is the collapse to a condensed form for over-threshold concentrations of H-NS. The collapse occurs within a few minutes following exposure to H-NS, which shows that it is not related to filamentation *per se*. As for sub-threshold suppression of elongation and contraction, divalent ions facilitate but are not required for DNA condensation. The enhanced sensitivity of the conformation to H-NS mediated attraction is plausibly related to DNA segment orientation order induced by confinement inside the channels with cross-sectional diameters on the order of a few times the DNA persistence length. The architectural role of H-NS is hence not only related to its binding modes but also DNA conformation as affected by one or two-dimensional confinement is of paramount importance<sup>[33]</sup>. The interplay among confinement, H-NS-mediated bridging, and filamentation controls the conformation and compaction of DNA. Furthermore, since the typical dimensions of the bacterial nucleoid

are comparable to those of our channel systems, these specific effects are likely to play a role in H-NS mediated gene silencing and chromosome organisation<sup>[1,3,14]</sup>.

This chapter was published in softmatter journal (2013) with minor changes.

### 3.6 Bibliography

- [1] Browning, D., Grainger, D., & Busby, S. (2010) Curr. Opin. Microbiol. **13**, 773–780. 77, 106
- [2] Amit, R., Oppenheim, A., & Stavans, J. (2003) Biophys. J. **84**, 2467–2473. 77, 97, 99, 100
- [3] Bouffartigues, E., Buckle, M., Badaut, C., Travers, A., & Rimsky, S. (2007) Nat. Struct. Mol. Biol. **14**, 441–448. 77, 97, 106
- [4] Woldringh, C. & Nanninga, N. (2006) J. Struct. Biol. **156**, 273–283. 78
- [5] Dame, R., Wyman, C., & Goosen, N. (2000) Nucleic Acids Res. **28**, 3504–3510. 78, 100, 102
- [6] Liu, Y., Chen, H., Kenney, L., & Yan, J. (2010) Gene. Dev. **24**, 339–344. 78, 97, 100, 102
- [7] Bloomfield, V. (1996) Curr. Opin. Struc. Biol. **6**, 334–341. 78, 104
- [8] Reisner, W., Pedersen, J., & Austin, R. (2012) Rep. Prog. Phys. **75**. 78

- [9] Levy, S. & Craighead, H. (2010) Chem. Soc. Rev. **39**, 1133–1152. 78
- [10] Dai, L., Siow, Y. N., Doyle, P. S., & van der Maarel, J. R. C. (2012) ACS Macro Lett. **1**, 1046–1050. 78
- [11] Zhang, C., Shao, P., van Kan, J. A., & van der Maarel, J. R. C. (2009) Proc. Natl. Acad. Sci. U.S.A. **106**, 16651–16656. 78, 99, 101
- [12] Jones, J. J., van der Maarel, J. R. C., & Doyle, P. S. (2011) Nano Lett. **11**, 5047–5053. 78, 99
- [13] Zhang, C., Gong, Z., Guttula, D., Malar, P. P., van Kan, J. A., Doyle, P. S., & van der Maarel, J. R. C. (2012) J. Phys. Chem. B **116**, 3031–3036. 78, 99, 101
- [14] Wang, W., Li, G.-W., Chen, C., Xie, X., & Zhuang, X. (2011) Science **333**, 1445–1449. 79, 106
- [15] Zhang, C., Zhang, F., Van Kan, J. A., & van der Maarel, J. R. C. (2008) J. Chem. Phys. **128**. 79, 83
- [16] van Kan, J. A., Bettiol, A. A., & Watt, F. (2006) Nano Lett. **6**, 579–582. 79, 83
- [17] van Kan, J. A., Zhang, C., Malar, P. P., & van der Maarel, J. R. (2012) Biomicrofluidics **6**, 036502. 79, 83
- [18] Zhang, C., Jiang, K., Liu, F., Doyle, P. S., van Kan, J. A., & van der Maarel, J. R. C. (2013) Lab. Chip **13**, 2821–2826. 80, 83, 91, 93, 102
- [19] Egawa, Y., Hayashida, R., Seki, T., & Anzai, J.-i. (2008) Talanta **76**, 736–741. 82

- [20] van Kan, J. A., Shao, P. G., Wang, Y. H., & Malar, P. (2011) Microsyst. Technol. **17**, 1519–1527. 84
- [21] Dai, L., van der Maarel, J. R. C., & Doyle, P. S. (2012) ACS Macro Lett. **1**, 732–736. 86, 97
- [22] Dai, L., Jones, J., van der Maarel, J. R. C., & Doyle, P. (2012) Soft Matter **8**, 2972–2982. 86, 97
- [23] Tegenfeldt, J., Prinz, C., Cao, H., Chou, S., Reisner, W., Riehn, R., Wang, Y., Cox, E., Sturm, J., Silberzan, P., & Austin, R. (2004) Proc. Natl. Acad. Sci. U.S.A. **101**, 10979–10983. 88
- [24] Daoud, M. & De Gennes, P. (1977) J. Phys. (Paris) **38**, 85–93. 97, 102
- [25] De Gennes, P. G. (1979) Scaling concepts in polymer physics (Cornell university press). 97
- [26] van der Maarel, J. R. (2008) Introduction to biopolymer physics (World Scientific). 97, 99
- [27] Baumann, C., Smith, S., Bloomfield, V., & Bustamante, C. (1997) Proc. Natl. Acad. Sci. U.S.A. **94**, 6185–6190. 99
- [28] Tupper, A., Owen-Hughes, T., Ussery, D., Santos, D., Ferguson, D., Sidebotham, J., Hinton, J., & Higgins, C. (1994) EMBO J. **13**, 258–268. 100
- [29] Stella, S., Falconi, M., Lammi, M., Gualerzi, C., & Pon, C. (2006) J. Mol. Biol. **355**, 169–174. 100

- [30] Spassky, A., Rimsky, S., Garreau, H., & Buc, H. (1984) Nucleic Acids Res. **12**, 5321–5340. 101
- [31] Makita, N., Yoshikawa, Y., Takenaka, Y., Sakaue, T., Suzuki, M., Watanabe, C., Kanai, T., Kanbe, T., Imanaka, T., & Yoshikawa, K. (2011) J. Phys. Chem. B **115**, 4453–4459. 102
- [32] Dai, L., Mu, Y., Nordenskiöld, L., & van der Maarel, J. R. C. (2008) Phys. Rev. Lett. **100**, 118301. 102
- [33] Joyeux, M. & Vreede, J. (2013) Biophys. J. **104**, 1615–1622. 103, 105
- [34] Hud, N. & Vilfan, I. (2005) Ann. Rev. Biophys. Biomol. Struct. **34**, 295–318. 104



## Chapter 4

# Effect of HU protein on the conformation and compaction of single DNA molecules in a nanospace

### 4.1 Introduction

The genome of *Escherichia coli* (*E. coli*) bacteria has a contour length of 1.6 mm, yet it is contained inside a nucleoid of about 1  $\mu\text{m}$  diameter. This compaction by 3 orders of magnitude has been attributed to many factors, including supercoiling, nucleoid associated proteins (NAPs), and macromolecular crowding. Despite being a topic of long-standing interest, the exact mechanism is not clear. In particular, the interplay between the above-mentioned compaction factors and confinement within a nanospace

is not clear.

In *E.coli*, HU is considered as the most abundant protein. There are 30,000 copies in the logarithmic phase, and 7,500 in the stationary phase<sup>[1,2]</sup>. In the logarithmic phase, this corresponds to 300 to 400 bp of the *E.coli* genome. HU exists as a dimer with molecular weight  $\sim 18$ KDa and  $pI$  9.5. In most cases it exists as a heterodimer  $HU_{\alpha}$  and  $HU_{\beta}$ , encoded by the *hupA* and *hupB* gens. It also exists as a homo-dimer forms as  $HU_{\alpha\alpha}$  and  $HU_{\beta\beta}$  with low percentage. All forms of HU are having different binding properties<sup>[3,4,5]</sup>. HU is a structural homologue of IHF. It induces a bending angle of  $160^{\circ}$  to DNA. The binding of HU to DNA causes two sharp kinks, at a space of 9bp via the insertion of prolines<sup>[6,7]</sup>. Moreover, the two kinks are not co-planar, which results in a dihedral angle and leads to an under-winding of the DNA helix<sup>[6]</sup>. Binding of HU to DNA is sequence unspecific. The bending of DNA by HU requires interactions between adjacent HU dimers<sup>[8,9]</sup>, but recent studies have shown that a single HU dimer is sufficient for bending<sup>[10]</sup>. HU can stabilise and constrain supercoiling. The bend induced by HU is not as rigid as the DNA bend induced by IHF; moreover it is a flexible hinge<sup>[6]</sup>. At a high concentration of HU, the HU coats along the DNA and forms rigid filaments due to protein-protein interactions<sup>[11]</sup>.

The bending caused by a single HU at random positions would change the apparent flexibility. At a low concentration of HU ( $\leq 50$  nM), the HU-DNA complex is more flexible (compacted by 50 %), and at a relatively high HU concentration the HU-DNA complex is less flexible (which leads to filamentation)<sup>[8,12]</sup>. Recent studies, with magnetic tweezers have reported

that the persistence length of the DNA-HU complex is also dependent on the salt concentration<sup>[13]</sup>. Compaction and extension (Bimodal) was observed for  $\leq 100$  nM of NaCl salt and compaction is observed for  $\geq 150$  nM only. Kundukad *et al.* have reported that the persistence length and contour length of the HU-DNA complex changes with incubation time<sup>[14]</sup>.

Advances in nanofabrication have made it possible to produce quasi-one-dimensional channel devices with cross-sectional diameters to the order of tens to hundreds of nanometers. Our chips are made of polydimethylsiloxane (PDMS) cast on a high quality master stamp, obtained by proton beam writing and UV lithography<sup>[15,16,17]</sup>. The advantage of this technology is that about a hundred replicas can be made with a single stamp, so that a fresh chip can be used for every experiment. These channel devices are used to study, among others, the conformation, folding, and compaction of single DNA molecules<sup>[18]</sup>. Furthermore, confinement in a nanospace results in significant modification of certain important biophysical phenomena, such as the knotting probability of circular DNA and the effect of macromolecular crowding<sup>[19,20,21]</sup>. In particular, it has been shown that DNA can be compacted into a condensed form for over-threshold concentrations of a crowding agent such as dextran or like-charged proteins such as bovine serum albumin and hemoglobin. DNA condensation with DNA-binding protein H-NS has also been reported<sup>[22]</sup>.

Here, this chapter reports the effect of HU, in conjunction with confinement inside a nanochannel, on the conformation and compaction of DNA. For this purpose, series of experiments were done with nanochannels having different cross-sections. These experiments focused on the equi-

librium properties of DNA molecules that were pre-incubated with HU. Super-resolution fluorescence imaging of HU in living *Escherichia coli* cells has shown that it is composed of clusters distributed within the nucleoid, which has a diameter of a few hundred nanometers<sup>[23]</sup>. This diameter of the nucleoid is comparable to the diameters of our channel systems. Accordingly, it may be surmised that our results for nanochannel confined DNA have implications for gene silencing and chromosome organisation.

T4-DNA (166 kbp) was incubated in buffers of various ionic composition and various concentrations of HU for at least 24 h. Some of the buffers also contained divalent magnesium ions (400 nM). The DNA molecules were stained with YOYO-1 with an intercalation ratio of 100 base-pairs per dye molecule. For such a low level of intercalation, the distortion of the secondary DNA structure is minimal. Furthermore, there is no appreciable effect on the bending rigidity, as inferred from previously reported measurements of the extension of DNA in nanochannels with different concentrations of dye<sup>[15]</sup>. The pre-incubated molecules were subsequently electrophoresed into a single array of long and rectangular nanochannels with average cross-sectional diameters of 200 or 250 nm. The chips are made of polydimethylsiloxane (PDMS) cast on a high quality HSQ master stamp, obtained by proton beam writing and UV lithography<sup>[15,16,17]</sup>. The advantage of this technology is that about a hundred replicas can be made with a single stamp, so that a fresh chip can be used for every experiment. Once the pre-incubated molecules were equilibrated after, the electric field was switching off, their extensions along the direction of the channel (stretch) were measured with fluorescence microscopy. Depending on solution conditions, we observed only contraction of the DNA molecules with respect

to the protein-free state. Furthermore, in recent studies with H-NS we observed elongation or contraction of the DNA molecules and as in the case of macromolecular crowding, we observed a collapse to a condensed form for over-threshold concentrations of the macromolecular crowding agent.

## 4.2 Materials and methods

### 4.2.1 Isolation and purification of HU

DNA plasmid pET Duet-1, which has been designed for the co-expressing of two genes  $HU_\alpha$  and  $HU_\beta$  ( $HU_\alpha$  tagged with N terminal his), was transformed into *Escherichia coli BL21*. The cells were grown at 37°C in a Luria Broth medium containing ampicillin and the overproduction of HU was induced with the addition of 4 mM IPTG at 20°C. The cells were lysed with a high pressure homogeniser. The lysate was cleared by centrifugation at 35,000 rpm for 30 min at 4°C. The lysate was then diluted with a buffer containing 250 mM NaCl, 10 mM Tris, and 10% glycerol, and loaded into a HisTrap HP column. The column was eluted with imidazole. The protein was further purified with a Superdex 75 gel filtration column and dispersed in a buffer comprising 500 mM KCl and 10 mM Tris. The concentration was determined by UV absorbance at 230 nm with  $A_{230} = 2.3$  per 1 g of HU/L<sup>[24]</sup>. Protein purification was done in Assoc Prof. Yan Jie's lab in MBI-NUS and Physics-NUS.

### 4.2.2 Sample preparation

The sample preparation was the same as that described in section (3.2.2); briefly, T4 GT7 DNA (165.65 kbp) were purchased from Nippon Gene, Tokyo and used without further purification. The integrity of the T4-DNA was verified with pulsed gel electrophoresis. No fragments of ones to tens of kbps were observed. Samples were prepared by dialysing solutions of DNA against 10 mM Tris-HCl with the relevant concentration of NaCl and/or MgCl<sub>2</sub> in micro-dialysers. Solutions of HU in the same buffer were also prepared. The Tris-HCl concentration was 10 mM Tris adjusted with HCl to pH 7.5, (*i.e.* 8.1 mM TrisCl and 1.9 mM Tris). The ionic strength of the buffer was calculated with the Davies equation for estimating the activity coefficients of the ions, and a dissociation constant  $pK = 8.08$  for Tris. For the measurement of the pre-equilibrated DNA molecules, solutions of HU and DNA were subsequently mixed and incubated for 6 h at 277 K. YOYO-1 fluorescence staining dye was purchased from Invitrogen, Carlsbad, CA. The T4-DNA was stained with YOYO-1 with an incubation time of 24 h and an intercalation ratio of 100 base-pairs per dye molecule. No anti-photo bleaching agent was used, since it might have interfered with DNA-protein binding. The final DNA concentration was 3 mg per L.

### 4.2.3 Fabrication of the Nanofluidic Chips

The nanofluidic devices were fabricated by replication in PDMS of patterned master stamps.<sup>[15,17]</sup> The nanochannels were made in HSQ resist (Dow Corning, Midland, MI) using a lithography process with proton beam writing.<sup>[16]</sup> (the process is described in section 2.2). For the measurement

#### 4.2.4. Single-channel array

---

of the pre-incubated DNA molecules, a single array of nanochannels was connected to two loading reservoirs through a superposing set of microchannels made in SU-8 resin with UV lithography. The heights and widths of the positive channel structures on the stamps were measured with atomic force microscopy (Dimension 3000, Veeco, Woodbury, NY) and scanning electron microscopy, respectively. For the single-array device, two stamps were made featuring nanochannels of length  $60\ \mu\text{m}$  and rectangular cross-sections of  $150 \times 250$  and  $200 \times 300\ \text{nm}^2$ , respectively. The connecting microchannels had a width and height of  $30$  and  $5\ \mu\text{m}$ , respectively. The stamp was coated with a  $5\ \text{nm}$  thick teflon layer to guarantee perfect release of the replicated PDMS chips.<sup>[25]</sup> The stamps were replicated in PDMS followed by curing with a curing agent (Sylgard, Dow Corning) at  $338\ \text{K}$  for  $24\ \text{h}$ . The PDMS replica was sealed with a glass coverslip, after both substrates were plasma oxidised (Harrick, Ossining, NY).

#### 4.2.4 Single-channel array

The pre-incubated and stained DNA molecules dispersed in the relevant solution were loaded into one of the two reservoirs connected to the single array of nanochannels. The DNA molecules were subsequently driven into the channels by electrophoresis. For this purpose, two platinum electrodes were immersed in the reservoirs and connected to an electrophoresis power supply with a relatively low voltage in the range of  $0.1\text{-}10\ \text{V}$  (Keithley, Cleveland, OH). Once the DNA molecules were localised inside the nanochannels, the electric field was switched off and the molecules were allowed to relax to their equilibrium state for at least  $60\ \text{sec}$ . The stained

DNA molecules were visualised with a Nikon Eclipse Ti inverted fluorescence microscope equipped with a 200 W metal halide lamp, a filter set, and a 100 $\times$  oil immersion objective. A UV light shutter controlled the exposure time. Images were collected with an electron multiplying charge coupled device (EMCCD) camera (iXon X3, Andor Technology, Belfast, UK) and the extension of the DNA molecules inside the channels was measured with IMAGEJ software (<http://rsb.info.nih.gov/ij/>). For the intensity threshold, a signal to background noise ratio of 2:1 was used.

## 4.3 Results and Discussion

### 4.3.1 Compaction and Condensation of pre-incubated DNA

The T4-DNA molecules were incubated with the relevant buffer for at least 24 h before they were brought into the channels of the single-array device. Montages of images of single DNA molecules confined in rectangular channels with a cross-section of 200 $\times$  300 nm<sup>2</sup> are shown in Figure (4.2). The images refer to well-equilibrated conformations. After the electric field was switched off, the molecules relaxed to their equilibrium state within 60 s. There was no further change in the size of the molecules for more than 3 h. Furthermore, no difference was observed between the extensions of molecules inserted by electrophoresis or those inserted by pressure. The equilibrated stretch in the longitudinal direction of the channel depends on the buffer conditions. In a buffer with a moderate ionic strength of around 11 mM (T-buffer with 3 mM NaCl; T-buffer is 8.1 mM TrisCl and



### 4.3.1. Compaction and Condensation of pre-incubated DNA

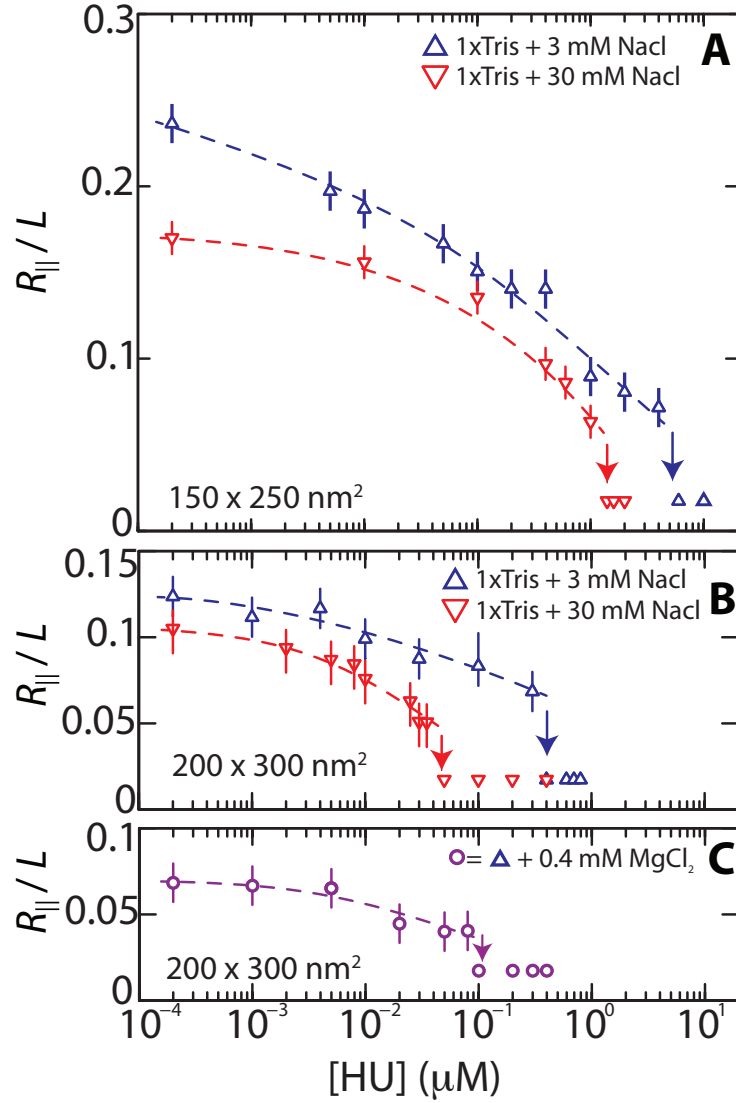


**Fig. 4.1** Relative extension  $R_{||}/L$  of T4-DNA in T-buffer with 3 ( $\Delta$ ) or 30 ( $\nabla$ ) mM NaCl versus the concentration of HU. The molecules are pre-incubated and inside  $150 \times 250 \text{ nm}^2$  channels. (B) As in panel (A), but in  $200 \times 300 \text{ nm}^2$  channels. (C) As in panel (A), but in T-buffer with 3 mM NaCl and 0.4 mM  $\text{MgCl}_2$  ( $\circ$ ), inside  $200 \times 300 \text{ nm}^2$  channels. The dashed curves are drawn as an aid to the eye and the arrows denote the condensation thresholds.

### 4.3.1. Compaction and Condensation of pre-incubated DNA

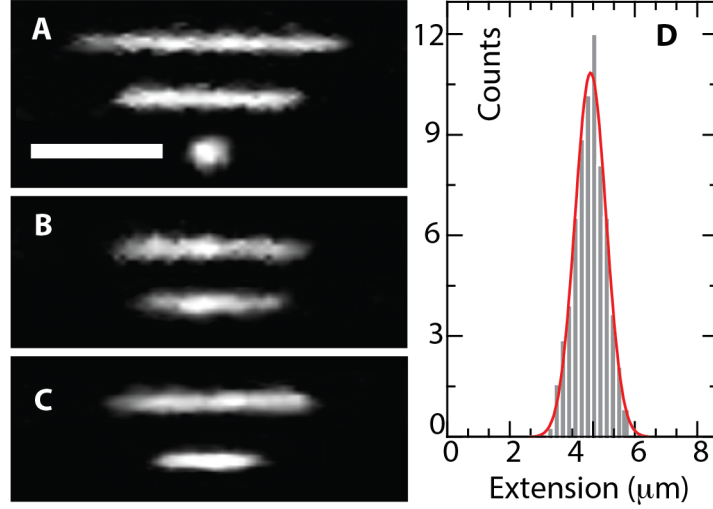


**Fig. 4.2** (A) Montage of fluorescence images of T4-DNA in T-buffer with 3 mM NaCl and inside  $200 \times 300 \text{ nm}^2$  channels. T-buffer is 8.1 mM TrisCl and 1.9 mM Tris, pH 7.5. The HU concentration is 10, 100, and 400 nM from top to bottom. The scale bar denotes  $3 \mu\text{m}$ . (B) As in panel (A), but in T-buffer with 30 mM NaCl. The HU concentrations are 10 and 30 nM from top to bottom. (C) As in panel (A), but in T-buffer with 3 mM NaCl and 0.4 mM  $\text{MgCl}_2$ . The HU concentrations are 10 and 80 nM from top to bottom. (D) Distribution in extension of a population of 80 molecules in T-buffer with 3 mM NaCl and 100 nM HU, inside  $200 \times 300 \text{ nm}^2$  channels. A Gaussian fit gives  $R_{||} = 4.5 \pm 1.0 \mu\text{m}$ .

1.9 mM Tris, pH 7.5), the DNA molecules slowly contracted compared to buffer with a higher ionic strength of about 38 mM, with respect to the protein-free situation. In the presence of sub-milli molar concentration of magnesium ions, HU-induced compaction was observed. And over a threshold concentration of HU, condensation DNA molecules into a compact form was observed. In channels with a smaller cross-section of  $150 \times 250 \text{ nm}^2$ , we observed the same qualitative behaviour. The quantitative differences are the values of the critical concentration of HU for DNA condensation.

The extension of the DNA molecules in channels with two different cross-sections of  $200 \times 300$  and  $150 \times 250 \text{ nm}^2$  was measured. For each

### 4.3.1. Compaction and Condensation of pre-incubated DNA

---

experimental condition, that is buffer composition, channel diameter, and HU concentration, a fresh PDMS replica was used, and about 50 molecules were measured. The distribution in extension was close to Gaussian<sup>[26]</sup>. An example of such a distribution is shown in Figure(4.2D). Fragmented DNAs can easily be discerned, because their extensions clearly fall below the values pertaining to the intact molecules. For the cut-off, we have used the mean value minus two times the standard deviation. Resolution broadening could be neglected, because the optical resolution was one order of magnitude smaller than the variance. The mean relative extension  $R_{||}/L$ , that is the mean extension divided by the YOYO-1 corrected contour length of  $57 \mu\text{m}$ , is set out in figure(4.1) as a function of the HU concentration. In a buffer with moderate ionic strength without Magnesium (T-buffer with 3 mM NaCl), a slow contraction in length was observed. In the case of a buffer with high concentration (T-buffer with 30 mM NaCl), the contraction was faster compared with molecule bathed in moderate ionic strength buffer. The same effect was also observed in 0.4 mM  $\text{MgCl}_2$  in a T- buffer with 3 mM NaCl(moderate ionic strength buffer). Note that for sub-threshold concentrations of HU, the relative extensions were in the range of 0.05-0.2, which implies that the DNA molecules remained coiled. Furthermore, the same decrement in length was observed in the  $150 \times 250 \text{ nm}^2$  channel system which had stronger confinement than the  $200 \times 300 \text{ nm}^2$  system.

For over-threshold concentrations of HU, the DNA molecules compacted into a condensed form. This was facilitated by the confinement in the nanochannel, because we did not observe condensation in the feeding microchannels and/or the reservoirs of the chip. To the best of our knowledge, condensation of DNA by HU has not been reported before. In 200

$\times 300 \text{ nm}^2$  channels, the critical concentrations of HU for condensation were  $0.3 \pm 0.05$  and  $0.04 \pm 0.01 \text{ }\mu\text{M}$  HU in moderate (T-buffer with 3 mM) and high (T-buffer with 30mM Na) buffers respectively. On the other hand, in a  $150 \times 250 \text{ nm}^2$  channel system, the values for the condensation concentration of HU were  $1.1 \pm 0.1$  and  $5 \pm 1$  in high and moderate monovalent buffers respectively. The threshold concentration for condensation increased in value, as the channel cross-sectional diameter decreased. The concentration of monovalent salts had a significant effect on condensation, because as monovalent salt concentration increases the condensation concentration of HU decreases. On the other hand, the critical concentration for condensation was lowered from 0.3 to  $0.09 \text{ }\mu\text{M}$  of HU in the presence of sub millimolar concentration (i.e 0.4 mM) of magnesium ions. The effect of magnesium was smaller than that of the change in monovalent salt concentration from high to moderate for condensation, while the effect of magnesium was more prominent in H-NS<sup>[22]</sup>

## 4.4 Conclusions

As the concentrations of HU increased, the molecules are contracted with respect to the protein-free state for 24 h incubation, because of the *bridging* of different segments of DNA by HU protein. The DNA molecules are condensed more easily in high-salt concentration than low-salt condition. With the addition of a sub-milli-molar concentration of magnesium, the threshold concentration for condensation is lowered, but the effect of divalent ion is low (unlike with H-NS), as compared with the increase in monovalent salt from 3 to 30 mM. The critical concentration for condensation is

also depends on channel diameter, i.e in wider channels DNA-HU complex condense more easily. Condensation of DNA with HU in the bulk phase and/or the microchannels of the chip in the prevalent solution conditions was not observed. It should be noted that for sufficiently low HU concentrations, the molecules contract but do not compact into a condensed form. A unique feature of the confinement in a nanospace is that the molecules do compact into a condensed form for over-threshold concentrations of HU. This phenomenon also be observed in neutral crowding agents and like charge proteins, but condensation induced by bacterial proteins HU and H-NS occurs at an order of magnitude lower, with a concentration of about one micromolar. Our results show that the effects of architectural proteins on the conformation and folding of DNA do not depend on DNA-protein interaction and crowding per se, but the interplay with the confinement in a nanospace such as within a bacterial cell is of paramount importance<sup>[23]</sup>.

## 4.5 Bibliography

- [1] Azam, T. A., Iwata, A., Nishimura, A., Ueda, S., & Ishihama, A. (1999) J. Bacteriol. **181**, 6361–6370. 111
- [2] Dixon, N. E. & Kornberg, A. (1984) Proc. Natl. Acad. Sci. U.S.A. **81**, 424–428. 111
- [3] Claret, L. & Rouviere-Yaniv, J. (1997) J. Mol. Biol. **273**, 93–104. 111
- [4] Pinson, V., Takahashi, M., & Rouviere-Yaniv, J. (1999) J. Mol. Biol. **287**, 485–497. 111

- [5] Tanaka, H., Goshima, N., Kohno, K., Kano, Y., & Imamoto, F. (1993) J. Biochem **113**, 568–572. 111
- [6] Swinger, K. K., Lemberg, K. M., Zhang, Y., & Rice, P. A. (2003) EMBO J. **22**, 3749–3760. 111
- [7] Swinger, K. K. & Rice, P. A. (2007) J. Mol. Biol. **365**, 1005–1016. 111
- [8] Tanaka, I., Appelt, K., Dijk, J., White, S. W., & Wilson, K. S. (1984) Nature **310**, 376–381. 111
- [9] Tanaka, H., Yasuzawa, K., Kohno, K., Goshima, N., Kano, Y., Saiki, T., & Imamoto, F. (1995) Mol. Gen. Genet. **249**, 570–570. 111
- [10] Goodman, S. D., Nicholson, S. C., & Nash, H. A. (1992) Proc. Natl. Acad. Sci. U.S.A. **89**, 11910–11914. 111
- [11] Dame, R. T. (2005) Mol. MicroBiol. **56**, 858–870. 111
- [12] van Noort, J., Verbrugge, S., Goosen, N., Dekker, C., & Dame, R. T. (2004) Proc. Natl. Acad. Sci. U.S.A. **101**, 6969–6974. 111
- [13] Xiao, B., Johnson, R. C., & Marko, J. F. (2010) Nucleic Acids Res. **38**, 6176–6185. 112
- [14] Kundukad, B., Cong, P., van der Maarel, J. R. C., & Doyle, P. S. (2013) Nucleic Acids Res. **41**, 8280–8288. 112
- [15] Zhang, C., Zhang, F., Van Kan, J. A., & van der Maarel, J. R. C. (2008) J. Chem. Phys. **128**. 112, 113, 115
- [16] van Kan, J. A., Bettiol, A. A., & Watt, F. (2006) Nano Lett. **6**, 579–582. 112, 113, 115

- [17] van Kan, J. A., Zhang, C., Malar, P. P., & van der Maarel, J. R. (2012) Biomicrofluidics **6**, 036502. 112, 113, 115
- [18] Zhang, C., Shao, P., van Kan, J. A., & van der Maarel, J. R. C. (2009) Proc. Natl. Acad. Sci. U.S.A. **106**, 16651–16656. 112
- [19] Dai, L., Siow, Y. N., Doyle, P. S., & van der Maarel, J. R. C. (2012) ACS Macro Lett. **1**, 1046–1050. 112
- [20] Jones, J. J., van der Maarel, J. R. C., & Doyle, P. S. (2011) Nano Lett. **11**, 5047–5053. 112
- [21] Zhang, C., Gong, Z., Guttula, D., Malar, P. P., van Kan, J. A., Doyle, P. S., & van der Maarel, J. R. C. (2012) J. Phys. Chem. B **116**, 3031–3036. 112
- [22] Zhang, C., Guttula, D., Liu, F., Malar, P. P., Ng, S. Y., Dai, L., Doyle, P. S., van Kan, J. A., & van der Maarel, J. R. C. (2013) Soft Matter **9**, 9593–9601. 112, 121
- [23] Wang, W., Li, G.-W., Chen, C., Xie, X., & Zhuang, X. (2011) Science **333**, 1445–1449. 113, 122
- [24] Krylov, A. S., Zasedateleva, O. A., Prokopenko, D. V., Rouviere-Yaniv, J., & Mirzabekov, A. D. (2001) Nucleic Acids Res. **29**, 2654–2660. 114
- [25] van Kan, J. A., Shao, P. G., Wang, Y. H., & Malar, P. (2011) Microsyst. Technol. **17**, 1519–1527. 116
- [26] Tegenfeldt, J., Prinz, C., Cao, H., Chou, S., Reisner, W., Riehn, R., Wang, Y., Cox, E., Sturm, J., Silberzan, P., & Austin, R. (2004) Proc.

Natl. Acad. Sci. U.S.A. **101**, 10979–10983. 120



# Chapter 5

## Conclusions and future work

This chapter focuses on the conclusions of the study, followed by the overall conclusion and recommendations for future research. The main objective of this thesis is to investigate conformational changes of single DNA molecules induced by H-NS and HU proteins in nanospace.

### 5.1 Conclusions

#### (A) Effect of H-NS on the elongation and compaction of single DNA molecules in a nanospace

In the first project, the observations of nanochannel-confined DNA agree with the filamentation of H-NS on DNA and H-NS mediated bridging of distal DNA segments. Filamentation with a concomitant increase in bending rigidity occurs over a time span of about an hour, as determined from the elongation of DNA along the direction of the channel in a buffer of moderate ionic strength. Elongation is suppressed and the DNA molecule may even contract once bridging comes into play. For DNA in a nanospace, bridging is not only induced by

divalent ions such as magnesium, but also by screened electrostatics through the concentration of monovalent salts. Another unique feature of nano-confinement, in conjunction with H-NS mediated bridging, is the collapse to a condensed form for over-threshold concentrations of H-NS. The collapse occurs within a few minutes following exposure to H-NS, which shows that it is not related to filamentation *per se*. As for sub-threshold suppression of elongation and contraction, divalent ions facilitate but are not required for DNA condensation. The interplay among confinement, H-NS-mediated bridging, and filamentation controls the conformation and compaction of DNA.

**(B) Effect of HU protein on the conformation and compaction of single DNA molecules in a nanospace**

In the second project, the DNA-HU complex was contracted with increasing concentration of HU by bridging and finally compacted into a condensed form. The critical concentration for condensation not only depends on the salt concentration, but also nanochannel dimension. The critical concentration for condensation has higher value in the low ionic salt condition and lower value in high ionic salt condition. DNA-HU complex was easy to condense in more wider channels than in more narrow channels. A unique feature of the confinement in a nanospace is that the molecules do compact into a condensed form for over threshold concentrations of HU. In presence of sub-millimolar concentration of magnesium the threshold concentration shifts to lower value side. Magnesium alone does not condense the DNA such a low level magnesium concentration. There is no condensation of DNA with HU in the bulk phase and/or the microchannels of the

chip in the prevalent solution conditions.

#### 5.1.1 Overall conclusion

In nanochannels, DNA-protein interaction studies are different from the bulk phase. A unique feature of the nanochannel walls is that it imposes orientation order to juxtaposed segments of the DNA. As the concentration of protein increases, the DNA-HNS complex shows an increase in length at low ionic strength, and a decrease in length at high ionic strength. On the other hand, DNA-HU complex shows contraction by bridging at below the threshold concentration and at an over-threshold concentration of protein, the DNA molecules compact into a condensed form. This phenomenon is shared with neutral crowding agents as well as like charge proteins, but condensation induced by bacterial proteins HU and H-NS occurs at an order of magnitude lower concentration of about one micromolar.

Our results show that the effects of architectural proteins on the conformation and folding of DNA do not depend on DNA-protein interaction and crowding *per se*, but the interplay with the confinement in a nanospace such as within a bacterial cell is of paramount importance<sup>[1]</sup>.

## 5.2 Future work

There are various interesting topics to explore using the nano-fluidic device in the area of protein-DNA interaction studies. Further extensions from current studies described so far in this thesis are discussed in the following

sections, to provide further understanding of the conformational changes of DNA induced by nucleoid-associated proteins (NAPs).

- H-NS WT forms filamentation and bridging in the nano channel depending on environmental buffer conditions. H-NS has two domains, called as the C-terminal and N-terminal. Mutation in the C-terminal domain affect the DNA-binding, and mutation in the N-terminal domain affects the dimerisation of H-NS. The removal of proline in the C-terminal ( $\Delta P115$ ), or the substitution of it with alanine (P115A), has the ability to retard the dimerisation and cause condensation. L30P and L30D are a result of mutation in the N-terminal that affects the dimerisation. Other mutants R15C and R15H affect the DNA-binding ability. R12E and C21S have the ability to enhance oligomerisation. Recent studies show that L26P and L30P mutants causes large scale DNA condensation<sup>[2]</sup>. A study of some of these mutations provides a clear picture of gene silencing. In a nanochannel it is interesting to study the effect of mutation on the filamentation and bridging. H-NS has homology with other NAPs such as StpA, and forms heteromeric with them. To study the collective behaviour of the homomeric and heteromeric with DNA is a possible direction for future research work, because collectively these NAPs are organising the genome.
- All NAPs bind to DNA and changes conformation uniquely. NAPs have different copy numbers in different phases of the cell. Some of them are abundant in the logarithmic phase (E.g. Hfq, HU, StpA, H-NS etc.), and some in the stationary phase (E.g. Dps and IHF). In-

terestingly, a few NAPs are very most abundant in one of the phases and much less abundant or even not present in another phases. For example, Fis is abundant in the exponential phase and not present in the stationary phase, and Dps is the most abundant protein in the stationary phase, with more than 1,00,000 copies, and much less abundant in the exponential phase, with only 100 copies<sup>[3]</sup>. These NAPs control the conformational changes of the chromatin. Conformation of the chromatin is diffuse in the exponential phase and compact in the stationary phase. The investigation of conformational changes of DNA in nanospace by other NAPs like as Fis and Dps would thus be an interesting research direction.

- HU produce a flexible kink to in the DNA and is not as strong as the kink produced by IHF. The HU-DNA complex length in nano channels shows more fluctuation than the HNS-DNA complex. It would be interesting to investigate the dynamics of the HU-DNA complex in nanochannels. Temporal response of the DNA by HU is in progress.
- Advancement in nanofabrication and DNA labelling can provide DNA sequencing by the linearisation of DNA<sup>[4]</sup>. Linearisation of DNA in an array of nanochannels with specific labelling gives sequencing resolution of few kilo bases. Recently, Matsuoka *et al.* have reported the linearisation of chromatin with nanochannels (epigenetic profiling)<sup>[5,6]</sup>. This type of epigenetic profiling has problems with histone modification and labelling with antibodies, and thus is time consuming and also not robust. Zhang *et al.* have developed a nanofluidic

device to study single molecules with *in situ* control of environmental solution conditions<sup>[7]</sup>. Through a combination of the linearisation of the chromatin technique and a crossed micro-nanochannel array for change of buffer and/or antibody labels, it might be possible to do epigenetic profiling in a single chip.

- Finally, the distribution of H-NS and HU around the DNA is still completely unknown. Nanofluidic devices are useful in investigating conformational changes of DNA induced by proteins, but are too constrained by optical resolution and the fabrication of nanochannels to see the distribution of protein around the DNA. Therefore, to know the distribution of protein around the DNA, other experimental tools such as Neutron and/or X-ray scattering are needed. The small-angle neutron scattering technique is useful to estimate the distribution of other molecules around the DNA and also the DNA conformational changes induced by the other molecules. In 1999, polyamine distribution around the DNA<sup>[8]</sup> was reported by Zakharova et al. The effect of crowding on the conformation of interwound DNA strands<sup>[9]</sup> using SANS has also been reported. It is also possible to estimate the distribution of H-NS and HU around the DNA. Small angle neutron scattering experiments with solvent contrast matching to derive the DNA-Protein (H-NS and HU) and protein partial structure functions are in progress. The structural functions will be interpreted in terms of a radial distribution of protein density and possible protein density correlation along the duplex in register with the phosphate moieties.

### 5.3 Bibliography

- [1] Wang, W., Li, G.-W., Chen, C., Xie, X., & Zhuang, X. (2011) Science **333**, 1445–1449. 128
- [2] Lim, C. J., Lee, S. Y., Kenney, L. J., & Yan, J. (2012) Sci. Rep. **2**. 129
- [3] Azam, T. A., Iwata, A., Nishimura, A., Ueda, S., & Ishihama, A. (1999) J. Bacteriol. **181**, 6361–6370. 130
- [4] Zhang, C., Hernandez-Garcia, A., Jiang, K., Gong, Z., Guttula, D., Ng, S. Y., Malar, P. P., van Kan, J. A., Dai, L., Doyle, P. S., Vries, R. d., & van der Maarel, J. R. C. (2013) Nucleic Acids Res. **41**, e189. 130
- [5] Matsuoka, T., Kim, B. C., Huang, J., Douville, N. J., Thouless, M., & Takayama, S. (2012) Nano Lett. **12**, 6480–6484. 130
- [6] Matsuoka, T., Kim, B. C., Moraes, C., Han, M., & Takayama, S. (2013) Biomicrofluidics **7**, 041301. 130
- [7] Zhang, C., Jiang, K., Liu, F., Doyle, P. S., van Kan, J. A., & van der Maarel, J. R. C. (2013) Lab. Chip **13**, 2821–2826. 131
- [8] Zakharova, S., Egelhaaf, S., Bhuiyan, L., Outhwaite, C., Bratko, D., & van der Maarel, J. (1999) The Journal of Chemical Physics **111**, 10706. 131
- [9] Zhu, X., Ng, S. Y., Gupta, A. N., Feng, Y. P., Ho, B., Lapp, A., Egelhaaf, S. U., Forsyth, V. T., Haertlein, M., Moulin, M., Schweins, R., & van der Maarel, J. R. C. (2010) Phys. Rev. E **81**, 061905. 131

# Chapter 6

## Over all references

### 6.1 References

- [1] Dahm, R. (2008) Hum. Genet. **122**, 565–581.
- [2] Downie, A. (1972) J. Gen. Microbiol. **73**, 1–11.
- [3] Avery, O., MacLeod, C., & McCarty, M. (1944) J. Exp. Med. **79**, 137–158.
- [4] Watson, J. D. (2011) The double helix: A personal account of the discovery of the structure of DNA (Scribner).
- [5] Bates, A. D. & Maxwell, A. (2005) DNA topology (Oxford university press).
- [6] Holmes, V. F. & Cozzarelli, N. R. (2000) Proc. Natl. Acad. Sci. U.S.A. **97**, 1322–1324.
- [7] Ellis, R. J. (2001) Trends Biochem. Sci. **26**, 597–604.



## References

---

- [8] Zimmerman, S. B. & Minton, A. P. (1993) Ann. Rev. Biophys. Biomol. Struct. **22**, 27–65.
- [9] Sear", R. (1998) Phys. Rev. E **58**, 724–728.
- [10] Robinow, C. & Kellenberger, E. (1994) Microbiol. Rev. **58**, 211.
- [11] Zimmerman, S. B. (2006) J. Struct. Biol. **153**, 160–175.
- [12] Stavans, J. & Oppenheim, A. (2006) Phys. Biol. **3**, R1.
- [13] Egan, E., Fogel, M., & Waldor, M. (2005) Mol. MicroBiol. **56**, 1129–1138.
- [14] Wang, J. C. (1985) Annu. Rev. Biochem. **54**, 665–697.
- [15] Higgins, N. P. & Vologodskii, A. (2004) Topological behavior of plasmid DNA (Washington, DC: American Society for Microbiology Press).
- [16] Zechiedrich, E. L., Khodursky, A. B., & Cozzarelli, N. R. (1997) Gene. Dev **11**, 2580–2592.
- [17] Azam, T. A. & Ishihama, A. (1999) J. Biol. Chem. **274**, 33105–33113.
- [18] Ishihama, A. (2009) EcoSal–Escherichia coli and Salmonella: Cellular and Molecular Biology .
- [19] Kim, J., Yoshimura, S. H., Hizume, K., Ohniwa, R. L., Ishihama, A., & Takeyasu, K. (2004) Nucleic Acids Res. **32**, 1982–1992.
- [20] Jacquet, M., Cukier-Kahn, R., Pla, J., & Gros, F. (1971) Biochem. Bioph. Res. Co. **45**, 1597–1607.

## References

---

- [21] Cukier-Kahn, R., Jacquet, M., & Gros, F. (1972) Proc. Natl. Acad. Sci. U.S.A. **69**, 3643–3647.
- [22] Varshavsky, A., Nedospasov, S., Bakayev, V., Bakayeva, T., & Georgiev, G. (1977) Nucleic Acids Res. **4**, 2725–2746.
- [23] Spassky, A., Rimsky, S., Garreau, H., & Buc, H. (1984) Nucleic Acids Res. **12**, 5321–5340.
- [24] Dame, R. R. T. & Dorman, C. J. (2010) Bacterial chromatin (Springer).
- [25] Rimsky, S., Zuber, F., Buckle, M., & Buc, H. (2001) Mol. MicroBiol. **42**, 1311–1323.
- [26] Bouffartigues, E., Buckle, M., Badaut, C., Travers, A., & Rimsky, S. (2007) Nat. Struct. Mol. Biol. **14**, 441–448.
- [27] Schröder, O.oder, O. & Wagner, R. (2002) Biol. Chem. **383**, 945–960.
- [28] Rimsky, S. (2004) Curr. Opin. Microbiol. **7**, 109–114.
- [29] Fang, F. C. & Rimsky, S. (2008) Curr. Opin. Microbiol. **11**, 113–120.
- [30] Lucchini, S., Rowley, G., Goldberg, M. D., Hurd, D., Harrison, M., & Hinton, J. C. (2006) PLoS Pathog. **2**, e81.
- [31] Navarre, W. W., McClelland, M., Libby, S. J., & Fang, F. C. (2007) Gene. Dev. **21**, 1456–1471.
- [32] Bertin, P., Benhabiles, N., Krin, E., Laurent-Winter, C., Tendeng, C., Turlin, E., Thomas, A., Danchin, A., & Brasseur, R. (1999) Mol. MicroBiol. **31**, 319–329.

## References

---

- [33] Shindo, H., Iwaki, T., Ieda, R., Kurumizaka, H., Ueguchi, C., Mizuno, T., Morikawa, S., Nakamura, H., & Kuboniwa, H. (1995) FEBS lett. **360**, 125–131.
- [34] Shindo, H., Ohnuki, A., Ginba, H., Katoh, E., Ueguchi, C., Mizuno, T., & Yamazaki, T. (1999) FEBS lett. **455**, 63–69.
- [35] Renzoni, D., Esposito, D., Pfuhl, M., Hinton, J. C., Higgins, C. F., Driscoll, P. C., & Ladbury, J. E. (2001) J. Mol. Biol. **306**, 1127–1137.
- [36] Bloch, V., Yang, Y., Margeat, E., Chavanieu, A., Augé, M. T., Robert, B., Arold, S., Rimsky, S., & Kochoyan, M. (2003) Nat. Struct. Mol. Biol. **10**, 212–218.
- [37] Dorman, C. J. (2004) Nat. Rev. Micro. **2**, 391–400.
- [38] Williams, R. M., Rimsky, S., & Buc, H. (1996) J. Bacteriol. **178**, 4335–4343.
- [39] Kajitani, M. & Ishihama, A. (1991) Nucleic Acids Res. **19**, 1063–1066.
- [40] Liu, Q. & Richardson, C. C. (1993) Proc. Natl. Acad. Sci. U.S.A. **90**, 1761–1765.
- [41] Donato, G. M. & Kawula, T. H. (1998) J. Biol. Chem. **273**, 24030–24036.
- [42] Nieto, J., Madrid, C., Miquelay, E., Parra, J., Rodriguez, S., & Juarez, A. (2002) J. Bacteriol. **184**, 629–635.
- [43] Falconi, M., Colonna, B., Prosseda, G., Micheli, G., & Gualerzi, C. O. (1998) EMBO J. **17**, 7033–7043.

## References

---

- [44] Tupper, A., Owen-Hughes, T., Ussery, D., Santos, D., Ferguson, D., Sidebotham, J., Hinton, J., & Higgins, C. (1994) EMBO J. **13**, 258–268.
- [45] Amit, R., Oppenheim, A., & Stavans, J. (2003) Biophys. J. **84**, 2467–2473.
- [46] Caramel, A. & Schnetz, K. (1998) J. Mol. Biol. **284**, 875–883.
- [47] Dame, R., Wyman, C., & Goosen, N. (2000) Nucleic Acids Res. **28**, 3504–3510.
- [48] Dame, R. T., Noom, M. C., & Wuite, G. J. (2006) Nature **444**, 387–390.
- [49] Woldringh, C. & Nanninga, N. (2006) J. Struct. Biol. **156**, 273–283.
- [50] Spurio, R., Dürrenberger, M., Falconi, M., La Teana, A., Pon, C. L., & Gualerzi, C. O. (1992) Mol. Gen. Genet. **231**, 201–211.
- [51] Dame, R. T., Wyman, C., Wurm, R., Wagner, R., & Goosen, N. (2002) J. Biol. Chem. **277**, 2146–2150.
- [52] Zhang, W., Carneiro, M. J., Turner, I. J., Allen, S., Roberts, C. J., & Soutanas, P. (2005) J. Mol. Biol. **351**, 66–75.
- [53] Liu, Y., Chen, H., Kenney, L., & Yan, J. (2010) Gene. Dev. **24**, 339–344.
- [54] Dixon, N. E. & Kornberg, A. (1984) Proc. Natl. Acad. Sci. U.S.A. **81**, 424–428.
- [55] Azam, T. A., Iwata, A., Nishimura, A., Ueda, S., & Ishihama, A. (1999) J. Bacteriol. **181**, 6361–6370.

## References

---

- [56] Claret, L. & Rouviere-Yaniv, J. (1997) J. Mol. Biol. **273**, 93–104.
- [57] Pinson, V., Takahashi, M., & Rouviere-Yaniv, J. (1999) J. Mol. Biol. **287**, 485–497.
- [58] Tanaka, H., Goshima, N., Kohno, K., Kano, Y., & Imamoto, F. (1993) J. Biochem **113**, 568–572.
- [59] White, S. W., Wilson, K. S., Appelt, K., & Tanaka, I. (1999) Acta Crystallographica Section D: Biological Crystallography **55**, 801–809.
- [60] Azam, T. A., Hiraga, S., & Ishihama, A. (2000) Genes. Cell. **5**, 613–626.
- [61] Swinger, K. K., Lemberg, K. M., Zhang, Y., & Rice, P. A. (2003) EMBO J. **22**, 3749–3760.
- [62] Rice, P. A. (1997) Curr. Opin. Struc. Biol. **7**, 86–93.
- [63] Bewley, C. A., Gronenborn, A. M., & Clore, G. M. (1998) Ann. Rev. Biophys. Biomol. Struct. **27**, 105–131.
- [64] Koh, J., Saecker, R. M., & Record Jr, M. T. (2008) J. Mol. Biol. **383**, 324–346.
- [65] Vis, H., Boelens, R., Mariani, M., Stroop, R., Vorgias, C. E., Wilson, K. S., & Kaptein, R. (1994) Biochemistry **33**, 14858–14870.
- [66] Vis, H., Mariani, M., Vorgias, C. E., Wilson, K. S., Kaptein, R., & Boelens, R. (1995) J. Mol. Biol. **254**, 692–703.
- [67] Tanaka, I., Appelt, K., Dijk, J., White, S. W., & Wilson, K. S. (1984) Nature **310**, 376–381.

## References

---

- [68] Tanaka, H., Yasuzawa, K., Kohno, K., Goshima, N., Kano, Y., Saiki, T., & Imamoto, F. (1995) Mol. Gen. Genet. **249**, 570–570.
- [69] Goodman, S. D., Nicholson, S. C., & Nash, H. A. (1992) Proc. Natl. Acad. Sci. U.S.A. **89**, 11910–11914.
- [70] Dame, R. T. & Goosen, N. (2002) FEBS lett. **529**, 151–156.
- [71] van Noort, J., Verbrugge, S., Goosen, N., Dekker, C., & Dame, R. T. (2004) Proc. Natl. Acad. Sci. U.S.A. **101**, 6969–6974.
- [72] Balandina, A., Claret, L., Hengge-Aronis, R., & Rouviere-Yaniv, J. (2001) Mol. MicroBiol. **39**, 1069–1079.
- [73] Flashner, Y. & Gralla, J. D. (1988) Cell **54**, 713–721.
- [74] Lewis, D. E., Geanacopoulos, M., & Adhya, S. (1999) Mol. MicroBiol. **31**, 451–461.
- [75] Kamashev, D. & Rouviere-Yaniv, J. (2000) EMBO J. **19**, 6527–6535.
- [76] Semsey, S., Geanacopoulos, M., Lewis, D. E. A., & Adhya, S. (2002) EMBO J. **21**, 4349–4356.
- [77] Haykinson, M. J. & Johnson, R. (1993) EMBO J. **12**, 2503.
- [78] Xiao, B., Johnson, R. C., & Marko, J. F. (2010) Nucleic Acids Res. **38**, 6176–6185.
- [79] Kundukad, B., Cong, P., van der Maarel, J. R. C., & Doyle, P. S. (2013) Nucleic Acids Res. **41**, 8280–8288.
- [80] Dame, R. T., Hall, M. A., & Wang, M. D. (2013) ChemBioChem **14**, 1954–1957.

## References

---

- [81] Rice, P. A., Yang, S.-w., Mizuuchi, K., & Nash, H. A. (1996) Cell **87**, 1295–1306.
- [82] Ali, B. J., Amit, R., Braslavsky, I., Oppenheim, A. B., Gileadi, O., & Stavans, J. (2001) Proc. Natl. Acad. Sci. U.S.A. **98**, 10658–10663.
- [83] Pan, C. Q., Finkel, S. E., Cramton, S. E., Feng, J.-A., Sigman, D. S., & Johnson, R. C. (1996) J. Mol. Biol. **264**, 675–695.
- [84] Schneider, R., Lurz, R., Lüder, G., Tolksdorf, C., Travers, A., & Muskhelishvili, G. (2001) Nucleic Acids Res. **29**, 5107–5114.
- [85] Luijsterburg, M. S., Noom, M. C., Wuite, G. J., & Dame, R. T. (2006) J. Struct. Biol. **156**, 262–272.
- [86] Luijsterburg, M. S., White, M. F., van Driel, R., & Dame, R. T. (2008) Crit. Rev. Biochem. Mol. Biol. **43**, 393–418.
- [87] Kuhn, W. (1934) Kolloid. Z. **68**, 2–15.
- [88] Kuhn, W. (1936) Kolloid. Z. **76**, 258–271.
- [89] Flory, P. J. (1949) J. Chem. Phys. **17**, 303.
- [90] Flory & J., P. (1953) Principles of polymer chemistry (Cornell University Press).
- [91] Reisner, W., Beech, J. P., Larsen, N. B., Flyvbjerg, H., Kristensen, A., & Tegenfeldt, J. O. (2007) Phys. Rev. Lett. **99**, 058302.
- [92] Tegenfeldt, J., Prinz, C., Cao, H., Chou, S., Reisner, W., Riehn, R., Wang, Y., Cox, E., Sturm, J., Silberzan, P., & Austin, R. (2004) Proc. Natl. Acad. Sci. U.S.A. **101**, 10979–10983.

- [93] Odijk, T. (1983) Macromolecules **16**, 1340–1344.
- [94] Wang, Y., Tree, D. R., & Dorfman, K. D. (2011) Macromolecules **44**, 6594–6604.
- [95] Odijk, T. (2006) J. Chem. Phys. **125**, 204904.
- [96] Dai, L., Siow, Y. N., Doyle, P. S., & van der Maarel, J. R. C. (2012) ACS Macro Lett. **1**, 1046–1050.
- [97] Bustamante, C. (1991) Annu. Rev. Biophys. Bio. **20**, 415–446.
- [98] Volkmuth, W. & Austin, R. (1992) Nature **358**, 600–602.
- [99] Volkmuth, W., Duke, T., Austin, R., & Cox, E. (1995) Proc. Natl. Acad. Sci. U.S.A. **92**, 6887–6891.
- [100] Bakajin, O. B., Duke, T. A. J., Chou, C. F., Chan, S. S., Austin, R. H., & Cox, E. C. (1998) Phys. Rev. Lett. **80**, 2737–2740.
- [101] Guo, L. J., Cheng, X., & Chou, C.-F. (2004) Nano Lett. **4**, 69–73.
- [102] Reisner, W., Morton, K. J., Riehn, R., Wang, Y. M., Yu, Z., Rosen, M., Sturm, J. C., Chou, S. Y., Frey, E., Austin, R. H., et al. (2005) Phys. Rev. Lett. **94**, 196101.
- [103] De Gennes, P. G. (1979) Scaling concepts in polymer physics (Cornell university press).
- [104] Persson, F., Utko, P., Reisner, W., Larsen, N. B., & Kristensen, A. (2009) Nano Lett. **9**, 1382–1385.
- [105] Zhang, C., Zhang, F., Van Kan, J. A., & van der Maarel, J. R. C. (2008) J. Chem. Phys. **128**.



## References

---

- [106] Kim, Y., Kim, K. S., Kounovsky, K. L., Chang, R., Jung, G. Y., Jo, K., Schwartz, D. C., et al. (2011) Lab. Chip **11**, 1721–1729.
- [107] Chang, R. & Jo, K. (2012) J. Chem. Phys. **136**, 095101.
- [108] Zhang, C., Shao, P., van Kan, J. A., & van der Maarel, J. R. C. (2009) Proc. Natl. Acad. Sci. U.S.A. **106**, 16651–16656.
- [109] Dai, L. & Doyle, P. S. (2013) Macromolecules **46**, 6336–6344.
- [110] Wang, W., Li, G.-W., Chen, C., Xie, X., & Zhuang, X. (2011) Science **333**, 1445–1449.
- [111] Reisner, W., Pedersen, J., & Austin, R. (2012) Rep. Prog. Phys. **75**.
- [112] Levy, S. & Craighead, H. (2010) Chem. Soc. Rev. **39**, 1133–1152.
- [113] Jones, J. J., van der Maarel, J. R. C., & Doyle, P. S. (2011) Nano Lett. **11**, 5047–5053.
- [114] Zhang, C., Gong, Z., Guttula, D., Malar, P. P., van Kan, J. A., Doyle, P. S., & van der Maarel, J. R. C. (2012) J. Phys. Chem. B **116**, 3031–3036.
- [115] Browning, D., Grainger, D., & Busby, S. (2010) Curr. Opin. Microbiol. **13**, 773–780.
- [116] Bloomfield, V. (1996) Curr. Opin. Struc. Biol. **6**, 334–341.
- [117] Swinger, K. K. & Rice, P. A. (2007) J. Mol. Biol. **365**, 1005–1016.
- [118] Dame, R. T. (2005) Mol. MicroBiol. **56**, 858–870.

## References

---

- [119] Rye, H. S., Yue, S., Wemmer, D. E., Quesada, M. A., Haugland, R. P., Mathies, R. A., & Glazer, A. N. (1992) Nucleic Acids Res. **20**, 2803–2812.
- [120] Glazer, A. N. & Rye, H. S. (1992) Nature **359**, 859–861.
- [121] Larsson, A., Carlsson, C., Jonsson, M., & Albinsson, B. (1994) J. Am. Chem. Soc. **116**, 8459–8465.
- [122] Bennink, M. L., Schärer, O. D., Kanaar, R., Sakata-Sogawa, K., Schins, J. M., Kanger, J. S., de Grooth, B. G., & Greve, J. (1999) Cytometry **36**, 200–208.
- [123] Günther, K., Mertig, M., & Seidel, R. (2010) Nucleic Acids Res. **38**, 6526–6532.
- [124] Reuter, M. & Dryden, D. T. (2010) Biochem. Bioph. Res. Co. **403**, 225–229.
- [125] Watt, F., Breese, M. B., Bettiol, A. A., & van Kan, J. A. (2007) Mater. Today **10**, 20–29.
- [126] Wilson, K. M. & Walker, J. M. (2010) Principles and techniques of biochemistry and molecular biology (Cambridge University Press).
- [127] Tanaka, K., Yanada, H., Yoshida, T., & Mizuni, T. (1991) Agricultural and Biological Chemistry **55**, 3139–3141.
- [128] Porath, J. & Flodin, P. (1959) Nature **183**, 1657–1659.
- [129] Leonard, P. G., Ono, S., Gor, J., Perkins, S. J., & Ladbury, J. E. (2009) Mol. MicroBiol. **73**, 165–179.

## References

---

- [130] Krylov, A. S., Zasedateleva, O. A., Prokopenko, D. V., Rouviere-Yaniv, J., & Mirzabekov, A. D. (2001) Nucleic Acids Res. **29**, 2654–2660.
- [131] van Kan, J. A., Bettioli, A. A., & Watt, F. (2006) Nano Lett. **6**, 579–582.
- [132] van Kan, J. A., Zhang, C., Malar, P. P., & van der Maarel, J. R. (2012) Biomicrofluidics **6**, 036502.
- [133] Zhang, C., Jiang, K., Liu, F., Doyle, P. S., van Kan, J. A., & van der Maarel, J. R. C. (2013) Lab. Chip **13**, 2821–2826.
- [134] Egawa, Y., Hayashida, R., Seki, T., & Anzai, J.-i. (2008) Talanta **76**, 736–741.
- [135] van Kan, J. A., Shao, P. G., Wang, Y. H., & Malar, P. (2011) Microsyst. Technol. **17**, 1519–1527.
- [136] Dai, L., van der Maarel, J. R. C., & Doyle, P. S. (2012) ACS Macro Lett. **1**, 732–736.
- [137] Dai, L., Jones, J., van der Maarel, J. R. C., & Doyle, P. (2012) Soft Matter **8**, 2972–2982.
- [138] Daoud, M. & De Gennes, P. (1977) J. Phys. (Paris) **38**, 85–93.
- [139] van der Maarel, J. R. (2008) Introduction to biopolymer physics (World Scientific).
- [140] Baumann, C., Smith, S., Bloomfield, V., & Bustamante, C. (1997) Proc. Natl. Acad. Sci. U.S.A. **94**, 6185–6190.

## References

---

- [141] Stella, S., Falconi, M., Lammi, M., Gualerzi, C., & Pon, C. (2006) J. Mol. Biol. **355**, 169–174.
- [142] Makita, N., Yoshikawa, Y., Takenaka, Y., Sakaue, T., Suzuki, M., Watanabe, C., Kanai, T., Kanbe, T., Imanaka, T., & Yoshikawa, K. (2011) J. Phys. Chem. B **115**, 4453–4459.
- [143] Dai, L., Mu, Y., Nordenskiöld, L., & van der Maarel, J. R. C. (2008) Phys. Rev. Lett. **100**, 118301.
- [144] Joyeux, M. & Vreede, J. (2013) Biophys. J. **104**, 1615–1622.
- [145] Hud, N. & Vilfan, I. (2005) Ann. Rev. Biophys. Biomol. Struct. **34**, 295–318.
- [146] Zhang, C., Guttula, D., Liu, F., Malar, P. P., Ng, S. Y., Dai, L., Doyle, P. S., van Kan, J. A., & van der Maarel, J. R. C. (2013) Soft Matter **9**, 9593–9601.
- [147] Lim, C. J., Lee, S. Y., Kenney, L. J., & Yan, J. (2012) Sci. Rep. **2**.
- [148] Zhang, C., Hernandez-Garcia, A., Jiang, K., Gong, Z., Guttula, D., Ng, S. Y., Malar, P. P., van Kan, J. A., Dai, L., Doyle, P. S., Vries, R. d., & van der Maarel, J. R. C. (2013) Nucleic Acids Res. **41**, e189.
- [149] Matsuoka, T., Kim, B. C., Huang, J., Douville, N. J., Thouless, M., & Takayama, S. (2012) Nano Lett. **12**, 6480–6484.
- [150] Matsuoka, T., Kim, B. C., Moraes, C., Han, M., & Takayama, S. (2013) Biomicrofluidics **7**, 041301.
- [151] Zakharova, S., Egelhaaf, S., Bhuiyan, L., Outhwaite, C., Bratko, D., & van der Maarel, J. (1999) The Journal of Chemical Physics **111**,

10706.

- [152] Zhu, X., Ng, S. Y., Gupta, A. N., Feng, Y. P., Ho, B., Lapp, A., Egelhaaf, S. U., Forsyth, V. T., Haertlein, M., Moulin, M., Schweins, R., & van der Maarel, J. R. C. (2010) Phys. Rev. E **81**, 061905.